

EM41/Doris W. Hipp

CR-199817



(NASA-CR-199817) METHODS OF VIDEO  
AND SHEAROGRAPHY INSPECTION Final  
Report, 22 Sep. 1994 - 21 Sep. 1995  
(Alabama Univ.) 104 p

N96-16277

Unclas

G3/38 0086514

**Research Institute  
The University of Alabama in Huntsville**

Technical Report 5-33567  
Contract No. NAS8-38609  
Delivery Order No. 119

**Methods of Video and  
Shearography Inspection  
(5-33567)**

Final Technical Report for Period  
22 September 1994 through 21 September 1995

September 1995

Prepared by

Matthew D. Lansing  
Michael W. Bullock  
William J. Gnacek

Research Institute  
The University of Alabama in Huntsville  
Huntsville, Alabama 35899

Prepared for

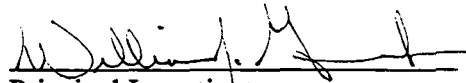
George C. Marshall Space Flight Center  
National Aeronautics and Space Administration  
Marshall Space Flight Center, AL 35812  
Attn: EH13 (Dr. Samuel S. Russell)

## PREFACE

This technical report was prepared by the staff of the Research Institute, The University of Alabama in Huntsville. The purpose of this report is to provide documentation of the work performed and results obtained under delivery order 119 of Marshall Space Flight Center (MSFC) Contract No. NAS8-38609. Mr. William J. Gnacek was Principal Investigator for this twelve month level of effort. Dr. Samuel S. Russell of the Nondestructive Evaluation Branch provided technical coordination.

The views, opinions, and/or findings contained in this report are those of the author(s) and should not be construed as an official NASA position, policy, or decision unless so designated by other official documentation.

I have reviewed this report, dated 20 Sept 95 and the report contains no classified information.

  
Principal Investigator

## TABLE OF CONTENTS

1.	INTRODUCTION	1
2.	BACKGROUND AND OBJECTIVES	1
2.1.	ELECTRONIC SHEAROGRAPHY	1
2.2.	SUB-PIXEL DIGITAL VIDEO IMAGE CORRELATION	3
3.	DELTA CLIPPER-EXPERIMENTAL ADVANCED	4
3.1.	COMPOSITE FUEL TANK	4
3.1.1.	SPECIMEN	4
3.1.2.	PROCEDURE	4
3.1.3.	RESULTS	5
3.1.4.	SUMMARY	6
3.2.	COMPOSITE LIQUID HYDROGEN FEED LINE	6
3.2.1.	JOINT COMPONENTS	6
3.2.2.	DEMONSTRATION TEST ARTICLE	7
3.2.3.	DEMONSTRATION TEST ARTICLE WITH REVISED BONDING	8
3.2.4.	PROTOTYPE	8
3.2.5.	FLIGHT ARTICLE	9
3.3.	COMPOSITE INTERTANK HONEYCOMB	9
4.	IMPACT DAMAGED FILAMENT WOUND PRESSURE VESSELS	11
4.1.	SPECIMEN	11
4.1.1.	GRAPHITE EPOXY	12
4.1.1.1.	EMPTY Gr-Ep CASES	12
4.1.1.2.	Gr-Ep CASES FILLED WITH INERT PROPELLANT	13
4.1.2.	KEVLAR EPOXY	13
4.2.	PROCEDURES	13
4.2.1.	ELECTRONIC SHEAROGRAPHY INSPECTION	13
4.2.1.1.	THERMAL EXCITATION	13
4.2.1.2.	PRESSURE EXCITATION	14
4.2.1.2.1.	INTERNAL VACCUUM	14
4.2.1.2.2.	INTERNAL PRESSURIZATION	15
4.2.2.	VIDEO IMAGE CORRELATION INSPECTION	15
4.3.	RESULTS	16
4.3.1.	EXAMPLES	16
4.3.2.	NEURAL NETWORK BURST PRESSURE PREDICTION	20
4.4.	SUMMARY	21
5.	SPACE SHUTTLE EXTERNAL TANK	22
5.1.	COMPOSITE NOSE CONE	22
5.1.1.	INTERNAL DELAMINATIONS	22
5.1.2.	FASTENER HOLES	23
5.1.2.1.	MACHINING DAMAGE TO CYLINDRICAL HOLES	23
5.1.2.2.	MACHINING DAMAGE TO CONICAL HOLES	25
5.1.2.3.	LOAD INDUCED DAMAGE TO CONICAL HOLES	25
5.1.2.4.	SUMMARY	28
5.2.	LIQUID OXYGEN FEED LINE FAIRING	28

6.	PEGASUS FAIRING THERMAL PROTECTION SYSTEM	29
6.1.	PROCEDURE	30
6.2.	ORBCOMM	30
6.3.	SEASTAR	33
7.	SOLAR X-RAY IMAGER TELESCOPE TUBE	37
8.	CRACK TIP STRESS INTENSITY FACTOR MEASUREMENT	37
8.1.	CRACK TIP PLASTIC ZONE	37
8.2.	ELASTIC DEFORMATION FIELD	40
9.	CONTROL SETTINGS INFLUENCE PROBABILITY OF DETECTION	41
	APPENDICES	46
A.1.	REFERENCES AND RELATED LITERATURE	47
A.2.	FWPV DATA	49
A.2.1.	GRAPHITE EPOXY	49
A.2.1.1.	EMPTY Gr-Ep CASES	49
A.2.1.2.	Gr-Ep CASES FILLED WITH INERT PROPELLANT	57
A.2.2.	KEVLAR EPOXY	66
A.2.2.1.	EMPTY K-Ep CASES	66
A.2.2.2.	K-Ep CASES FILLED WITH INERT PROPELLANT	73
A.3.	VICNET NEURAL NETWORK INTERFACE	78
A.3.1.	VICNET ABOUT BOX	78
A.3.2.	VICNET MAIN WINDOW	79
A.3.3.	SDVIC DATA FILE NAME REQUEST WINDOW	92
A.3.4.	SETTINGS FILE NAME REQUEST WINDOW	94
A.3.5.	FORM INDEPENDENT CODE	96

## 1. INTRODUCTION

The Research Institute at the University of Alabama in Huntsville (UAH) was tasked by the Nondestructive Evaluation (NDE) Branch (EH-13) at Marshall Space Flight Center (MSFC) to study methods of video image correlation and electronic shearography for nondestructive evaluation. The purpose of this task was to study and develop methods and tests to evaluate the structural integrity of aerospace components using these techniques. Methods of physical load application must be developed before interrogations with these methods may be used to qualify hardware. To that end, inspection procedures were developed for a variety of aerospace components and material systems. Experiments were also conducted from which the relationship between the control settings of the electronic shearography apparatus may be related to flaw detectability. A short feasibility study was conducted to determine the applicability of electronic shearography to the determination of the stress intensity factor of a Mode I crack tip by measurement of the localized zone of three dimensional plasticity.

## 2. BACKGROUND AND OBJECTIVES

The NDE Branch at MSFC maintains a laboratory for the application and development of the methods of video image correlation and electronic shearography. This facility is equipped with a Pratt-Whitney Electronic Holography/Shearography Inspection System (PW EH/SIS) and a Laser Technology, Inc. (LTI) SC-4000. Electronic shearography techniques provide non-contact real-time location and sizing of defects in many material systems.

### 2.1. ELECTRONIC SHEAROGRAPHY

Electronic shearography images a coherently illuminated object through an image shearing lens to produce an interference fringe pattern<sup>[1-3,5-7,12,14, 22-23,25-26]</sup>. The boundaries between light and dark fringes represent contours of constant change in surface slope due to some form of excitation. The PW EH/SIS at the MSFC NDE Branch Electronic Shearography Laboratory was used to interrogate most of the specimens for this study. This device utilizes a modified Michelson interferometer as an image shearing device, as shown in Figure 1. A frequency doubled Nd:YAG pumped diode laser ( $\lambda = 532$  nm) is used as a source of coherent illumination, the beam of which passes through a spatial filter and an etalon to produce a stable divergent speckle pattern on the surface of the test article. The light reflected from the object is collected by a telephoto lens, which provides a variable field of view, and imaged onto the sensor array of a CCD camera through the shearing interferometer.

Each ray passed through the telephoto lens is separated by the beam splitter into a reference beam and a sheared beam. The reference beam passes straight through the beam splitter, reflects from a phase stepping mirror back along its previous path, and is reflected from the back of the beam splitter toward the sensor array. The sheared beam is reflected from the front of the beam splitter toward the image shearing mirror, reflected back again at a tilted angle, then passed through the beam splitter toward the sensor array. The

sheared beam is incident on the sensor array at a point which is shifted, or sheared, from the reference beam. Each point on the surface of the object is thus imaged to two separate pixels on the camera sensor array. A more complicated reverse ray trace shows that, similarly, a single pixel on the camera sensor array images two sheared points on the surface of the object. Assuming a planar object, all points in the image are sheared by the same lateral distance, referred to as the image shearing distance,  $s$ . The sensitivity of the device is proportional to  $s$  and thus related to the angle at which the image shearing mirror is tilted. By varying the tilt angle and direction of the image shearing mirror, the operator may adjust the sensitivity of the device to suit the structure being evaluated and the type of excitation being applied.

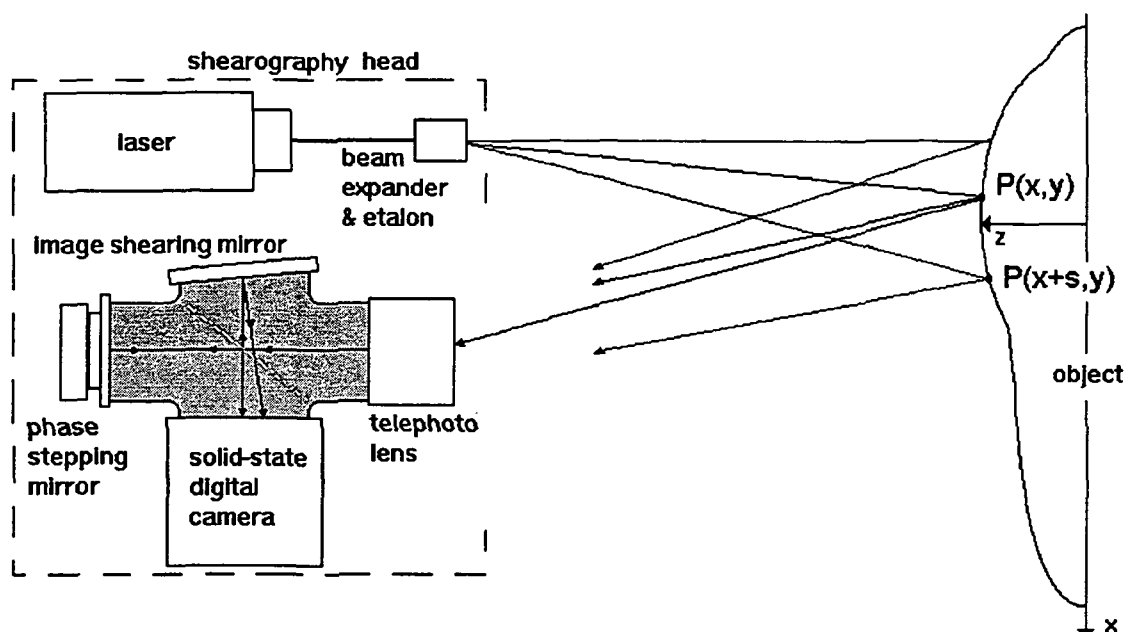


Figure 1. PW EH/SIS Optical Arrangement

Unlike electronic holography (EH), which produces fringe patterns indicative of object displacements toward the camera, ES senses changes in the slope of the surface of the object along intervals of the image shearing distance. That is, the fringes are produced by differences in motion toward (or away from) the camera between points separated by  $s$ . The ES technique is thus less sensitive overall than is EH. In addition, some EH techniques pass the reference beam directly from the laser to the sensor array inside an optical fiber and only the object beam reflects from the test article. Other EH techniques illuminate the test object with two coherent beams having almost entirely different optical paths in object space. The optical paths of the reference and sheared beam in ES differ only inside the interferometer. The ES technique is thus less sensitive to environmental effects (changes in vibration, temperature, etc.) than is EH. The ES apparatus does not require extensive environmental isolation, such as an optical air table, and is regularly used for field evaluations.

In the static test mode, sheared images are digitally acquired before and after some form of excitation is applied to the test article. The intensity recorded on each pixel is a

function of the relative phase between the light rays reflected from the two corresponding points separated by  $s$  in the direction of image shearing on the object surface, and thus a function of the relative slope across that interval of the image shearing distance. After the test object has been statically excited, typically by heating, cooling, or changing the pressure to which it is exposed, then a second sheared image is recorded. The digital frame subtraction of these two images results in a shearogram featuring a fringe pattern indicative of full-field values for the change in surface slope at each point on the object surface due to the excitation load.

## 2.2 SUB-PIXEL DIGITAL VIDEO IMAGE CORRELATION

Sub-pixel Digital Video Image Correlation<sup>[3,8-11,15-18,20-21,24]</sup> is a full-field non-contact computer vision technique for determination of in-plane displacements and strains in near-real-time. This technique utilizes readily available and inexpensive video equipment in conjunction with a Microsoft Windows environment image processing software package which is available from NASA COSMIC. Rather than qualitative fringe patterns, the results of SDVIC inspection are quantitatively scaled and indexed false-color plots indicating full-field values for both of the in-plane displacement components, both of the in-plane linear strain components, the in-plane shear strain, and in-plane rotations with sub-pixel resolution. A data file is also produced which contains the tabulated values for these measurements in a grid arrangement of points on the surface of interest. The separation distance and number of points for which data is tabulated is determined by the user.

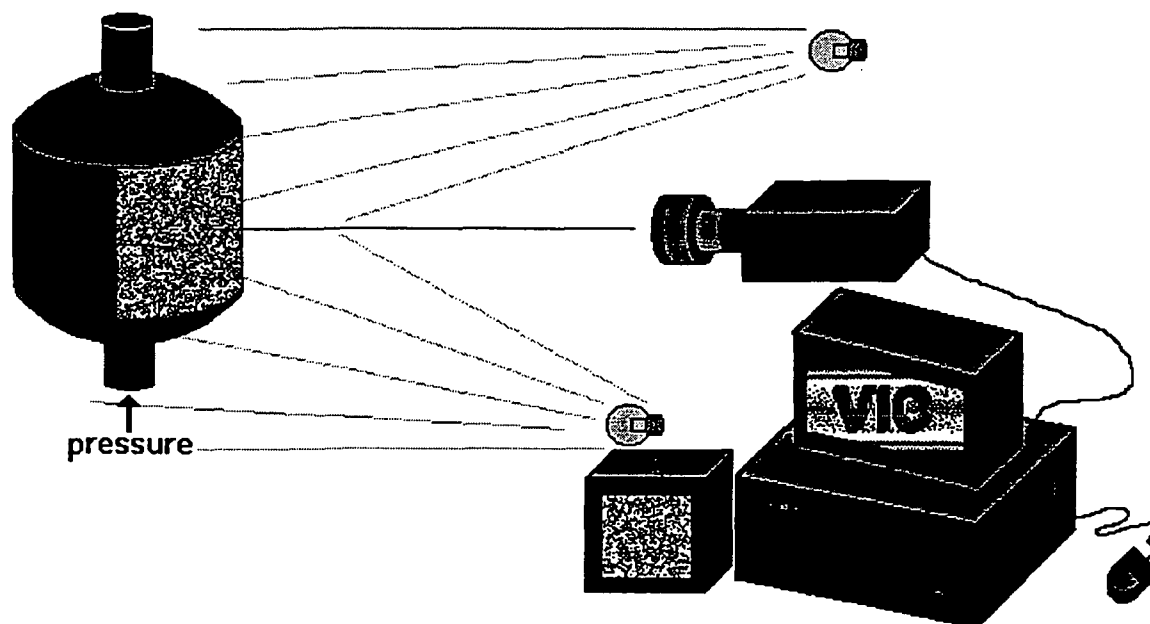


**Figure 2.** Apparatus used for SDVIC data acquisition.

The apparatus used to acquire and process images for SDVIC is shown in Figure 2. with a domed cylindrical pressure vessel as an example specimen. The over-spray from



black and white spray paint is used to apply a random black and white speckle pattern to the surface of the specimen. This pattern is illuminated by a white light source and imaged by a Sony XC-77 CCD camera with a Sigma 70-210 mm telephoto lens. The video images are captured and digitized by a Data Translation DT-2862 frame grabber board in an Intel compatible personal computer.

### 3. DELTA CLIPPER-EXPERIMENTAL ADVANCED

The NASA Office of Space Access and Technology has entered into cooperative agreements with private industry to develop a Reusable Launch Vehicle (RLV) with the aim of lower manufacturing, maintenance, and launch costs than the current Space Transportation System (STS) Space Shuttle. One of the Single Stage to Orbit (SSTO) vehicles under development is the McDonnell-Douglas Delta Clipper. As an improvement upon the Air Force sponsored Delta Clipper-Experimental (DC-X) vehicle, the NASA sponsored DC-XA (DC-X Advanced) proposes to reduce lifted mass, and thus increase payload capacity and decrease launch expenses, by utilizing composite components not only in the load bearing structure but also in the propulsion systems. Electronic Shearography methods were developed for inspection of several of these components.

#### 3.1. COMPOSITE FUEL TANK

The DC-XA will utilize Composite Overwrapped Filament Wound Pressure Vessels (CO-FWPV) to store liquid oxidizer (LOX) and liquid hydrogen (LH2) to fuel the vehicle propulsion systems. Tests were performed to explore the problem of hydrogen permeability in such structures. It was observed during helium pressurization tests of a subscale composite pressure vessel that delaminations on the dome section near an end boss caused considerable leakage. These delaminations were not visible to the unaided observer. The capability of Electronic Shearography for evaluation of such delaminations on the dome section of CO-FWPV has been demonstrated.

##### 3.1.1. SPECIMEN

The Nondestructive Evaluation Branch (EH13) was provided a graphite-epoxy (Gr-Ep) CO-FWPV with delamination leaks near an end boss. This was a 5.75" diameter filament wound bottle, similar to ASTM standard D2585-68 (1985), with pre-preg Gr-Ep tape over-wrap. Figure 3. schematically illustrates the structure of the bottle.

##### 3.1.2. PROCEDURE

The Pratt-Whitney Electronic Holography / Shearography Inspection System (PW EH/SIS) was used to evaluate the response of the bottle to

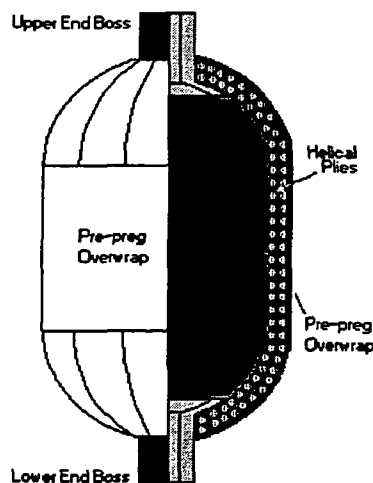


Figure 3. Specimen Geometry

thermal excitation. The image shearing distance was set to 1/8" horizontal at an object-to-lens distance of 4'. The telephoto lens was focused on the dome at maximum zoom with the optical axis of the camera approximately coincident with the longitudinal axis of the bottle. Static shearograms were obtained using speckle averaging and four frame averaging. No traveling fringes were displayed. A reference shearogram was obtained after the bottle had been slightly heated ( $\Delta T < 5^\circ\text{F}$ ) with an industrial heat gun. The deformed shearogram was taken after the bottle had cooled to approximately room temperature. The resulting interferogram is a superposition of these two images.

### 3.1.3 RESULTS

Electronic shearograms are interpreted by the light and dark fringe patterns they present. Each fringe represents a contour of change in surface slope produced by, in this case, thermal relaxation. Figure 2. is a shearogram of the end boss-dome section which did not leak. Away from the boss, the fringes are widely spaced and exhibit a smooth transition from dark to light. The pattern here is one of concentric parabolas. As the dome cools its radius of curvature changes. The positive slopes on the left decrease while the negative slopes on the right increase. Near the boss, the fringes are closer together, have sharper edges, and appear to be less regular. This is due to the local change in geometry (compared to the rest of the dome) and the interactive presence of the boss. However, the pattern of concentricity is still fairly evident.

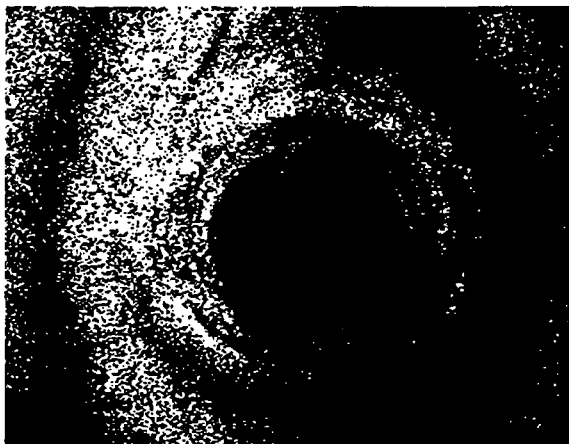


Figure 2. Sound Polar Boss



Figure 3. Leaking End Boss

Figure 3. is a shearogram of the end boss dome section which did leak. Identifying marks may be seen on the end of the boss. Away from this boss the fringe pattern is similar to that of the other end of the bottle. However, near to the boss the pattern becomes convoluted and irregular. This indicates a less directionally oriented and less uniform deformation pattern than would be expected of a sound lamination bond or was exhibited by the opposite dome section. Also, the fringes are sharper and more closely spaced, indicating more overall motion. Non-uniform deformation indications such as these tangled fringe patterns are typical of delamination indications in many composite materials.

### 3.1.4. SUMMARY

It has been demonstrated that, when inspected with electronic shearography, a leaking end boss in a composite overwrapped filament wound pressure vessel produces the same sort of fringe pattern discontinuity which is typical of a composite delamination. A sound end boss has been shown to produce a more regular and symmetrical pattern. The ability to distinguish a sound end boss from a leaking end boss indicates that electronic shearography is capable of assessing end boss delaminations without pressurizing the vessel.

### 3.2. COMPOSITE LIQUID HYDROGEN FEED LINE

In addition to the composite fuel tanks, the DC-XA will utilize composite feed lines for liquid hydrogen between the fuel tank and liquid-gas converter (LGC). The geometry of the flight article feed line is shown in Figure 4. The presence of delaminations in the composite components or bonded joints could lead to catastrophic vehicle loss. Throughout this development effort, specimens were provided to the MSFC NDE Branch for ES inspection to detect such delaminations. Thermal excitation was used for all inspections.

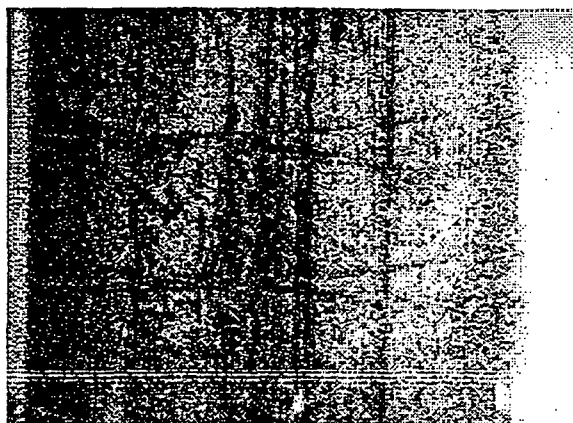


Figure 4. DCX-A composite liquid hydrogen feed line.

#### 3.2.1. JOINT COMPONENTS

Prior to joint bonding, specimens representative of the composite lay-up were inspected with ES. The image shearing distance was adjusted to 0.04 inch at an object distance of 4 feet with the telephoto lens focused on the surface of the tube closest to the shearography device. A typical shearogram is shown in Figure 5. Possible resin-rich areas along the edges of the axially oriented pre-preg strips were indicated by axial linear dark fringes. Possible wrinkles in the lay-up were also indicated by rows of parallel dark fringes

skewed from the axial direction. Gaps or wrinkles in the lay-up could be expected to form these resin-rich regions during consolidation.



**Figure 5.** Indications detected along the edges of both axial and helical strips in the feed line splice section \*



**Figure 6. (N)** Detection of an internal delamination simulated by a Teflon insert and indicated by a double bull's-eye.

Another specimen representing a section of feed line tube with simulated delaminations was inspected with an image shearing distance of 1/8 inch horizontal and 1/8 inch vertical. The delaminations were simulated by pillows fabricated from Teflon tape which were heat sealed along all four sides and inserted into the lay-up. A similar inspection procedure detected the inserts as indicated by the typical "double bull's-eye" in Figure 6.

### 3.2.2. DEMONSTRATION TEST ARTICLE

A demonstration test article (DTA#1-2) was inspected for bond line integrity with ES. This test article differed in geometry from the flight article in that a flat titanium flange attached to a straight composite tube replaced the tapered titanium flange and angled composite tube. X-ray computed tomography (CT) had detected a large delaminated region along the bond line between the inner feed line sections and the sleeve around the joint. The result of ES inspection of this portion of the feed line is shown in Figure 7. The unbonded region, indicated by large, feathery black fringes, appears larger than was indicated by CT. Subsequent radiographic inspections indicated similar unbonds which were, again, smaller in size than indicated by ES. It is likely that during ES inspection parts of the flaw were excited which were not detected by the other techniques because without loading the flaw surfaces remained in contact with each other. This is often referred to as a "kissing" delamination, and is among the most difficult flaws to detect with many methods.

\* This shearogram is shown as a negative image for clarity. Hereafter negative images will be noted (N).



Figure 7. (N) DTA#1-2, unbonded regions in the spliced joint with original bonding procedure.

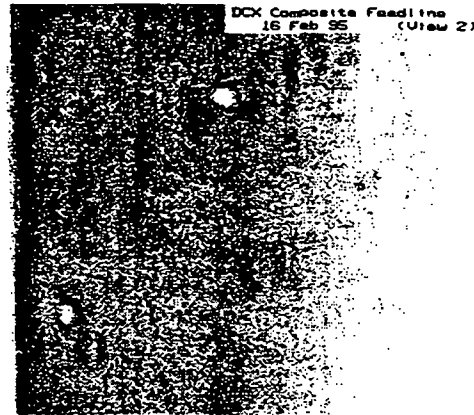


Figure 8. (N) DTA#1-2a, smaller unbonds detected with revised bonding, indications around epoxy injection holes.

### 3.2.3. DEMONSTRATION TEST ARTICLE WITH REVISED BONDING

A revised joint bonding procedure was developed to address the issue of the aforementioned unbonds. This procedure injects the epoxy between the inner feed line sections and the sleeve around the joint through 1/8 inch holes drilled in the sleeve. The sleeve was removed from the test article and replaced by another with the revised bonding procedure. The repaired part (DTA#1-2a) was inspected again with ES and no major indications were seen, as shown in Figure 8. Small circular indications were present at the epoxy injection holes, but the diameter of these indications were not significantly larger than the holes themselves, and the indications are believed to be the effect of a difference between the coefficient of thermal expansion of the feed line sleeve matrix and fiber and that of the joint bonding epoxy. The possibility exists that some machining damage was incurred during the drilling of the epoxy injection holes; however, such damage cannot be verified as there was no ES inspection prior to the bonding of the joint. Moreover, such machining damage may have been repaired to some degree by the injection of epoxy. The integrity of this repair cannot be verified because, again, no ES inspections of this type have been performed.

### 3.2.4. PROTOTYPE

A prototype feed line, identical in geometry and fabrication to the flight article, was inspected for bond line integrity similar to the preliminary test article. The results of this inspection are similar to that of the preliminary test article, with the same concerns about the epoxy injection holes. As shown in Figures 9. and 10., no major bond line delaminations were indicated. The injection holes appear as dark pairs of circles. The lay-up quality of the outer sleeve and inner feed line sections appears to have improved, as fewer minor anomalies were observed with an image shearing distance, and resulting sensitivity, up to four times that used for inspection of the demonstration test articles.

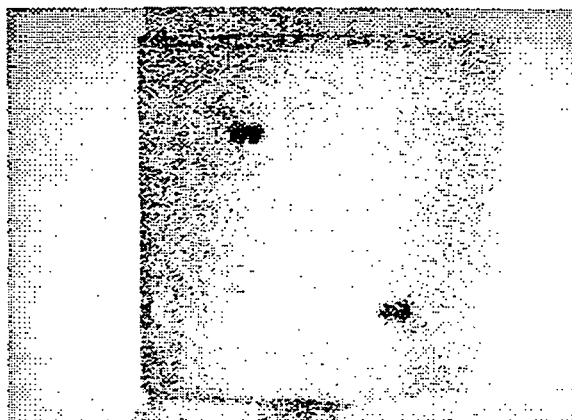


**Figure 9.** (N) Prototype, no unbonds detected in 90° to composite flange joint.

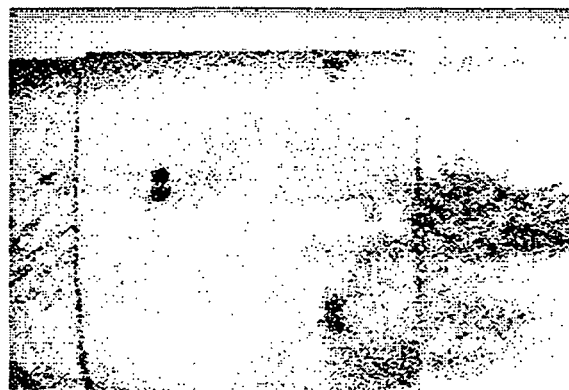


**Figure 10.** (N) Prototype, no unbonds detected in 90° to 45° bonded joint.

### 3.2.5. FLIGHT ARTICLE

Inspection of the flight article feed line assembly demonstrated that the bonded joints were of poorer quality than the prototype. As shown in Figures 11. and 12., respectively with and without indication labels, numerous small double bull's-eye indications appeared as well as an irregular vertical fringe pattern. The former indications are suspected to be small unbonds between the inner and outer tubes of the splice and the latter indication is suspected to be the influence of these small flaws on the surrounding material. However, the flight article was judged to be acceptable based upon the small size of the unbond indications.



**Figure 11.** (N) Numerous small unbonds detected in spliced joints of flight article produce complex fringe patterns.

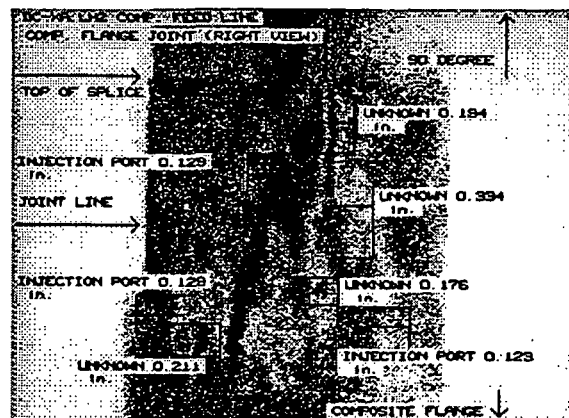


**Figure 12.** (N) Flight article unbonds, labeled here as UNKNOWN, judged to be acceptable based on small size.

### 3.3. COMPOSITE INTERTANK HONEYCOMB

The DC-XA composite intertank is being fabricated from an aluminum honeycomb with composite laminated inner and outer faces. This will provide significant weight reduction as compared to the current metallic structure. Areas of concern are the

presence of delaminations within the composite facing material, unbonds between the facing and the honeycomb core, and impact damage which may result in both types of delaminations as well as crushing of the honeycomb.

A specimen typical of the composite honeycomb with laminar facing for the DC-XA intertank was inspected with electronic shearography to determine the detectability of programmed impact damage. The specimen was cut from a larger coupon which had been impacted several times. This section contained two labeled impact points. A razor blade was used to separate the laminated plies in one corner to simulate a delamination in the facing material. Similarly, the facing material was unbonded from the honeycomb on one corner and in the middle of a free edge.

Figure 13. clearly indicates the location of the two impact points as a pair of large double bull's-eye fringe patterns. Several smaller double bull's-eye indications appear and are suspected to be damage caused by the c-clamps used to hold the specimen during impact. Figures 14. and 15. demonstrate the detection of delaminations between the laminant plies, between the facing and the honeycomb, and of unknown origin.



**Figure 13.** (N) Impact damage to intertank coupon indicated by 2 large double bull's-eyes. Other damage indicated by numerous smaller double bull's-eyes.

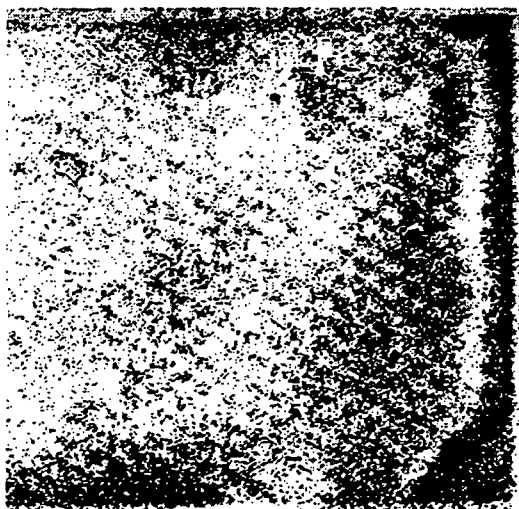


**Figure 14.** (N) Composite skin delamination (upper right) and skin to honeycomb (lower right) delaminations.

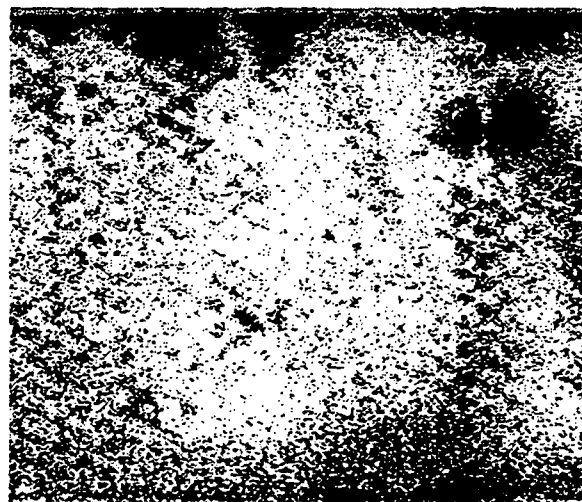


**Figure 15.** (N) Skin to honeycomb delamination (upper left) and unknown double bull's-eye (upper right).

#### 4. IMPACT DAMAGED FILAMENT WOUND PRESSURE VESSELS

Composite pressure vessels are being used with increased frequency for aerospace and other applications. The DC-XA, discussed in the previous section, will utilize filament wound pressure vessels (FWPV) to store liquid oxidizer (LOX) and liquid hydrogen (LH<sub>2</sub>) to fuel propulsion systems. The Transfer Orbital Stage (TOS) satellite boosters are solid rocket motors with filament wound cases. The possibility exists that during handling or service these composite structures may suffer impact damage. This damage may be in the form of highly localized fiber breaks and matrix cracking, more widespread internal delaminations, or some combination of the two. The nature of the impact damage is determined by the material system and the geometry and energy of the impactor.

Historically the complex material systems which give composite structures their desirable qualities have at the same time complicated the task of inspections for structural integrity. The hard x-rays typically used for radiography of metallic structures tend to wash out features which would otherwise indicate damage. The presence of solid rocket fuel in a composite case results in an inverse problem in that the filler material properties and thickness render it almost opaque to these x-rays. Likewise, the eddy-current techniques which are regularly used to locate and size cracks in metallic structures are ineffective for non-metallic composites. In many cases, a load or pressure proof test above that expected in service and perhaps as high as 90% of expected ultimate is used where other nondestructive evaluation (NDE) techniques are unavailable. These proof tests are expensive, potentially dangerous, and most likely induce damage which weakens the structure. If nothing else, then such a proof test is yet another high load fatigue cycle which shortens the service life of the structure.

This study demonstrates the complimentary abilities of two computer vision techniques to characterize the nature and extent of impact damage in filament wound pressure vessels with a single thermal cycle of less than five degrees Fahrenheit and a proof cycle of less than 25% of expected ultimate load. Electronic shearography (ES) and Sub-pixel Digital Video Image Correlation (SDVIC) are used to evaluate the structural integrity of these specimens with respect to internal delaminations, fiber breakage, and matrix cracking. ES is a variation of traditional holography which allows computer sensing of changes in surface slope components of the specimen due to some form of excitation. SDVIC is based upon the much older scribed grid technique for strain measurement and allows full-field non-contact measurement of in plane displacements and strains. ES and SDVIC results are shown to correlate well with the impact state and lowered burst pressures of these damaged vessels.

##### 4.1 SPECIMEN

The FWPV evaluated here conformed to ASTM standard D2585-68 (1985) and were fabricated by Thiokol Corporation at the Marshall Space Flight Center (MSFC) Productivity Enhancement Complex. The bottles were formed as shown in Figures 16. and 17. by a series of filament wound helical and hoop plies, with the outermost in the



cylindrical region being oriented in the hoop direction. Both ends of the bottle terminated in metallic polar bosses allowing access to the internal cavity.

Impact damages ranging from unapparent to the unaided observer to obvious indentions or partial perforations were produced in the FWPV by means of a calibrated dead weight drop fixture. Impact of the specimens was performed by the MSFC Polymers and Composites Branch. The impact energies used for this study were determined by preliminary testing. Micrographs of specimens impacted at various energies indicated the type of damage caused by each, and energies were thus chosen for this study which would produce significant damage as to effect burst pressures. All of these bottles contained a rubber liner to contain the pressurizing water after failure of the composite cylinder.

#### 4.1.1. GRAPHITE-EPOXY

The population spanned three epoxy resins and various levels of impact. All test articles were manufactured with continuous Hercules IM-7 graphite fiber pre-preg. One third of the FWPV were bound with each of the toughened epoxies ICI Fiberite 977-2 and Hercules X8553-45. The final one third contained the untoughened Hercules 3501-6 ATL epoxy resin.

##### 4.1.1.1. EMPTY Gr-Ep CASES

Three bottles from each resin class were impacted with a 1/2 inch diameter tip at 3.5 ft-lb. (low), 5.0 ft-lb. (medium), and 7.0 ft-lb. (high) respective energies. One vessel from each resin class was left undamaged as a reference. The geometry of these specimen is shown in Figure 16.

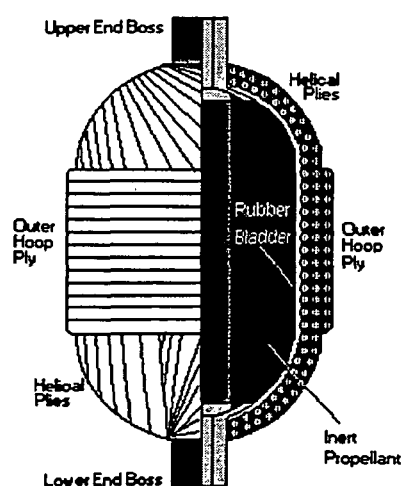
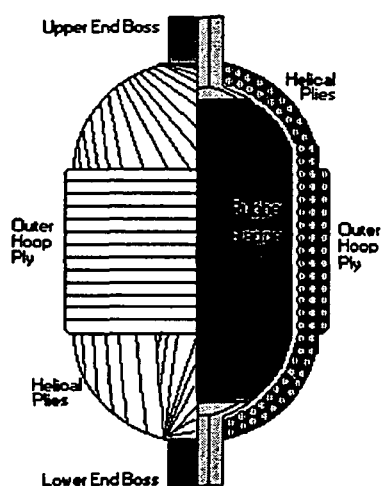


Figure 16. Geometry of empty specimens. Figure 17. Geometry of filled specimens.

#### **4.1.1.2. Gr-Ep CASES FILLED WITH INERT PROPELLANT**

All of these bottles were filled with an inert simulated solid propellant leaving an internal cavity approximately one inch in diameter running the entire axial length, as shown in Figure 17. This inert propellant was cast into the bottles and the internal cavity was then drilled out. The material was rubber-like and behaved mechanically similar to a pencil eraser.

#### **4.1.2 KEVLAR-EPOXY**

The kevlar-epoxy (K-Ep) FWPV evaluated here were manufactured in the same manner as the Gr-Ep bottles. The higher fracture toughness of the kevlar fibers as compared to that of the graphite fibers. Again, half of the population was unfilled and half was filled with the inert simulated propellant.

### **4.2. PROCEDURES**

#### **4.2.1. ELECTRONIC SHEAROGRAPHY INSPECTION**

The majority of the ES inspections performed on these FWPV were performed with thermal excitation. This method was chosen for its ease and speed. A single vacuum excitation inspection was performed to demonstrate that the method was feasible, although more complicated and time consuming. Attempts to perform ES inspections during internal pressurization proved to be prohibitively difficult, but the method is discussed below.

##### **4.2.1.1. THERMAL EXCITATION**

For this study, shearograms were obtained of each specimen after impact and prior to hydro-burst testing. The test articles were heated to surface temperatures slightly above ambient by thermal convection using an industrial heat gun. The heated specimens felt only slightly warm to the touch, and thus were minimally, if at all, harmed by the thermal cycle. Reference images were obtained while the FWPV were slightly warmer than ambient and these were digitally processed with later images at lower temperatures. The temperature differential between the two images was due to ambient cooling. The detected deformations are the result of thermal relaxation during this cooling.

The sensitivity of the ES apparatus was adjusted for these inspections such that the background motion of the structurally sound regions would lie within the first dark fringe. The greater motion of any damaged region would appear within a first light fringe and perhaps higher order dark and light fringes. Preliminary testing determined that an image shearing distance of 0.25 inches with a field of view approximately 6 inches wide at a lens-to-object distance of 8 feet provided the desired sensitivity. Upon the application of heat, delaminated regions expanded without the constraint of being bonded to the underlying laminae. The structurally sound regions, however, were subject to this constraint and deformed more uniformly with lower magnitudes. The surface above the delaminated

regions thus behaved like a buckling plate, and it is this deformation which appears in the shearogram.

This type of damage and indication is typical of what was observed in the shearograms of the blunt tip impacts. All of these shearograms are included in appendix A.2., and a few examples are discussed in section 4.3.1. While visible surface damage in almost every case was minimal, if existent at all, the results of ES inspection consistently reveal fairly large "rose-petal" or "butterfly" type indications. Indications with these appearances are respectively typical of non-uniform delaminations in laminar composites where the delamination meanders among the plies and delaminations which are more uniform, effecting a small number of plies. The blunt tip impacts at low energy were manifested as somewhat circular indications having a diameter of 2 to 3 inches. The blunt tip impacts at high energy, however, appear to be symmetrical only in the hoop and axial directions. The width of the indications appear to be similar in the hoop direction, but they extend almost completely across the outer hoops in the axial direction.

The overall appearance of the ES indications suggests that, at the impact energies used in this experiment, the damage caused by the blunt tip impacts were primarily delaminations. The geometry (size and shape) of the indications suggest that the higher energy impacts generally resulted in delaminations which were larger in area and thus effected a greater number of the outer hoop fibers.

Alternatively, the impact may have caused a more localized region of fiber breakage and matrix crushing rather than having generated delaminations. In this latter case, some of the damage would be visible to the unaided observer, but the question remains as to how far the damage extends beyond that which is visible. The region weakened by micro-cracking around the impact could be similarly expected to be somewhat less constrained than the undamaged regions away from the impact, and thus expand and deform more due to the application of heat and be detectable by ES interrogation.

This appears to be the case with the sharp tipped impacts in this study. Most of these test articles featured visible crush zones where the impact tip actually severed fibers in the outermost plies and indented into the bottle. In none of these specimens did the indentation visibly penetrate through to the rubber liner. The ES indications for the sharp tipped impacts are far more localized, and appear primarily as small double bull's-eye fringes. This type of indication is typical of a more uniform single-ply delamination than that observed with the blunt tip impacts. The indications for these bottles were in almost every case significantly larger than the 2 mm impact tip which resulted in the 2 mm visible indentions, and larger for the high energy impacts than those at low energy. ES inspection of a visible impact damage sight can thus determine how far the damage effected region extends beyond what is visible.

#### **4.2.1.2. PRESSURE EXCITATION**

##### **4.2.1.2.1. INTERNAL VACUUM**

A small vacuum pump was connected to the burst testing apparatus in place of the water pump. An internal vacuum of approximately 5 psig was pulled between reference

and subsequent images. Alternatively, the pressure was reduced prior to the reference image and restored before subsequent images. The image shearing distance, field of view, and object distance were adjusted to the same values used with thermal excitation. As illustrated in Figures 18. and 19., the delaminations in the test article were clearly evident.



**Figure 18.** (N) Vacuum application..

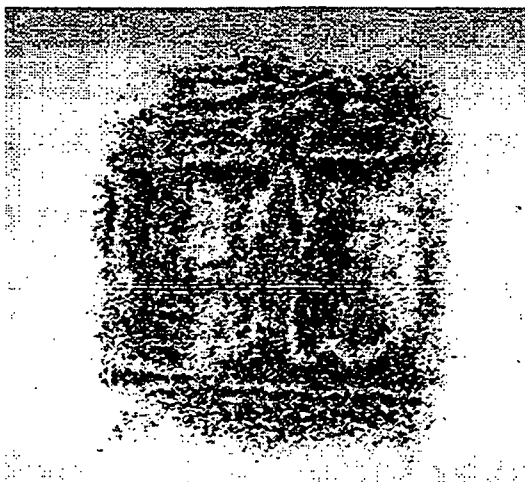


**Figure 19.** (N) Vacuum removal.

#### 4.2.1.2.2. INTERNAL PRESSURIZATION

An attempt was made to perform ES inspections while the FWPV were internally pressurized with the air driven water pump of the burst test apparatus. It was intended that while at house pressure (0 psig) or after the internal pressure had been increased to 250, 500, 750, or 1000 psig the manually controlled air regulator would gradually be adjusted to increase the pressure a few psig between reference and subsequent images. The problems faced included that adjusting the air regulator caused the water pump to cycle unpredictably, forcing a 100 psig jump in pressure, and that the  $\pm 25$  psig fluctuations in the house water supply did not provide a stable reference. The low resolution with which the pressure could be controlled prevented any meaningful shearograms from being obtained.

#### 4.2.2. VIDEO IMAGE CORRELATION INSPECTION

The SDVIC images were acquired during a proof test with a maximum pressure of approximately 25% of the manufacturer's predicted burst pressure (approximately 4000 psi) for an undamaged FWPV of this geometry and manufacturing technique and these material systems. A typical pressurization schedule is shown in Figure 20. Digital images were stored after the initial 800 psig proof at 250 psig intervals from 0 to 1000 psig. Following this second pressurization cycle, each bottle was pressurized to burst. This pressurization schedule was used for all cases except the empty Gr-Ep FWPV, for which the second pressurization schedule excluded holds and data acquisition at 250, 500, and 750 psig. All pressure ramps were at approximately 10 psig per second.

These stored images were later correlated by the SDVIC software in a Microsoft Windows environment. The image processing software calculates a correlation integral between a pixel subset of the undeformed image and an interpolated gray scale function which is fit to a subset of the deformed image. This correlation factor, the result of the correlation integral, is minimized by a Newton-Raphson routine to determine the displacements,

strains, and rotations which result in the best match between the undeformed subset and the interpolated deformed subset. The interpolation of the gray levels for the deformed subset allows deformation values to be determined with sub-pixel resolution. The software repeats this process, stepping across and down the undeformed image until results are determined for the entire field of interest with the desired resolution. The resulting deformation values may then be displayed as a scaled and indexed false-color plot. For this study, correlations were performed for each FWPV using the image taken at 0 psig prior to the pressurization cycle as the undeformed image. This image was then correlated with each of the images taken at each 250 psig incremental hold in the pressurization cycle. This process resulted in full-field hoop strain measurements from 0 psig to 250, 500, 750, and 1000 psig for the impact region of each bottle.

For the filled Gr-Ep and some of the K-Ep FWPV, in the interest of time, an initial low resolution correlation was performed for each load step with each FWPV over an area approximately 3 inches square. Impact damage was coarsely indicated as a subset or group of subsets with an anomalously large hoop strain as compared with the rest of the field. This initial correlation served to locate the impact zone. A second high resolution correlation was then performed over an area approximately 1 inch square. This second correlation more precisely indicated the geometry of the damage effected region and the strain values which occurred therein.

### 4.3. RESULTS

The results of ES and SDVIC inspections for all specimens in this study appear in appendix A.2. Shearograms and SDVIC hoop strain fields are tabulated for each class of specimen and ordered by impact state in each respective section.

#### 4.3.1. EXAMPLES

The generalized results discussed here in detail correspond to the filled Gr-Ep FWPV. SDVIC results for the empty Gr-Ep specimens are similar, and ES inspections were not performed for these specimen as part of this study. ES results for the K-Ep FWPV, as shown in the appendix, indicate more extensive delaminations. This

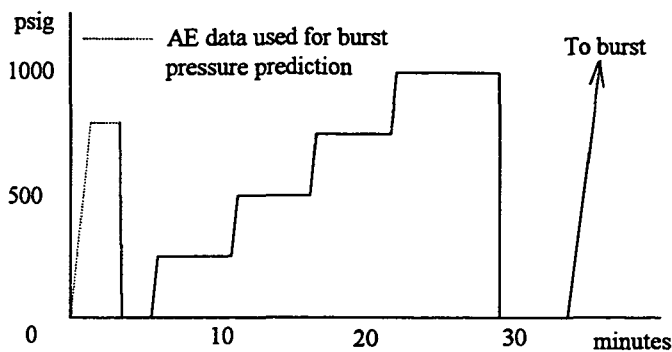


Figure 20. Typical Pressurization Schedule for Hydro-proof of FWPV (maximum pressure approximately 25% of expected burst for undamaged specimen.

delamination and the generally featureless SDVIC hoop strain fields are due to the greater fracture toughness of the kevlar fibers as compared to graphite.

As indicated by ES interrogations, the damage caused by blunt tip impacts was primarily delamination. The large field area of the initial correlation approximately circumscribed the area indicated as delaminated by ES for low energy impacts with the blunt tip impactor. However, the smaller field area of the second correlation generally lay within the ES delamination indications. In either case, the delaminations did not act as stress concentrators in the plane of the surface of the bottle, and thus are difficult to distinguish in the hoop strain fields determined from either correlation. In some cases, however, there was sufficient damage caused by the blunt tip impact that some fiber breakage and matrix cracking occurred, if not upon impact then during pressurization, as illustrated in Figure 23.a. The indicated damage is a concentrated strain region as high as 2% at 1000 psig. Failure at elevated pressure originated at this point.

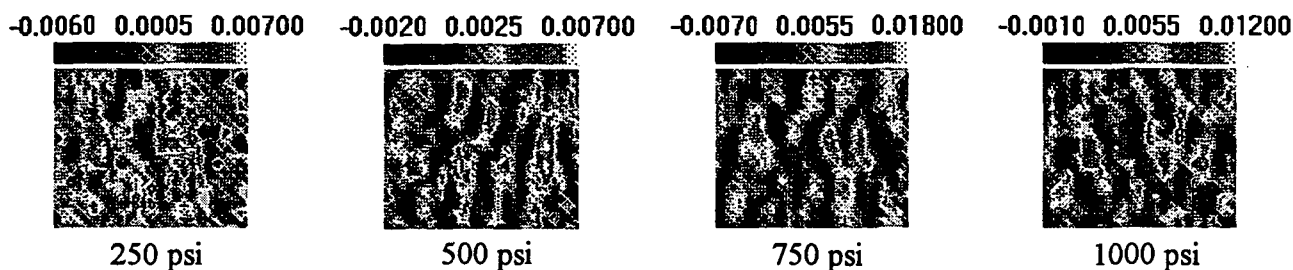


Figure 21.a. SDVIC Hoop Strain Measurements for No Impact  
(Bottle No. A003-004, Resin 3501-6 ATL)

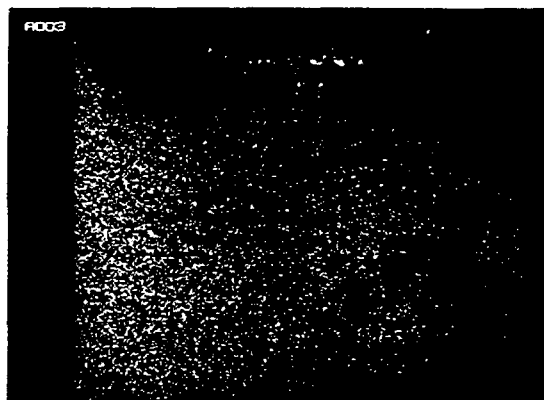
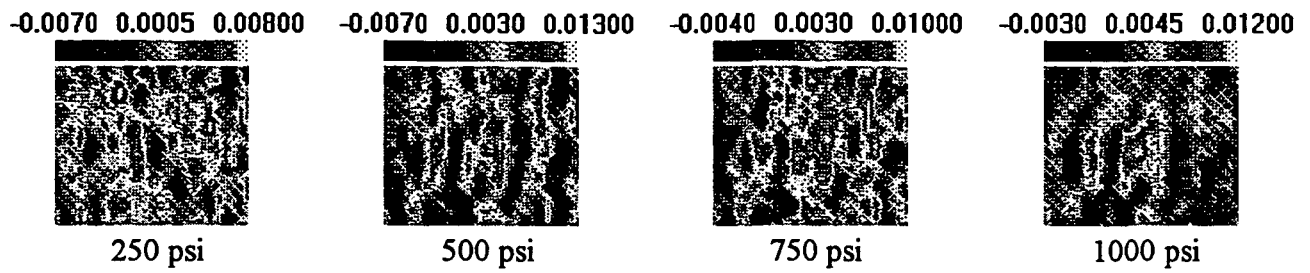
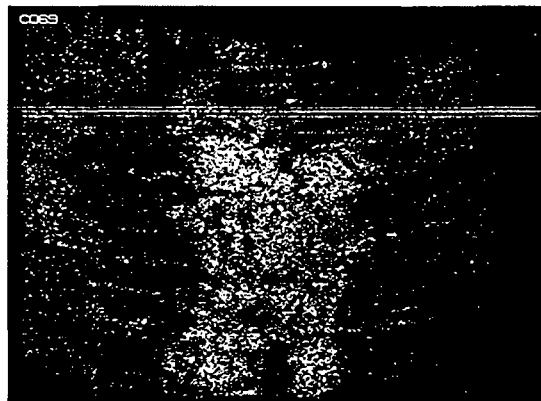


Figure 21.b. Static Shearogram for No Impact  
(Bottle No. A003-004, Resin 3501-6 ATL)

The more highly localized fiber breakage and matrix cracking caused by the sharp tipped impacts, however, did significantly concentrate the stress and strain in the damage effected zone and are readily apparent in most cases as low as 250 psig, about 6% of the expected burst pressure for the undamaged bottles. The strain fields indicate a region of intensified strain which grew larger in both size and strain magnitude with increasing pressure. In general, the ultimate failure of each FWPV was observed to have originated as the failure of hoop fiber bundles, or tows, with the same location and geometry as the hoop strain indication.



**Figure 22.a.** SDVIC Hoop Strain Measurements for a Blunt Tip Low Energy Impact  
(Bottle No. C069-070, Resin 3501-6 ATL)



**Figure 22.b.** Static Shearogram for a Blunt Tip Low Energy Impact  
(Bottle No. C069-070, Resin 3501-6 ATL)

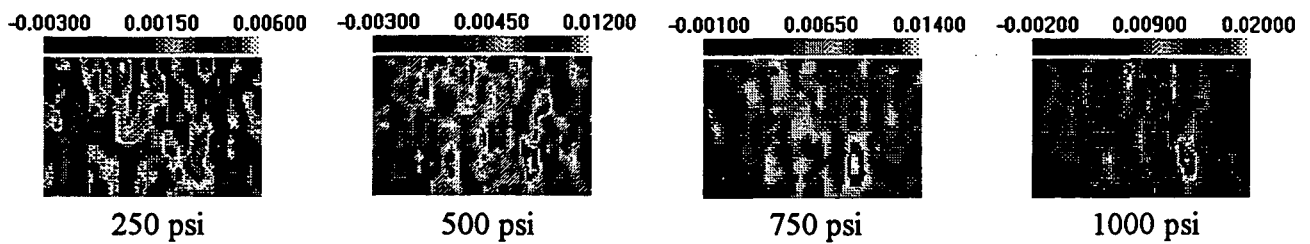


**Figure 23.a.** SDVIC Hoop Strain Measurements for a Blunt Tip High Energy Impact  
(Bottle No. A047-048, Resin X8553-45)

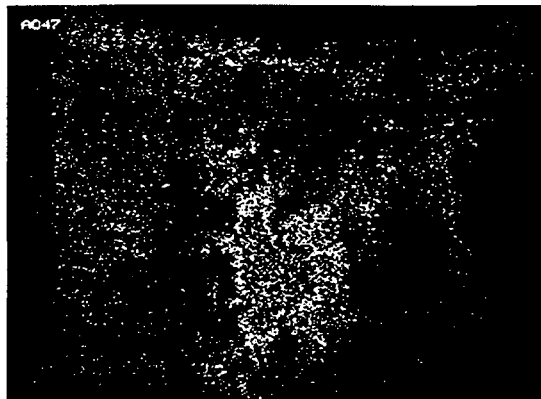


**Figure 23.b.** Static Shearogram for a Blunt Tip High Energy Impact  
(Bottle No. A047-048, Resin X8553-45)

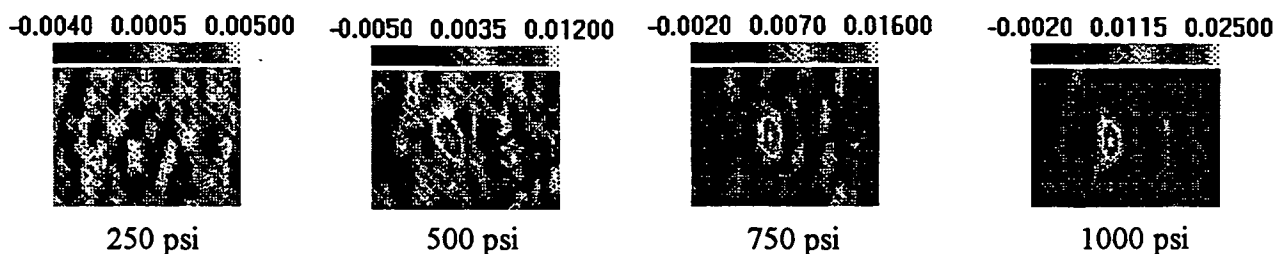


**Figure 24.a.** SDVIC Hoop Strain Measurements for a Sharp Tip Low Energy Impact  
(Bottle No. A013-014, Resin X8553-45)

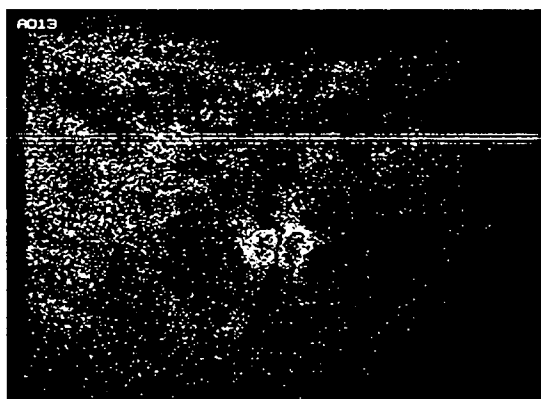


**Figure 24.b.** SDVIC Hoop Strain Measurements for a Sharp Tip Low Energy Impact  
(Bottle No. A013-014, Resin X8553-45)

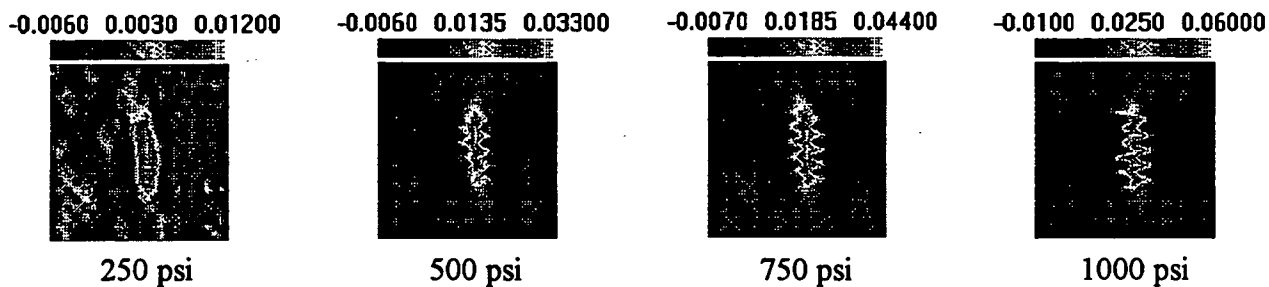


**Figure 25.a.** SDVIC Hoop Strain Measurements for a Sharp Tip High Energy Impact  
(Bottle No. C093-094, Resin X8553-45)

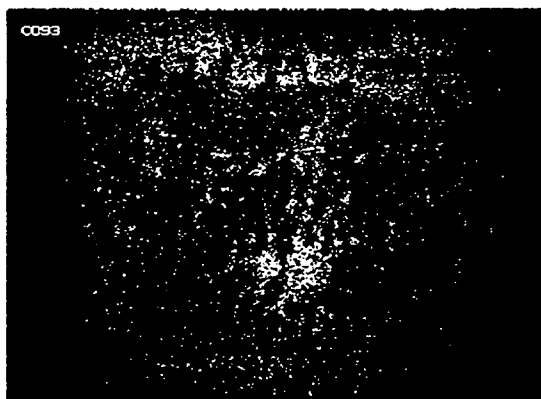


**Figure 25.b.** SDVIC Hoop Strain Measurements for a Sharp Tip High Energy Impact  
(Bottle No. C093-094, Resin X8553-45)



Among FWPV of the same resin class, the observed strain magnitude and the size of the strain concentrated region was larger at each pressure interval for the high energy sharp tip impact bottle than for the low energy sharp tip impact bottle, as illustrated in Figures 24.a. and 25.a.

In the case of the high energy impact with a sharp tip, Figure 25.a., a linear vertical strain concentrated region is clearly indicated, with much higher strains than the previous examples, up to 6%. The only visible damage at this pressure was the original indentation. The first indication of eminent failure was the appearance of a visible vertical crack at elevated pressure in the final ramp to burst. The geometry of the localized region of high strain closely resembled the geometry of the first graphite tow failures. Before any damage propagation was visible to the unaided observer, SDVIC predicted the location and nature of the initial tow failures.

#### 4.3.2. NEURAL NETWORK BURST PRESSURE PREDICTION

During burst testing of these FWPV, James Walker of the UAH Center for Automation and Robotics collected acoustic emission (AE) data for burst pressure prediction.<sup>[3,4]</sup> The AE amplitude distributions were supplied as input to a back propagation neural network (BPNN), which was trained on the data from a few FWPV and tested on the remainder. For the filled Gr-Ep FWPV, the burst pressures were estimated with an average error of 1.9%.

This success inspired development of a similar technique for use with SDVIC strain fields. However, the dissimilarities in the type of data required that some technique be found to preprocess the SDVIC data, resulting in a reduced data set of a form applicable to neural network analysis. Unfortunately, this technique was not found until most of the bottles had been burst and it required a modification in the SDVIC data acquisition.

The AE data used for BPNN analysis was in the form of a histogram, and the height of each category bar was input to a single neuron. This required as many input neurons as there were histogram categories or bars. A typical AE BPNN used 41 input neurons. In the case of SDVIC analysis, strain values are determined for a grid array of points on the bottle surface with sizes typically of 15,000 points or more. A direct input of this strain field into a BPNN would require an equal number of input neurons and would result in prohibitively time consuming analysis.

To overcome this problem, the VICNet Neural Network Interface software was developed. This program reduces the strain field data file to a histogram such as those shown in Figure 26. for two bottles with burst pressures of 2597 and 1701 psig.

In general, those FWPV with lower burst pressures tend to have a lower and wider strain distribution than those with higher burst pressures. In this form the SDVIC data may be input to a BPNN to produce a quantitative means for predicting burst pressure based upon SDVIC hoop strain measurements. Each input neuron may be assigned a strain category and assigned the number of SDVIC data points having strain values in that category. As the strain is related to FWPV failure by material properties more strongly than minor geometry differences, this technique may be capable of predicting the failure

strength of actual full scale rocket motor cases and storage vessels based upon training data obtained from smaller, less expensive specimens.

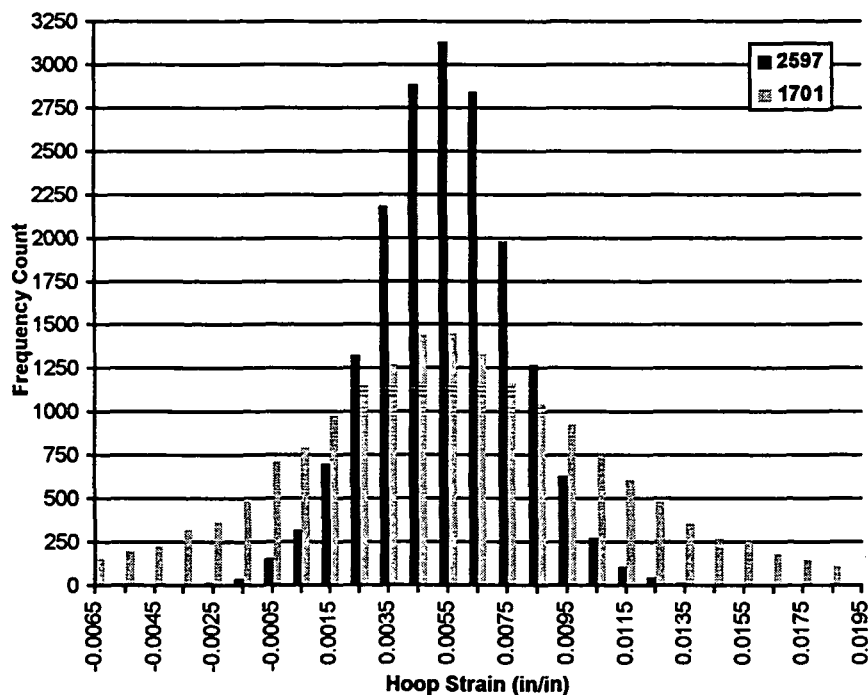


Figure 26. SDVIC Hoop Strain Histograms Generated by VICNet.

#### 4.4. SUMMARY

Electronic Shearography inspections provided a non-contact computer vision holography method of locating and sizing internal delaminations in impact damaged filament wound pressure vessels with a single low level thermal cycle. The character of the indications suggested whether those delaminations were limited to a few plies or effected a greater thickness of the material. The shape and size of indication correlated well with the type of impact.

Sub-pixel Digital Video Image Correlation provided a non-contact computer vision method of characterizing and predicting the propagation of impact induced fiber breakage and matrix cracking in filament wound pressure vessels with internal pressurization less than 25% of the manufacturer's predicted burst pressure. Full-field measurements of displacements and strains were made by SDVIC in near-real-time and displayed in an easily interpreted graphical form. The technique allowed the visualization of deformation measurements with sub-pixel resolution.

Neural network analysis based upon SDVIC measurements is now possible and may lead to a burst pressure prediction method which may be useful in inexpensively determining the remaining life of impact damaged flight articles such as solid rocket motor cases or storage vessels.

## 5. SPACE SHUTTLE EXTERNAL TANK

### 5.1 COMPOSITE NOSE CONE

MSFC is currently developing a composite nose cone proposed for use on the Space Shuttle external fuel tank. The graphite-phenolic (Gr-Ph) design provides a considerable weight reduction compared to the current aluminum structure and elimination of spray-on thermal protection system insulation. However, since the nose cone will be exposed to supersonic airflow during flight, the design must be aerodynamically as well as structurally sound. The presence of fastener holes in the external tank composite nose cone (ET-CNC) introduces the possibility of damage caused during their machining. The use of flat headed bolts assists in the design aerodynamics but necessitates that the fastener holes take on a conical geometry, which increases the possibility for service load induced damage. Additionally, the composite design introduces the possibility for the existence of serious delaminations within the material which may not be visible to the unaided observer. The capability of the Electronic Shearography for detection of internal delaminations, for assessment of machining induced fastener hole damage, and for assessment of load induced damage to conical fastener holes in the STS ET-CNC material systems has been demonstrated.

The PW EH/SIS was used to evaluate the response of each ET-CNC material specimen to thermal excitation. The telephoto lens was focused on each region of interest individually. Static shearograms were obtained using speckle averaging and four frame averaging. No traveling fringes were displayed. A reference shearogram was obtained after the test article had been slightly heated ( $\Delta T < 5^{\circ}\text{F}$ ) with an industrial heat gun. The deformed shearogram was taken after the specimen had cooled to approximately room temperature.

#### 5.1.1. INTERNAL DELAMINATIONS

The Nondestructive Evaluation Branch (EH13) was provided a Gr-Ph nose cone section containing three 1" square Teflon inserts. Located at increasing depths inside the nose cone wall, each insert simulates a material debond of equivalent size. The image shearing distance was set to 0.25 inches at a lens-to-object distance of 4 feet. The general vicinity but not the specific location of each insert was inspected until sufficient indication was given to locate the debonds.

Figure 27. indicates the response of an insert close to the material surface with the convex surface of the nose cone facing the shearography apparatus. The symmetric dark and light triangles in the center of the shearogram correctly indicate the size, shape, and orientation of the near-surface delamination. The boundary between the dark and light regions is approximately normal to the direction of image shear. The mottled gray region enclosing the debond indication and filling the lower left portion of the figure is the surface of the nose cone section. The lighter region above and to the right of this is the background behind the specimen. Although the debond closest to the front surface was detectable whether the concave or convex surface was facing the shearography device, inspections failed to detect the inserts at the mid-plane and near the surface away from the shearography device.

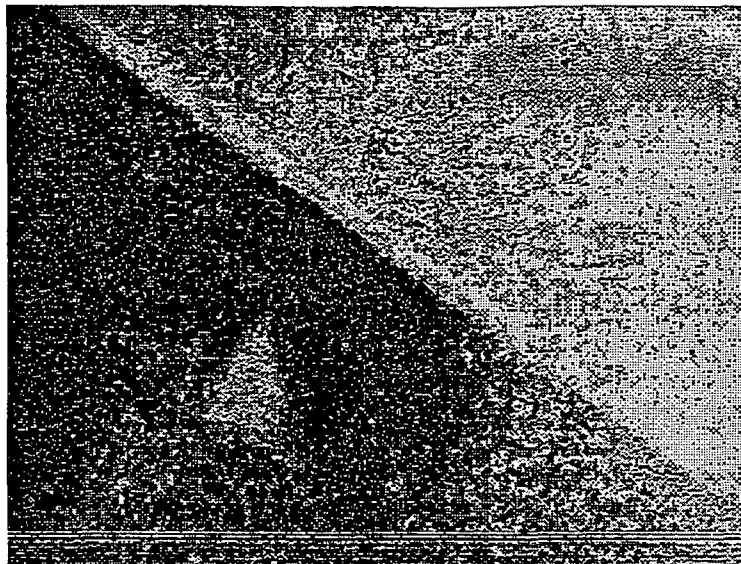


Figure 27. (N) Indication of a Simulated Delamination

### 5.1.2. FASTENER HOLES

The use of metallic bolts to fasten the ET-CNC to the internal structure requires characterization of machining and load induced damage around fastener holes of various proposed geometries. The capability of electronic shearography to detect such damage has been demonstrated.

#### 5.1.2.1. MACHINING DAMAGE TO CYLINDRICAL HOLES

The MSFC NDE Branch was provided a Gr-Ph coupon containing four drilled holes. The geometry of this specimen is shown in Figure 28. The specimen is 6" x 6" x 1/4" thick and curved to the same radius as the ET-CNC. A 1/4" hole has been drilled in each corner. The image shearing distance was set to 0.3" at a lens-to-object distance of 4.5". The telephoto lens was focused on each hole individually at maximum zoom.

For this experiment, the sensitivity has been adjusted such that the small motion of the undamaged part produces a dark zero-order fringe, while the greater motion of the damaged regions produces bright one-half-order and greater fringes. Electronic shearograms of two machined holes appear in

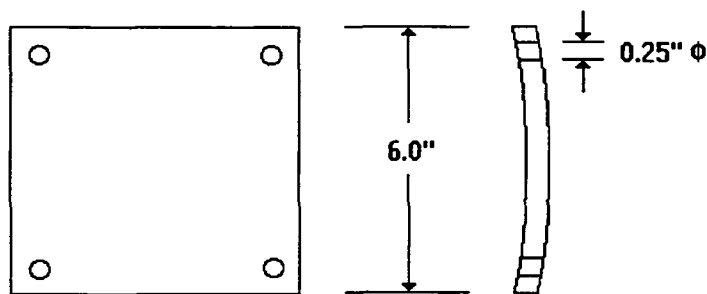


Figure 28. Gr-Ph ET-CNC Coupon with Machined Holes

Figures 28. and 30. Each image contains the appearance of each hole twice due to an image shearing distance 0.05 inches greater than the diameter of the holes.

Figure 29. is a shearogram of a hole with no damage visible to the unaided observer. However, the shearogram indicates a damaged region with a diameter of 0.290 inches. That is, the damage extends radially 0.02 inches beyond the drilled hole.

Figure 30. is a shearogram of a hole with visible machining damage in the form of frayed material inside the hole at the surface. The shearogram also indicates a damaged region with a diameter of 0.485 inches. That is, the damage extends radially 0.118 inches beyond the drilled hole. The latter damage is not visible to the unaided observer, but extends to almost twice the diameter of the intended hole.

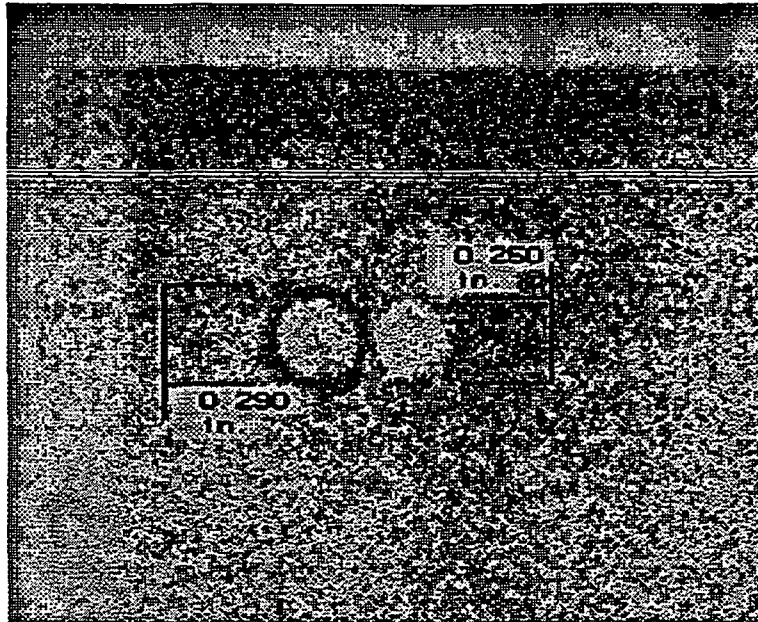


Figure 29. (N) Electronic Shearogram of Machined Hole with No Visible Damage

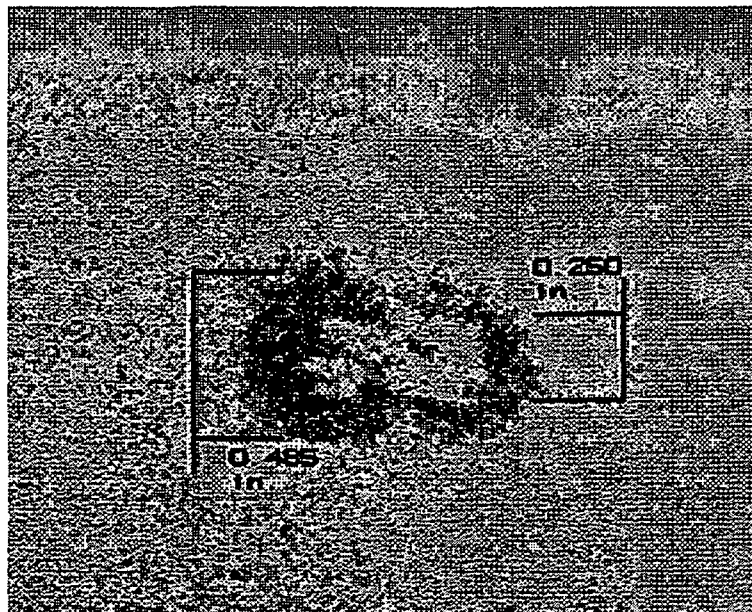
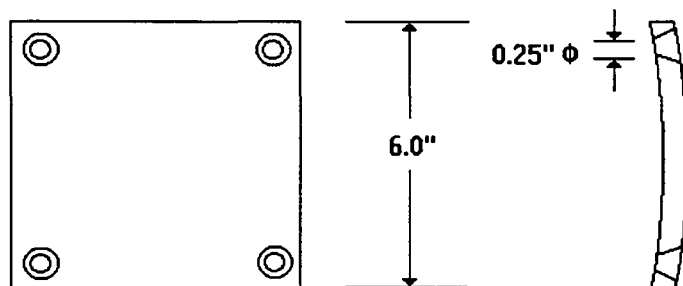


Figure 30. (N) Electronic Shearogram of Machined Hole with Visible Damage

### 5.1.2.2. MACHINING DAMAGE TO CONICAL HOLES

The MSFC NDE Branch was provided a Gr-Ph coupon containing four drilled holes tapered to accommodate flat-headed fasteners. The geometry of this specimen is shown in Figure 31. The specimen is 6"  $\times$  6"  $\times$  1/4" thick and curved to the same radius as the ET-CNC. A 0.25 in. ID conical hole has been drilled in each corner. The image shearing distance was set to 0.063 inches at a lens-to-object distance of 4.5 feet.



**Figure 31.** Gr-Ph ET-CNC Coupon with Conical Holes

For this experiment, the sensitivity has been adjusted such that the small motion of the undamaged part produces a dark zero-order fringe, while the greater motion of the damaged regions produces bright one-half-order and greater fringes. An electronic shearogram of these machined holes appears in Figure 32.

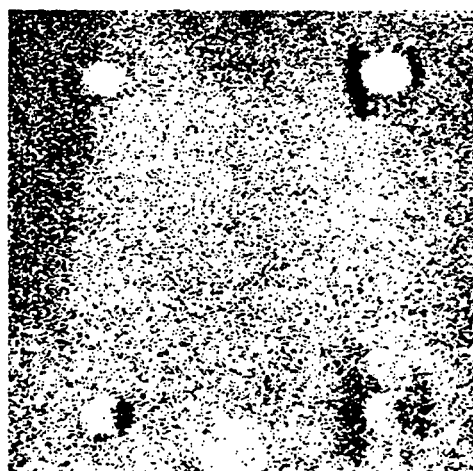


**Figure 32.** (N) Machining damage in conical fastener holes.

### 5.1.2.3. LOAD INDUCED DAMAGE TO CONICAL HOLES

The MSFC NDE Branch was provided a Gr-Ph coupon containing three conical holes. The geometry of this specimen is shown in Figure 33. A bolt in each hole was used to apply load, as illustrated in Figure 34. Tension was applied such that the coupon and the bolts were pulled in opposite directions. The direct bearing load between the metal

fastener and the Gr-Ph coupon caused visible damage inside the conical shaped holes. The image shearing distance was set to 0.13 inches at a lens-to-object distance of 4 feet. The telephoto lens was focused on each hole individually.

For this experiment, like the previous one, the sensitivity has been adjusted such that the small motion of the undamaged part produces a dark zero-order fringe, while the greater motion of the damaged regions produces bright one-half-order and greater fringes. Electronic shearograms of the three machined holes appear in Figures 35., 36., and 37. The appearance of each hole is elongated somewhat horizontally due to image shearing in that direction. However, the material was loaded in the vertical direction and, as there is no vertical shear, measurements of the extent of the damage may be made in this direction.

The shearograms of all three holes feature bright crescent shaped indications above the holes. This is the side against which the bearing load was applied by the bolts and upon which damage was observed visually.

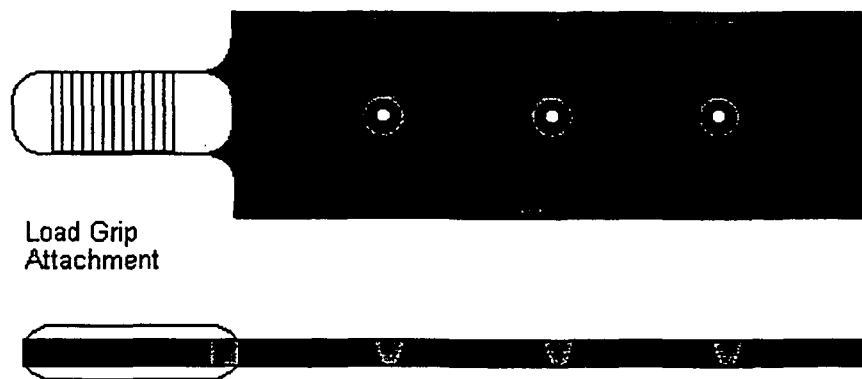


Figure 33. Specimen Geometry

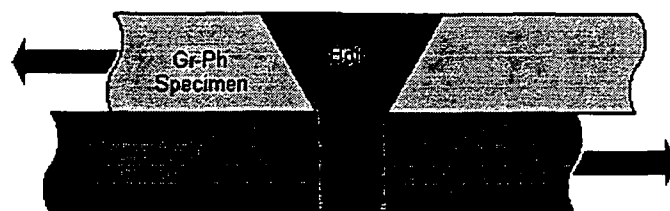
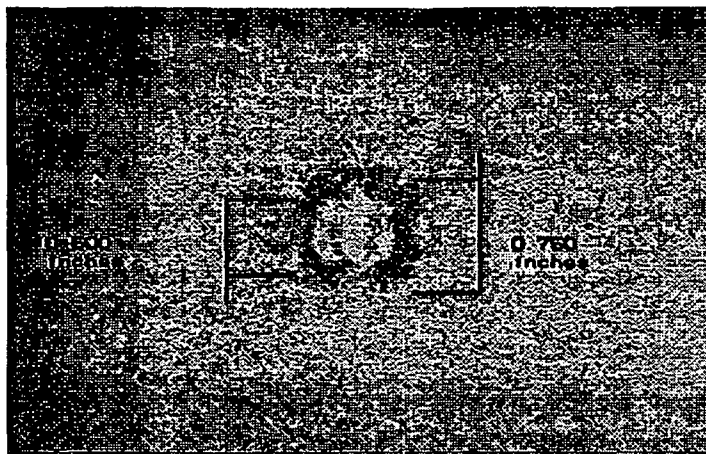
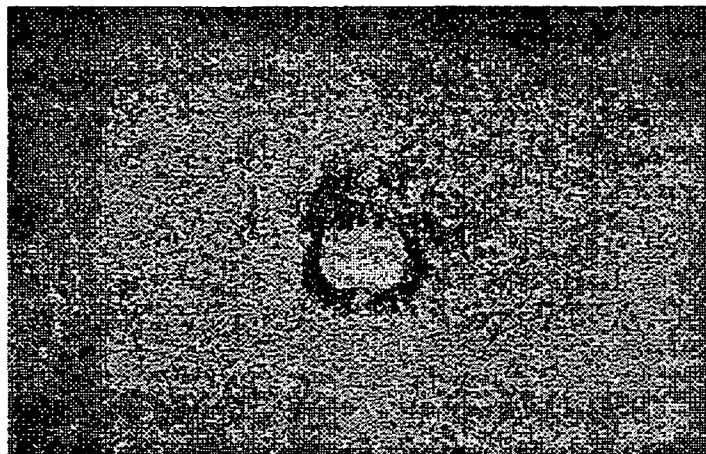


Figure 34. Bolt Loading Arrangement



**Figure 35. (N) Electronic Shearogram of Conical Hole Nearest to Load Grip.**



**Figure 36. (N) Electronic Shearogram of Middle Conical Hole.**

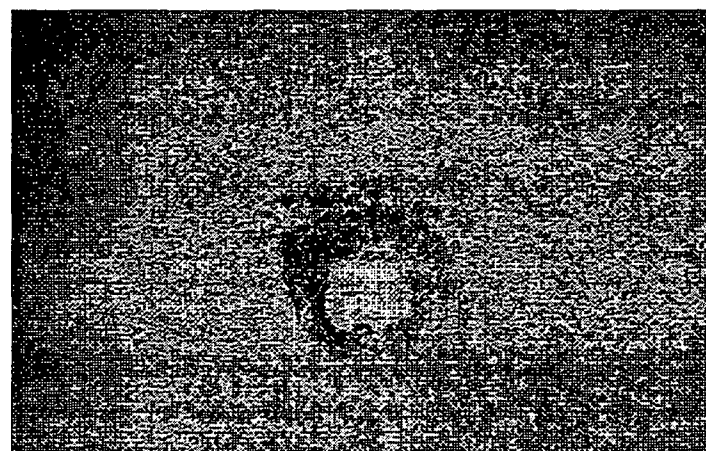


**Figure 37. (N) Electronic Shearogram of Conical Hole Farthest from Load Grip.**



#### 5.1.2.4. SUMMARY

It has been demonstrated that electronic shearography is capable of detecting near-surface delaminations in Gr-Ph composite materials. Inspections may be performed for both the concave and convex surfaces of the nose cone. However, debonds near the mid-plane of the nose cone wall may not be detected.

It has been demonstrated that electronic shearography is capable of assessing the extent of damage induced during the machining of Gr-Ph composite materials. While most machining operations introduce some localized damage, determination of the degree to which this has occurred may be made quickly and easily based upon the indication size

It has been demonstrated that electronic shearography is capable of assessing the extent of damage induced during the loading of conical fastener holes in Gr-Ph composite materials. The indicated damage lies outside the conic section of the holes. Electronic shearography thus provides a non-contact technique for nondestructively evaluating load induced damage around these holes without removing the fastener.

#### 5.2. LIQUID OXYGEN FEED LINE FAIRING

This fairing covers the junction between the space shuttle external tank and the liquid oxygen feed line which supplies the space shuttle main engines (SSME). It is constructed as a graphite-polyimide (Gr-Pim) composite. The possibility exists that delaminations could form as a result of exposure to the heat and stress created during atmospheric flight. To simulate this, a hot gas stream was blown across a curved Gr-Pim coupon. Two delaminations were subsequently visible along the same edge of the specimen at different depths; one close to the outer surface and one closer to the mid plane than the inner surface. Ultrasonic testing (UT) conducted by Mike Suits and Jeff Leak of the NDE branch resulted in a large indication along that edge and extending into the heart of the acreage of the coupon. This UT indication was the cumulative effect of all delaminations, and it was indeterminate how much of the indication was produced by each of the delaminations visible on edge. It was also unknown whether the indications were influenced by internal flaws which were not visible on edge.

An ES inspection was conducted for this specimen with radiant thermal excitation. Two 500 Watt Halogen bulbs were directed toward the specimen surface for five minutes. Static shearograms were recorded as the specimen cooled and the excited delaminations relaxed. As shown in Figures 38. and 39., a large circular delamination extending to the edge was detected near the outer surface of the specimen and no delaminations were detected near the outer surface. Based upon these inspections, it is concluded that the portion of the UT indication along the specimen edge corresponds to the visible delamination near the mid plane which was not detected with ES. The portion of the UT indication which extends into the acreage of the coupon corresponds to the circular ES indication and the visible delamination near the outer surface of the material. There is nothing to suggest that any other delaminations of the same magnitude are present in the coupon.

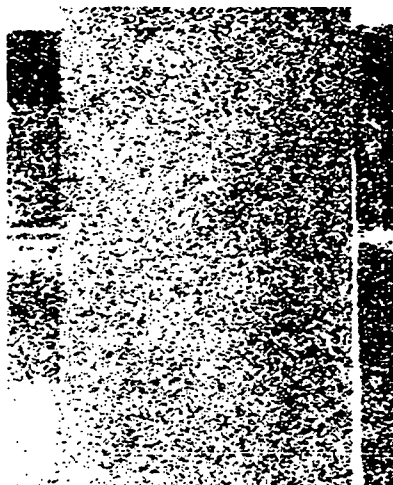


**Figure 38.** (N) No delaminations detected from inner surface.



**Figure 39.** (N) Large delamination detected from outer surface.

## 6. PEGASUS FAIRING THERMAL PROTECTION SYSTEM

The Pegasus launch vehicle is a multiple stage rocket manufactured by Orbital Science Corporation (OSC). Originally, the Pegasus and its payload of up to five satellites were carried to an initial altitude and then launched from beneath the wing of an Air Force B-52. OSC subsequently purchased a Lockheed L-1011 and outfitted it such that Pegasus rockets could be carried to altitude and launched from beneath the belly of the aircraft. Such a launch attempt in March of 1995 was aborted prior to release of the Pegasus when the Thermolag T230 thermal protection system (TPS) peeled off of the rocket's nose cone. The TPS is a thin layer of material designed to insulate the satellites inside the nose cone from the frictional heating on the outer surface of the rocket while it is accelerating through the atmosphere. The fairing shell, composed of graphite epoxy composite skins over an aluminum honeycomb core, may also be subject to thermal damage without the presence of the TPS. The L-1011 landed with the Pegasus still attached. Two of the satellites aboard the aborted launch vehicle were the NASA Orbital Transient Detector, an atmospheric lightning tracking device with development and operation managed by MSFC, and the ORBCOMM communications satellite, for which the vehicle was named.

Three engineers from MSFC, Sam Russell (Non-Destructive Evaluation Branch), Mike Prince (Polymers and Composites Branch), and Floyd Roberts (Ceramics and Coatings Branch), traveled to OSC's Pegasus assembly facility in Phoenix, Arizona to assist in the evaluation of the TPS problems. The NDE Branch shipped to OSC their Laser Technology, Inc. (LTI) electronic shearography device by next day air freight for evaluation of the TPS bond line integrity before and after repair attempts. The NASA engineers were accompanied by a UAH Research Associate to study the application of electronic shearography in an actual service environment, as well as to assist in the development of techniques for inspection of the Pegasus TPS and training of OSC personnel in the operation of the shearography apparatus.

After the remaining TPS was stripped from the nose cone, it was replaced with an inner layer of cork and an outer layer of RTV. Other areas were repaired by injecting adhesive beneath the unbonded Thermolag. ES inspections were conducted over the

majority of the surface of each fairing before and after these repairs. The repaired ORBCOMM Pegasus was launched successfully on 3 April 1995.

## 6.1. PROCEDURE

The Pegasus fairing consists of a right and left half with the nose cone attached to the left side. The nose cone is quasi-hemispherical and attached to the cylindrical section by a short frustum as shown in Figure 40. During inspection the fairings were supported from the inside on a wheeled cart. In this position, the actual side of the fairing appears to be the top. The two halves of the fairing are bound with steel bands during launch and there are two black rings around the fairing which are bare of TPS to accommodate these straps. The optical head, containing the laser illumination source and the optics and CCD camera for image acquisition, was positioned on its tripod approximately 3 to 6 feet from the fairing. The apparatus is visible in the left portion of Figure 40., and the laser illumination is apparent as a bright circle on the side of the fairing at the aft retaining band ring. ES inspections were not possible for a region approximately two feet wide and extending from approximately two feet behind the nose cone to approximately two feet ahead of the aft edge because the tripod did not provide sufficient elevation.



**Figure 40.** Electronic Shearography inspection of ORBCOMM Pegasus fairing at OSC manufacturing facility in Phoenix, Arizona.

Inspections were conducted with convective thermal excitation provided by an industrial heat gun. The heated delaminations expanded in a curved fashion away from the surrounding bonded regions due to the constraint provided there. Reference images were acquired while the region was still warm and these were processed with subsequent images after the region had cooled. The cooled delaminations had relaxed back toward their original shape, and the change in surface contour during this relaxation appears in the shearograms as bright fringes.

## 6.2. ORBCOMM

The location of each unbond detected on the ORBCOMM fairing is indicated in Figures 41. through 43. Each indication is shown and discussed individually in Figures 44. through 53.

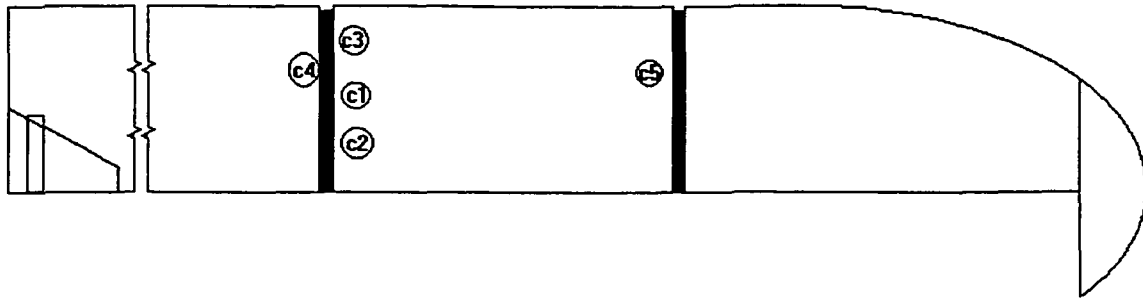


Figure 41. Left Fairing/Top Side

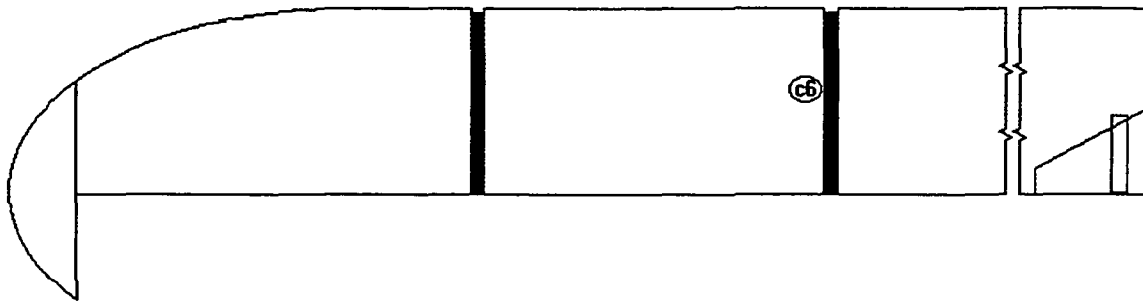


Figure 42. Left Fairing/Bottom Side

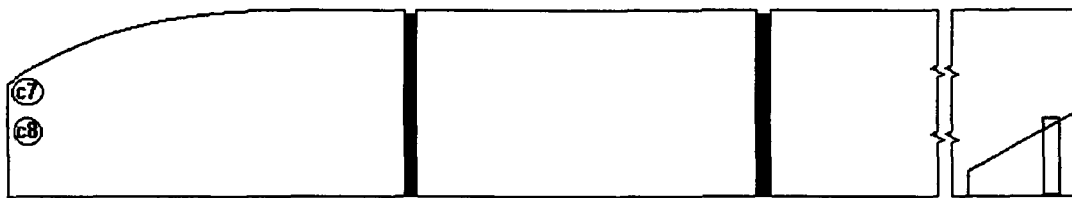
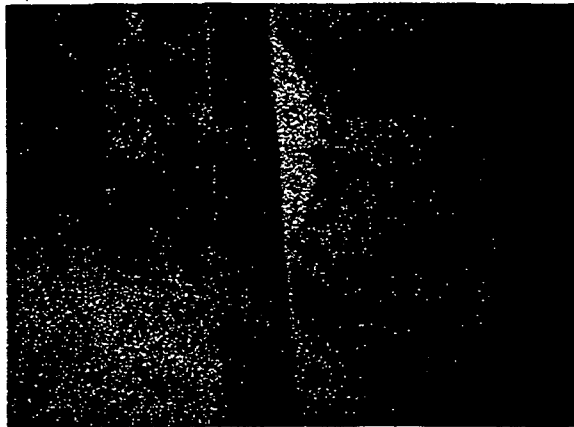


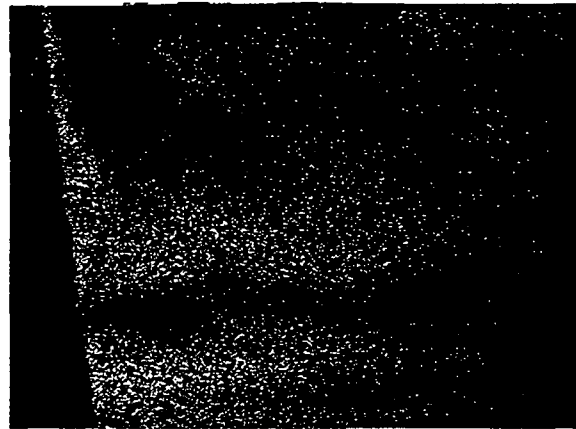
Figure 43. Right Fairing/Top Side



Figure 44. Glued joint filler indications in cork nose cone repair.



**Figure 45.** Indication C1.



**Figure 46.** Indication C2.

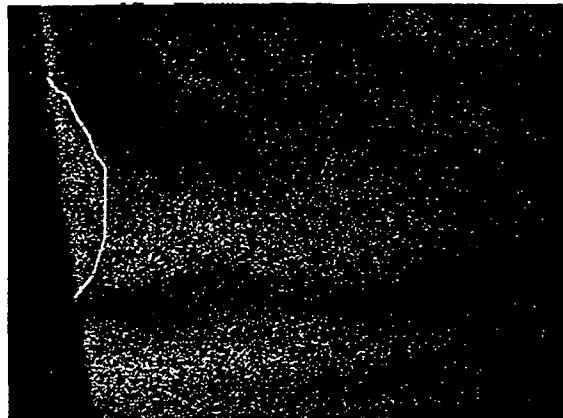


**Figure 47.** Indication C2 outlined for clarity.

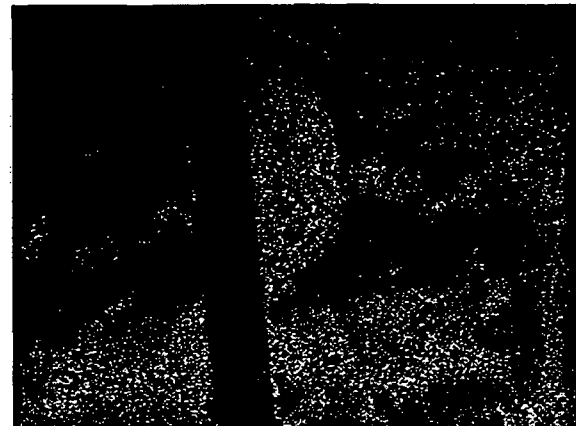


**Figure 49.** Indications C3 and C4.

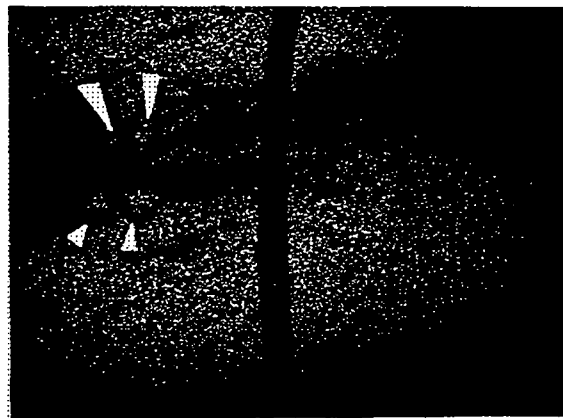


**Figure 50.** Indication C5, four circular test plugs through the composite beneath TPS.



**Figure 51.** Indication C6.

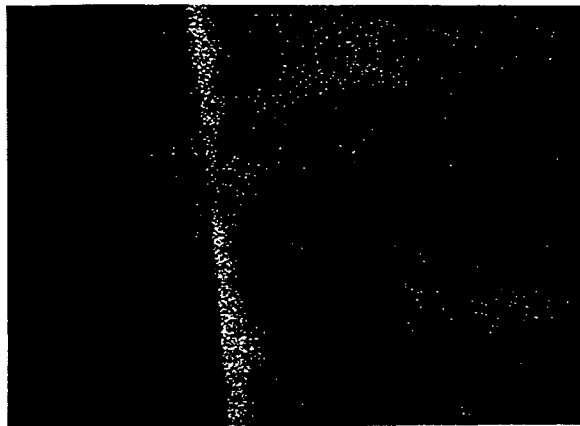


**Figure 52.** Indications C7 and C8, prior to repair.



**Figure 53.** Indications C7 and C8, following repair.

### 6.3. SEASTAR

At the same time that the ORBCOMM Pegasus fairing was being repaired, another fairing was being manufactured for use in the upcoming SEASTAR launch. This second fairing was also inspected, and numerous unbonds were detected. The location of each unbond detected on the SEASTAR fairing is indicated in Figures 54. through 57. Each indication is shown and discussed individually in Figures 58. through 71.

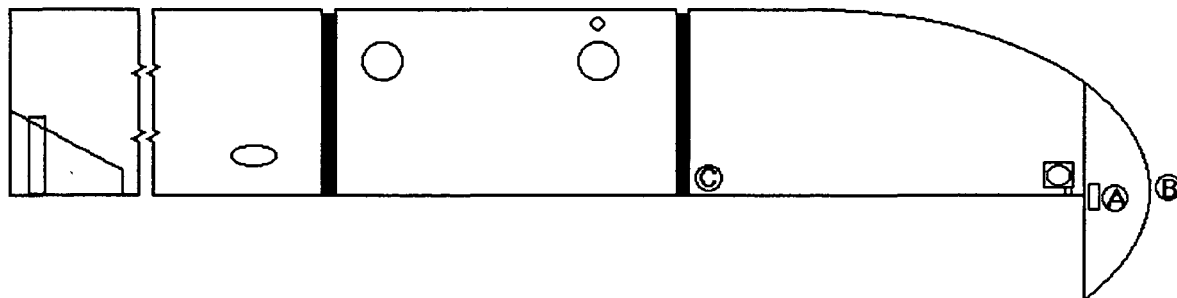


**Figure 54.** Left Fairing/Top Side

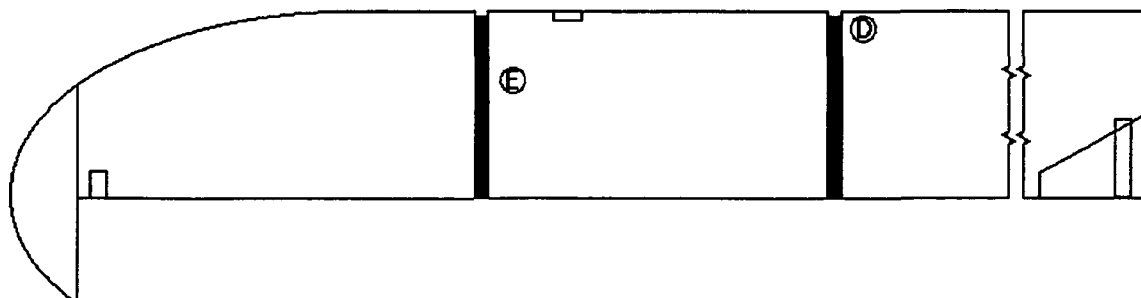


**Figure 55.** Left Fairing/Bottom Side

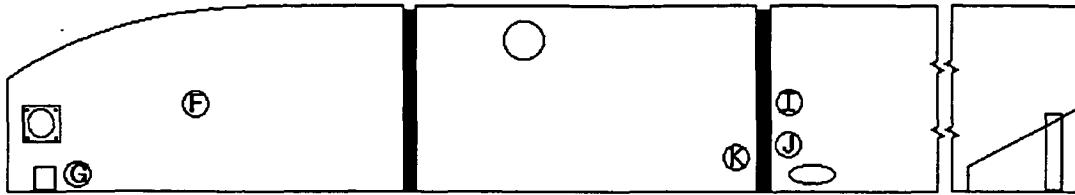


Figure 56. Right Fairing/Top Side

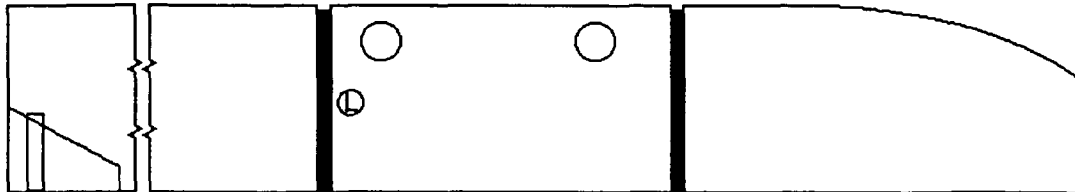


Figure 57. Right Fairing/Bottom Side

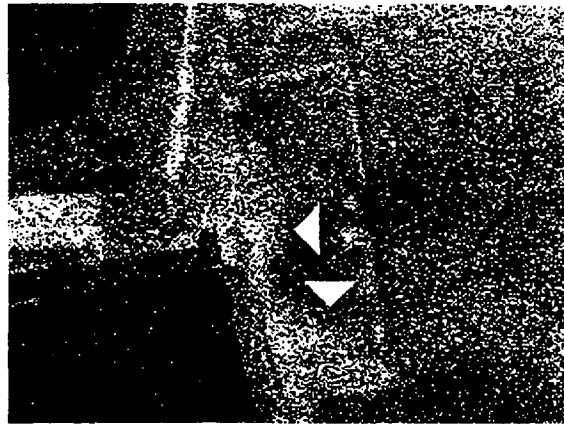


Figure 58. Indication A, unbonds along the edge of a rectangular cork insert adjacent to a square and a circular cutout.

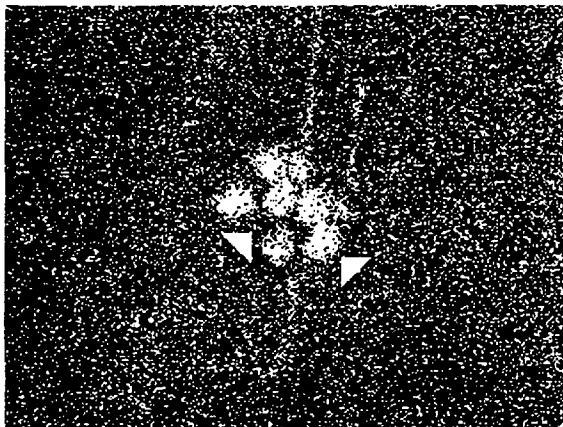


Figure 59. Indication B, diagonally sheared.

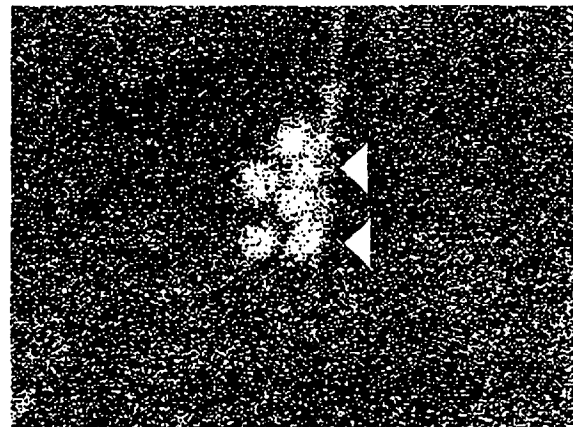


Figure 60. Indication B, vertically sheared.

This indication is that of three separate anomalies, each of which appears twice due to image shearing. In each of these two figures, the two spots with pointers are dual images of the same anomaly. This was later learned to be a glob of RTV used to position a thermocouple during curing. The other four indications in each figure are the dual images of two anomalies, holes drilled through the composite beneath the cork TPS.

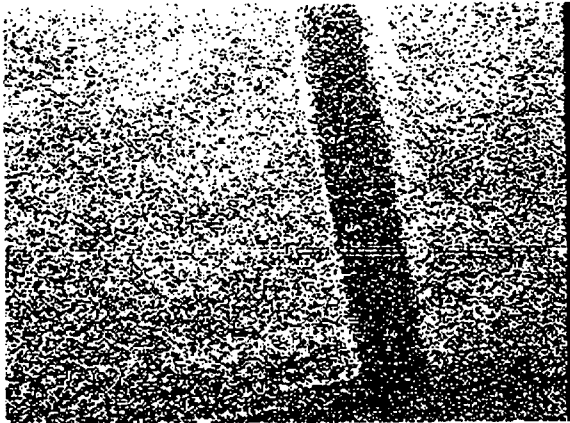


Figure 61. Indication C.

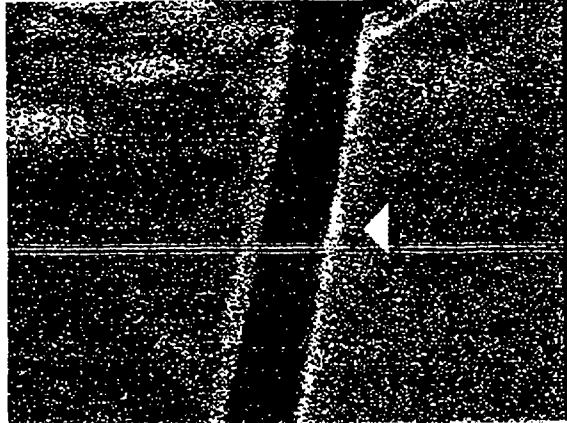


Figure 62. Indication D.

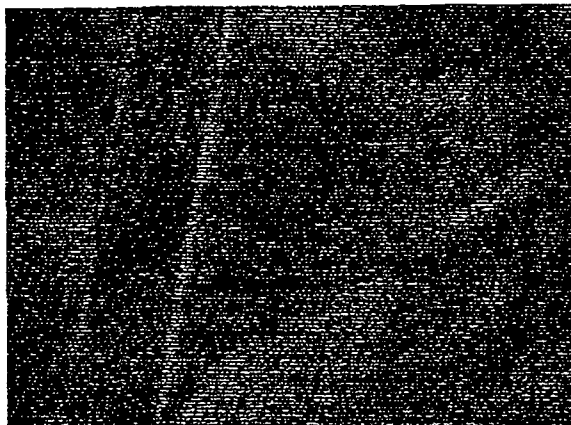


Figure 63. Indication E.

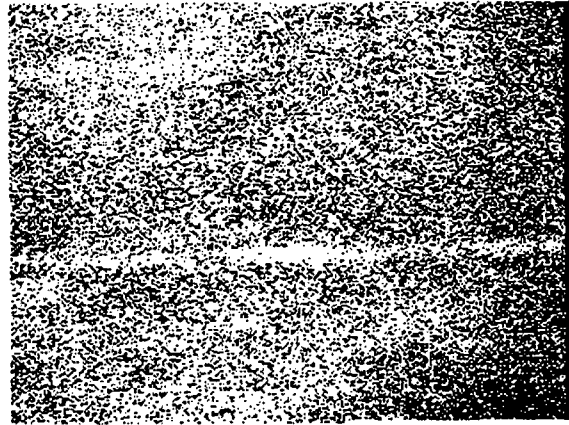


Figure 64. Indication F.

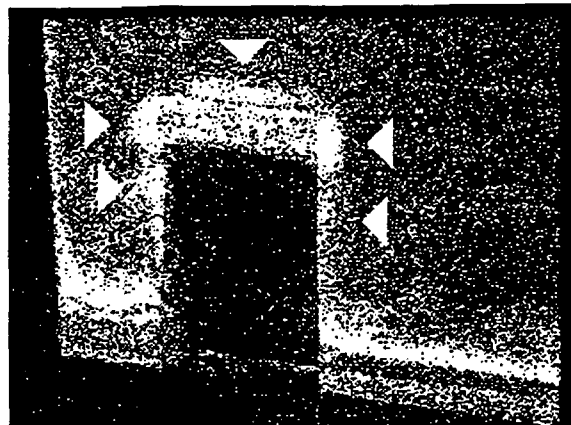


Figure 65. Indication G, vertical shear.

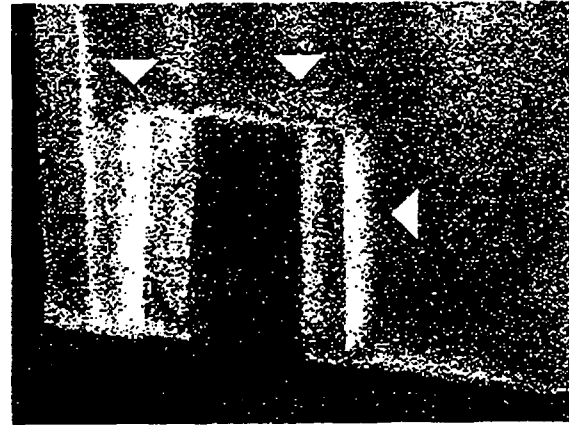


Figure 66. Indication G, horizontal shear.



Delaminations were indicated along all three edges of this cutout, as indicated by the pointers in the figures. Shearograms were recorded with both horizontal and vertical shearing vectors to separate the delamination indications from edge effects.



**Figure 67.** Indication H, low heat.

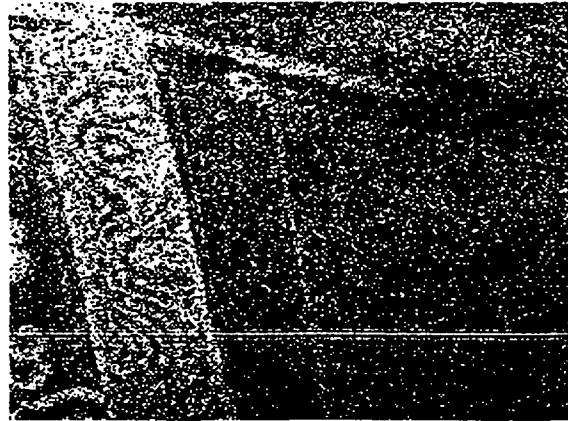


**Figure 68.** Indication H, high heat.

These indications were obtained from a section of cork which had been positioned with tape but not yet bonded. This simulated delamination was used to develop inspection procedures for other regions. Heating the region longer with the heat gun produced more fringes, but reflected the same modal distortion as evidenced by the similar fringe pattern in both figures.

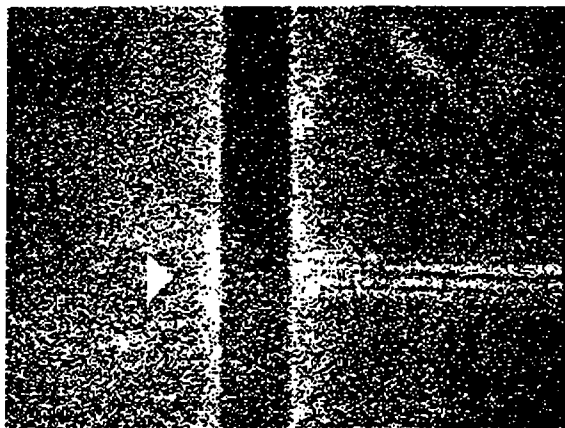


**Figure 69.** Indication I.

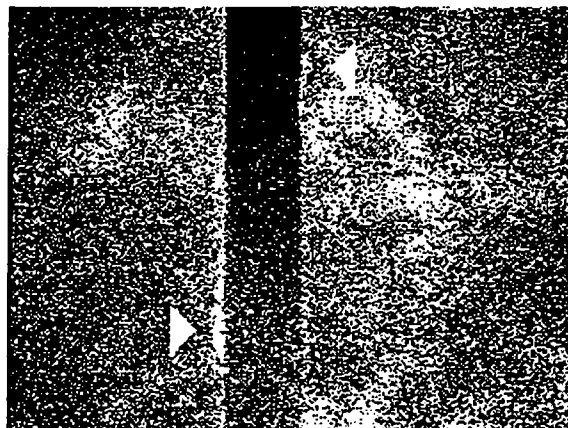


**Figure 70.** Indications J and K.

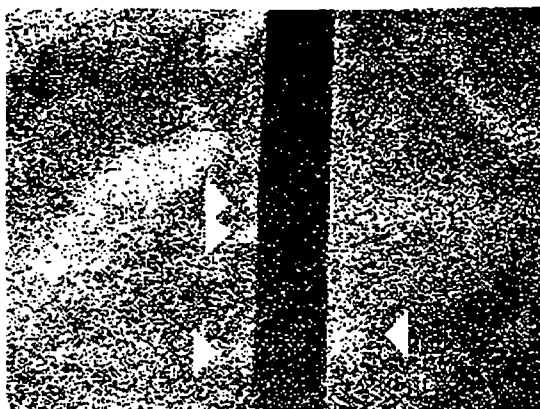


Figure 71. Indication L.

## 7. SOLAR X-RAY IMAGER TELESCOPE TUBE

The Solar X-ray Imager (SXI) telescope, to be incorporated into a Geostationary Operational Environment Satellite (GOES), utilizes a graphite-cyanate ester tube body. A cursory inspection was made of the ends of the tube to check for machining damage incurred during trimming of the cured lay-up. Inspections were performed with thermal excitation. The image shearing distance was adjusted to 1 inch with a field of view of 6 inches at an object distance of 5 feet. Figure 72. is typical of these inspection results, which indicated no significant flaws. Although a removable flat white coating is typically used for ES inspection of such dark and shiny surfaces as that of this tube, none was used in this instance due to the optical application of this flight article. Inspection reliability may have been compromised by glare and optical absorption, as well as the lack of procedural development.

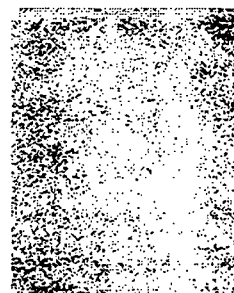


Figure 72. No significant flaws detected.

## 8. CRACK TIP STRESS INTENSITY FACTOR MEASUREMENT

### 8.1. CRACK TIP PLASTIC ZONE

The elevated stress state at the tip of a crack may cause the material in that region to yield although the material away from the crack tip remains elastic. The boundary between the plastic near field and elastic far field provides a boundary condition or constraint which may force the material in the near field to "dimple", or deform more in the thickness direction than the surrounding material. The degree to which the near field stress is elevated is often characterized in terms of a fracture mechanics parameter referred to as the stress intensity factor ( $K$ ). Several analytical forms have been found for the size and shape of this 3-D plastic zone, which compare with varying favor to experimental attempts at empirical measurement<sup>[13, p111-112; 18, p106-107]</sup>. Many of these experimental methods, such as replication, require data to be collected after the load has been removed from the specimen. In this case, the removal of the far field load induces compressive

residual forces which reduce the apparent size of the 3-D zone. Other techniques, such as moiré interferometry, are overly sensitive to environmental conditions, such as load frame motor vibration, and require extensive isolation.

A short feasibility study was conducted to determine the potential for measurement of  $K$  with shearography. A single edge notch (SEN) specimen was constructed as shown in Figure 73. from polycarbonate for Mode I, or opening mode, loading. The specimen was loaded at a displacement controlled rate of 0.005 inch per minute. The image shearing distance was adjusted to approximately 0.004 inch at an object distance of 3.5 feet.

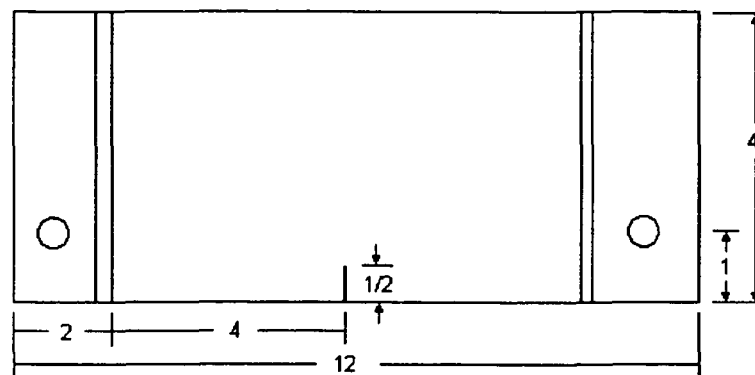


Figure 73. SEN specimen geometry, all dimensions in inches.

After an extension of 0.005 to 0.010 inches, the crosshead motion was stopped while static shearograms were acquired. The background vibration of the part and load relaxation due to creep during each hold, rather than interfering with shearography measurements, served as a source of motion for shearography measurements. That is, the vibration and relaxation caused the plastic zone to change shape between reference and subsequent images, thus indicating the reference size and shape of the 3-D zone. The 3-D zone was observed to increase in size as far field extension was increased and displayed an expected cardioid shape, as shown in Figures 74. through 79.

Image processing may be used to enhance the shearograms for determination of a closed form description of the plastic zone size and shape. An portion of an original shearogram is shown in Figure 80. Figure 81. contains the same shearogram after having been smoothed by the Blur utility from Adobe PhotoShop 4.0. Smoothing is necessitated by the speckle pattern superimposed upon the image by the nature of electronic shearography. By applying a threshold, or contrast enhancement, to the smoothed image, an outline of the detected 3-D zone may be obtained, as shown in Figure 82. A least squares regression may be utilized to fit a cardioid, as given by EQ.1., to the indicated boundary, and the solution used to predict  $K_I$ .

$$r = a(1 - \cos\theta)$$

< EQ.1. >

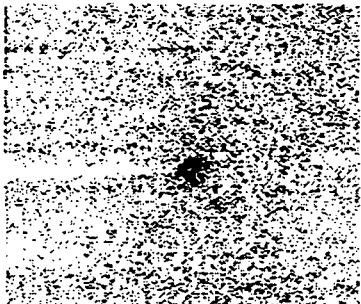


Figure 74. (N) 0.180 in. end displacement.

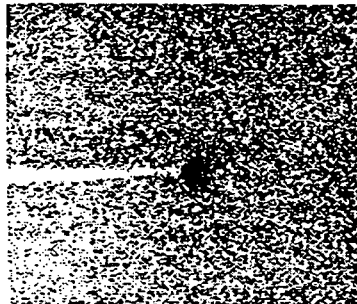


Figure 75. (N) 0.190 in. end displacement.

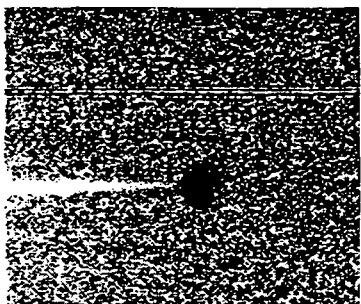


Figure 76. (N) 0.195 in. end displacement.

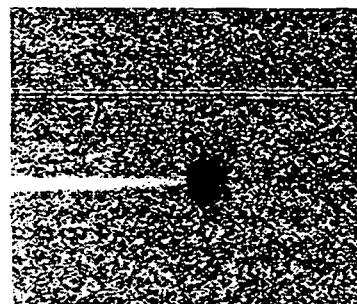


Figure 77. (N) 0.200 in. end displacement.

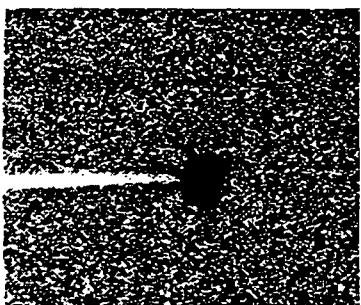


Figure 78. (N) 0.205 in. end displacement.

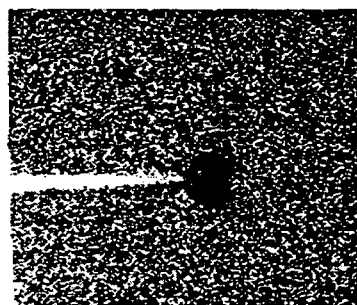


Figure 79. (N) 0.210 in. end displacement.

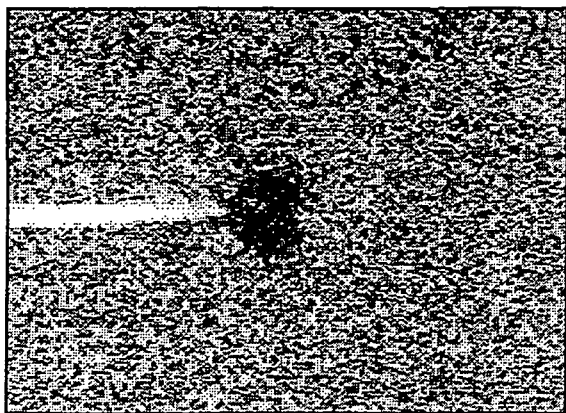


Figure 80. (N) Original Shearogram.

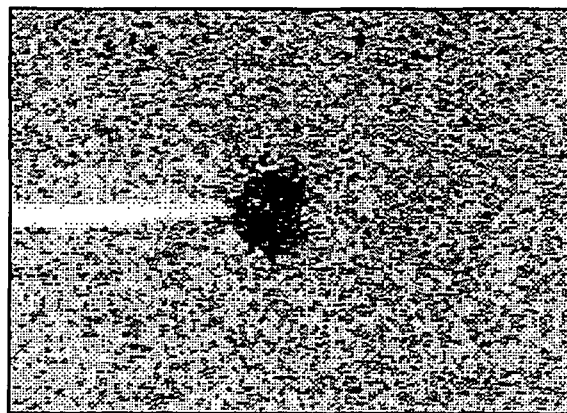


Figure 81. (N) Smoothed Shearogram.

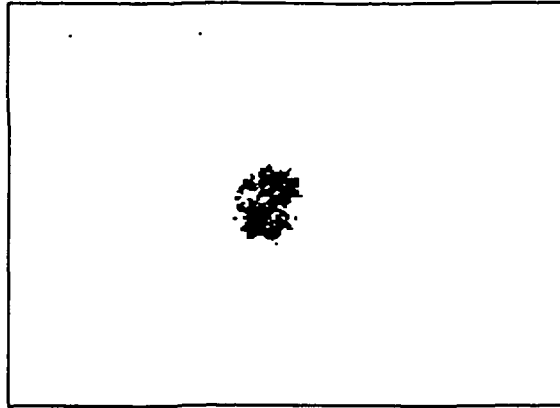


Figure 82. (N) Contrast Enhanced and Smoothed Shearogram.

## 8.2. ELASTIC DEFORMATION FIELD

The presence of a plastic zone at the tip of a crack effectively reduces  $K_I$ , as the crack influences the far field as though it were more blunt than it actually is. More accurate measurements of  $K_I$  may be made with less theoretical difficulty and more experimental effort from the far field deformation around a crack tip with little plasticity.

The elastic change in thickness of a specimen due to an applied load may be expressed as<sup>[13, p377]</sup>.

$$\Delta t = -\frac{t\nu}{E}(\sigma_{xx} + \sigma_{yy}) \quad \langle \text{EQ.2.} \rangle$$

Assuming symmetrical deformation, the out-of-plane displacements on each surface are one-half of the change in thickness.

$$w = \frac{\Delta t}{2} = -\frac{t\nu}{2E}(\sigma_{xx} + \sigma_{yy}) \quad \langle \text{EQ.3.} \rangle$$

$$\therefore \frac{\partial w}{\partial x} = -\frac{t\nu}{E} \frac{\partial}{\partial x} \left[ \frac{1}{2}(\sigma_{xx} + \sigma_{yy}) \right] \quad \langle \text{EQ.4.} \rangle$$

Following the elasticity theory used in similar isopachic photoelastic fringe analysis<sup>[13, p517]</sup>, directly ahead of the crack tip ( $\theta = 0$ ,  $r = x$ ),

$$\frac{1}{2}(\sigma_{xx} + \sigma_{yy}) = \frac{K_I}{\sqrt{2\pi x}} + B_0 + A_1\sqrt{x} + B_1x + A_2\sqrt{x^3} + B_2x^2 \quad \langle \text{EQ.5.} \rangle$$

$$\therefore \frac{\partial}{\partial x} \left[ \frac{1}{2}(\sigma_{xx} + \sigma_{yy}) \right] = \frac{-K_I}{2\sqrt{2\pi x^3}} + \frac{A_1}{2\sqrt{x}} + B_1 + \frac{3}{2}A_2\sqrt{x} + 2B_2x \quad \langle \text{EQ.6.} \rangle$$

Substitution of EQ.6. into EQ.4. gives:

$$\frac{\partial w}{\partial x} = \frac{t\nu}{E} \left[ \frac{K_I}{2\sqrt{2\pi x^3}} - \frac{A_1}{2\sqrt{x}} - B_1 - \frac{3}{2} A_2 \sqrt{x} - 2B_2 x \right] \quad \langle \text{EQ.7.} \rangle$$

Optical consideration of the ES apparatus indicates that, with proper apparatus setup<sup>[6]</sup>,

$$\frac{\partial w}{\partial x} = \frac{n\lambda}{2s} \quad \langle \text{EQ.8.} \rangle$$

where  $\partial w/\partial x$  is the change in surface slope,  $n$  is the fringe count,  $\lambda$  is the illumination wavelength, and  $s$  is the image shearing distance.

$$\therefore n = \frac{st\nu}{\lambda E} \left[ \frac{K_I}{\sqrt{2\pi x^3}} - \frac{A_1}{\sqrt{x}} - 2B_1 - 3A_2 \sqrt{x} - 4B_2 x \right] \quad \langle \text{EQ.9.} \rangle$$

An experiment similar to the feasibility study discussed above, with a sharp crack instead of a notch and greater vibration isolation, could be used to estimate  $K_I$  using EQ.9.

Plasticity at the crack tip should be minimized, and shearograms should be obtained with a reference at no load processed with images at load. The appearance of five fringe orders, and the measurement of their position straight ahead of the crack tip, are necessary for substitution into EQ.9. This gives five equations and five unknowns, from which values may be obtained for  $K_I$ ,  $A_1$ ,  $B_1$ ,  $A_2$ , and  $B_2$ .

This experimental measurement may be compared with theoretical values. For a Mode I single edge crack (SEC) specimen<sup>[19, p85]</sup>:

$$K_I = Y\sigma\sqrt{a} \quad \langle \text{EQ.9.} \rangle$$

$$\text{where } Y = 1.99 - 0.41\left(\frac{a}{W}\right) + 18.7\left(\frac{a}{W}\right)^2 - 38.48\left(\frac{a}{W}\right)^3 + 53.85\left(\frac{a}{W}\right)^4$$

For the specimen to be tested in this study,  $a/W = 0.125$ ,  $t = 0.093$  in., with  $E = 360$  ksi. and  $\nu = 0.38$ <sup>[13, p478]</sup>, EQ.9. results in  $Y = 2.17$  and  $K_I = 1.53 \sigma \text{ in}^{1/2}$ .

## 9. CONTROL SETTINGS INFLUENCE PROBABILITY OF DETECTION

Under ideal circumstances, the change in surface slope indicated by electronic shearography may be related to the fringe count by EQ.8.

$$\frac{\partial w}{\partial x} = \frac{n\lambda}{2s} \quad \langle \text{EQ.8.} \rangle$$

This expression indicates that for a given amount of motion, the number of fringes indicated is directly proportional to the image shearing distance. Similarly, a smaller amount of motion may be detected as a single fringe if  $s$  is increased. Since the amount of motion produced by a flaw depends on such properties as its size, shape, orientation, etc. as well as the type and extent of excitation, it becomes obvious that the result of a shearography inspection is dependent upon certain control settings, such as image shearing distance and excitation, as well as the characteristics of the flaw being inspected. As with any optical or electronic inspection method, ES results may also be influenced by noise such as unwanted light entering the optical path or random temperature variations.

It was desired that an experimental relationship be found between the output of the shearography device and the various control settings and noise levels. From this relationship, the influence of noise and control variables on the probability of detection (POD) curve was to be determined. During a NASA/ASEE summer faculty fellowship at MSFC, Dr. Enoch C. Temple of Alabama A&M University developed a statistical optimization methodology<sup>[1]</sup> to provide such analysis based upon Genichi Taguchi's method for process control, maximum likelihood analysis of variance, and response surface theory. This technique relates the values of a set of control variables,  $\underline{X} = [x_1, x_2, \dots, x_k]^T$ , and noise variables,  $\underline{Z} = [z_1, z_2, \dots, z_k]^T$ , to the instrumentation output  $y$  within an error of  $\epsilon$  by the relationship shown in EQ.10.

$$y = B_0 + \underline{X} \cdot \underline{B} + \underline{Z} \cdot \underline{D} + \underline{X} \cdot (\underline{CZ}) + \epsilon \quad \langle \text{EQ.10.} \rangle$$

Empirical values were obtained for the null response,  $B_0$ , the control influence coefficients,  $\underline{B}$ , the noise influence coefficients,  $\underline{D}$ , and the covariance matrix,  $\underline{C}$ , from the statistical regression analysis of a factorially designed experiment. The control variables used in this study were the image shearing distance,  $s$ , heat exposure time,  $h$ , and object distance,  $d$ . The noise variables explored here were ambient lighting,  $l$ , flaw size,  $a_i$ , and flaw orientation,  $r$ . The levels used for these variables are shown in Table 1. Table 2. indicates the combination of levels used in this study.

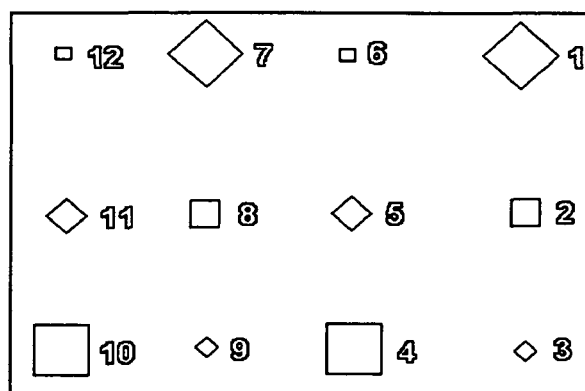
**Table 1. Control and Noise Levels Investigated**

Variable Type	Variable Name	Low (-)	Medium (0)	High (+)
Control	s	0 mm	3 mm	6 mm
Control	h	5 min.		10 min.
Control	d	4 ft.		8 ft.
Noise	l	Overhead Lights Off		Overhead Lights On
Noise	$a_i$	3 mm	6 mm	9 mm
Noise	r	0°		45°

**Table 2. Level Combinations For Each Inspection***i* = inspection number

<i>i</i>	<i>d</i>	<i>s</i>	<i>h</i>	<i>l</i>	<i>i</i>	<i>d</i>	<i>s</i>	<i>h</i>	<i>l</i>
1	-	-	-	-	13	+	-	-	-
2	-	-	-	+	14	+	-	-	+
3	-	-	+	-	15	+	-	+	-
4	-	-	+	+	16	+	-	+	+
5	-	0	-	-	17	+	0	-	-
6	-	0	-	+	18	+	0	-	+
7	-	0	+	-	19	+	0	+	-
8	-	0	+	+	20	+	0	+	+
9	-	+	-	-	21	+	+	-	-
10	-	+	-	+	22	+	+	-	+
11	-	+	+	-	23	+	+	+	-
12	-	+	+	+	24	+	+	+	+

Variations in flaw size and orientation were incorporated into the specimen. A painted panel was prepared containing programmed unbonds of the predetermined sizes and orientations. These flaws were simulated by the presence of 0.5 mil thick aluminum foil inserts between the enamel spray paint and the D6AC steel substrate, preventing a region of controlled geometry from bonding. For repetition, the test panel contained 2 flaws of each of the 6 size/orientation combinations, as shown in Figure 83. and Table 3.

**Figure 83.** Arrangement of simulated unbonds on test panel.



**Table 3. Size and Orientation of Each Simulated Unbond**

FLAW NUMBER	$a_i$	$r$
1	+	+
2	0	-
3	-	+
4	+	-
5	0	+
6	-	-
7	+	+
8	0	-
9	-	+
10	+	-
11	0	+
12	-	-

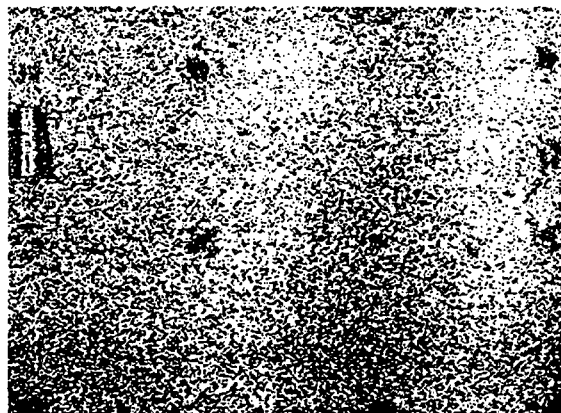


Figure 84. (N) Low level indications.

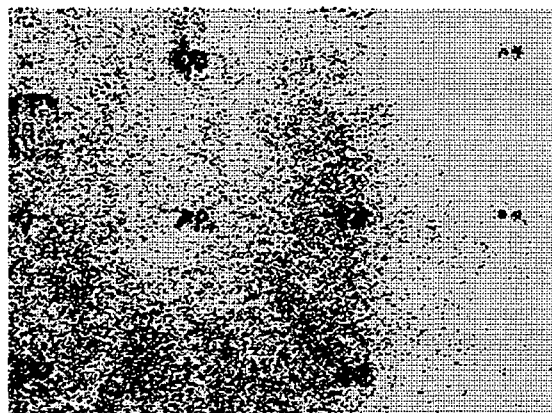


Figure 85. (N) High level indications.

The PW EH/SIS was used to conduct this experiment with thermal excitation supplied by two 500 watt halogen lamps at a distance of 6 inches from the panel. Static shearograms were recorded with four frame and speckle averaging. The reference image was recorded after the part had been exposed to excitation for the required amount of time, and this image was processed with a later image as determined by the experimenter. The detected flaws were recorded and the panel was allowed to return to room temperature before the next cycle began. Figures 84. and 85., for example, show the shearograms acquired during inspection numbers 2 and 24, respectively.

Dr. Temple's analysis based upon this experimental data indicated that, with the levels used here, ambient lighting and object distance had relatively insignificant influence upon flaw detection. A mathematical manipulation and substitution of experimental values into EQ.10., including significant terms only, gives

$$\ln\left(\frac{P_i}{1-P_i}\right) = 0.634a_i h + 0.850a_i s - 4.10r + 1.86a_i r + 0.227hr \quad \langle \text{EQ.11.} \rangle$$

where  $P_i$  is the average probability of detection of a flaw of size  $a_i$ . The influence coefficients of the first two terms on the right hand side of EQ. 11. indicate that, for the specimen used here, the POD is maximized by using the highest level of heat and shear. The levels used here could be adopted as an inspection standard for this material system. Although the last two terms indicate that POD is increased somewhat by interactions of heating level and flaw size with a higher angle of orientation, the third term reveals that the angle of orientation generally decreases POD. Further theoretical analysis is needed to establish the means by which POD confidence may be determined, and a repetition of this experiment with more levels may be used to optimize this confidence relationship.

Since the thermo-mechanical properties of the material system and the coating thickness determine the amount of motion generated by excitation, EQ. 11. is valid only for the specimens utilized here. Given that POD depends upon the material system and geometry in question, a study similar to that discussed here is necessary to establish an inspection standard for each class of test article. A generalized inspection standard cannot be relied upon for optimum performance with a variety of specimen.

**APPENDICES**

## A.1. REFERENCES AND RELATED LITERATURE

1. Temple, E.C., "Statistical Optimization of Shearography Inspections", Final Report, NASA/ASEE Summer Faculty Fellowship Program, August 1995.
2. Russell, S.S., Lansing, M.D., Horton, C.M., Gancek, W.J., *Probability of Detection of Defects in Coatings With Electronic Shearography*, NASA Technical Memorandum 108493, June 1995.
3. Walker, J., Lansing, M.D., Russell, S.S., Workman, G.L., "Materials Characterization of Damage in Filament Wound Composite Pressure Vessels", *American Society for Nondestructive Testing (ASNT), 1995 Spring National Conference*, 20-24 March 1995.
4. Walker, J., Workman, G.L., Hill, E.v.K., Russell, S.S., "A Neural Network/Acoustic Emission Analysis of Impact Damaged Graphite/Epoxy Pressure Vessels", *American Society for Nondestructive Testing (ASNT), 1995 Spring National Conference*, 20-24 March 1995.
5. Lansing, M.D., Russell, S.S., "Shearography Detection of Unbonds in Coatings and Qualification of the Method", *American Society for Nondestructive Testing (ASNT), 1995 Spring National Conference*, 20-24 March 1995.
6. Workman, G.L., Walker, J., Lansing, M.D., *Acoustic Method of Damage Sensing in Composite Materials*, Final Report for Contract NAS8-38609, Delivery Order 99, University of Alabama in Huntsville, Center for Automation & Robotics, 20 October, 1994.
7. Maddux, G.A., Horton, C.M., Lansing, M.D., Gnacek, W.J., Newton, P.L., *Probability of Detection of Defects in Coatings with Electronic Shearography*, Technical Report No. 5-33267, University of Alabama in Huntsville, Research Institute, March 1994.
8. Maddux, G.A., Horton, C.M., McNeill, S.R., Lansing, M.D., *Field Methods to Measure Surface Displacement and Strain with the Video Image Correlation Method*, Technical Report No. 5-33282, University of Alabama in Huntsville, Research Institute, July 1994.
9. Lansing, M.D., Russell, S.S., Nettles, A., McNeill, S.R., "Video Image Correlation Strain Field Evaluation of Impact Damaged Graphite Epoxy Pressure Vessels", *American Society for Nondestructive Testing (ASNT), 1994 Spring National Conference*, 21-25 March 1994.
10. McNeill, S.R., Russell, S.S., Lansing, M.D., "Sub-pixel Digital Video Image Correlation for Full-field Strain Measurement", approved by *NASA TechBriefs* January, 1994 (pending publication).
11. Durig, B., Zhang, F., McNeill, S.R., Chao, Y.J., Peters, W.H., "A Study of Mixed Mode Fracture by Photoelasticity and Digital Image Analysis", *Optics and Lasers in Engineering, Vol. 14*, 1991.
12. Maji, A.K., Wang, J.L., Lovato, J., "Electronic Speckle Pattern Interferometry for Fracture Mechanics Testing", *Experimental Techniques*, May/June 1991.
13. Dally, J.W., Riley, W.F., *Experimental Stress Analysis*, McGraw-Hill, Inc., 1991.
14. Newman, J.W., "Inspection of Aircraft Structure with Advanced Shearography", *American Society for Nondestructive Testing (ASNT), 1990 Fall National Conference*, 10 October 1990.

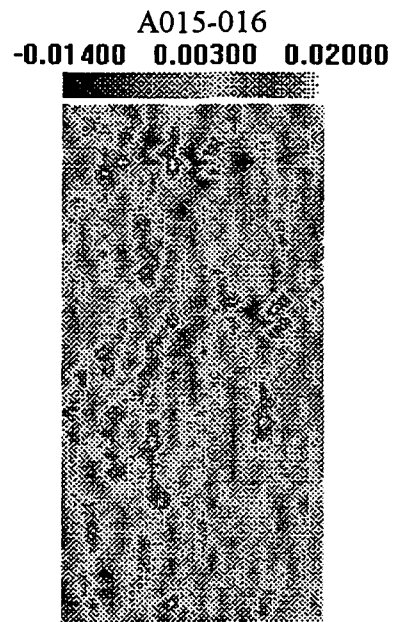
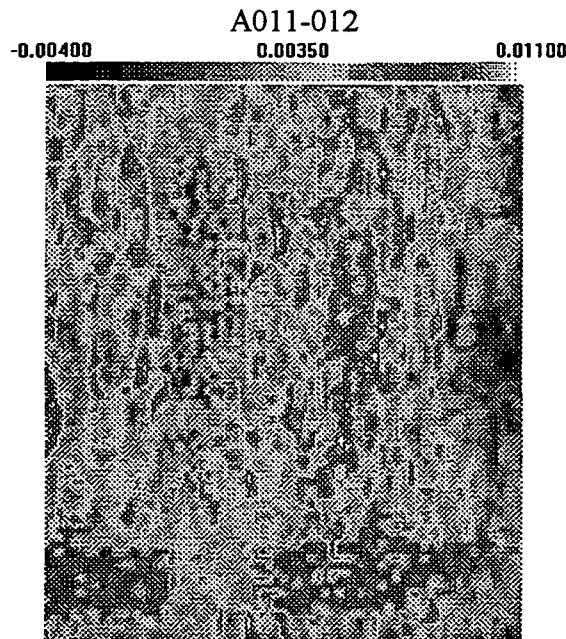
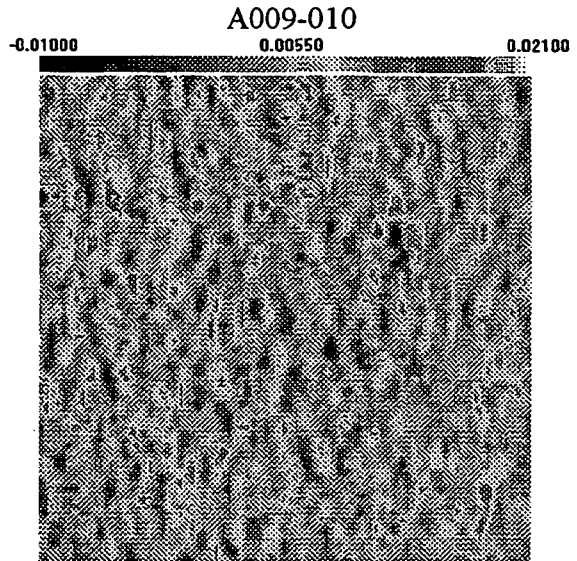
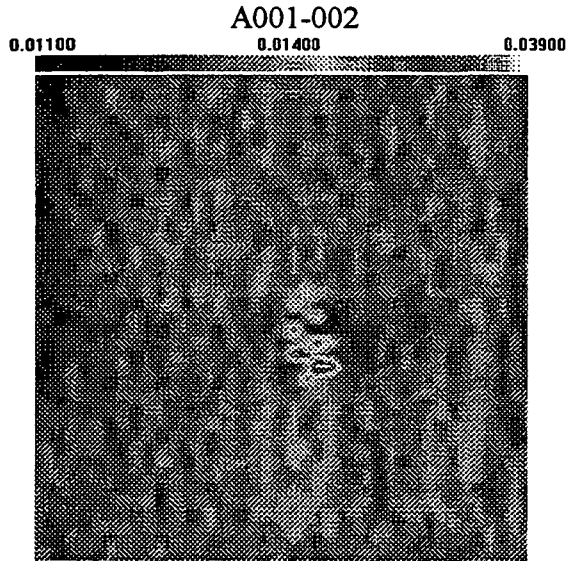
15. Parsi, F., Husband, D.M., Lisk, J.S., Gadala-Maria, F., McNeill, S.R., Sutton, M.A., "Application of Digital Image Processing to the Analysis of Two Phase Materials with Spherical Inclusions", *Polymer Composites*, Vol. 11, June 1990.
16. Bruck, H.A., McNeill, S.R., Sutton, M.A., Peters, W.H., "Digital Image Correlation Using Newton-Raphson Method of Partial Differential Correction", *Experimental Mechanics*, September 1989.
17. Bruck, H.A., McNeill, S.R., Russell, S.S., Sutton, M.A., "Use of Digital Image Correlation for Determination of Displacements and Strains", *Nondestructive Testing Monographs and Tracts, Volume 5: Nondestructive Evaluation for Aerospace Requirements*, 1989.
18. Sutton, M.A., McNeill, S.R., Jang, J., Babai, M., "Effects of Subpixel Image Restoration on Digital Correlation Estimates", *Optical Engineering*, October 1988.
19. Broek, D., *Elementary Engineering Fracture Mechanics*, Martinus Nijhoff Publishers, 1987.
20. McNeill, S.R., Peters, W.H., Sutton, M.A., "Estimation of Stress Intensity Factor by Digital Image Correlation", *Engineering Fracture Mechanics*, Vol. 28, No. 1.
21. Sutton, M.A., Cheng, M., Peters, W.H., Chao, Y.J., McNeill, S.R., "Application of an Optimized Digital Correlation Method to Planar Deformation Analysis", *Image and Vision Computing*, August 1986.
22. Mohanty, R.K., Joenathan, C., Sirohi, R.S., "High Sensitivity Tilt Measurement by Speckle Shear Interferometry", *Applied Optics*, Vol. 25, No. 10, 15 May 1986.
23. Mohanty, R.K., Joenathan, C., Sirohi, R.S., "Speckle and Speckle-shearing Interferometers Combined for the Simultaneous [sic] Determination of Out-of-plane Displacement and Slope", *Applied Optics*, Vol. 24, No. 18, 15 September 1985.
24. Sutton, M.A., Wolters, W.J., Peters, W.H., Ranson, W.F., McNeill, S.R., "Determination of Displacements Using an Improved Digital Correlation Method", *Computer Vision*, August 1983.
25. Hung, Y.Y., "Shearography: A New Optical Method for Strain Measurement and Nondestructive Testing", *Optical Engineering*, Vol. 21, No. 3, May/June 1982.
26. Boone, P.M., "Determination of Slope and Strain Contours by Double-exposure Shearing Interferometry", *Experimental Mechanics*, August 1975.

A.2. FWPV DATA

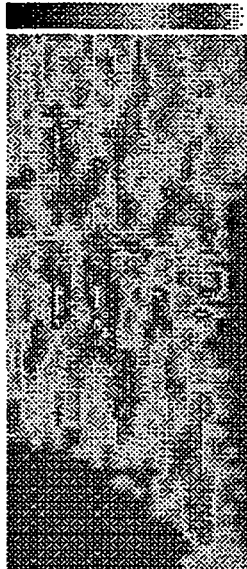
A.2.1. GRAPHITE-EPOXY

A.2.1.1. EMPTY Gr-Ep CASES

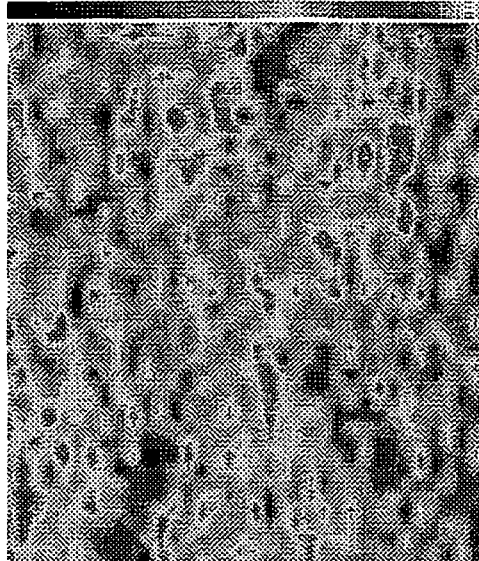
3501-ATL Resin



A019-020  
-0.0040 0.0040 0.0120



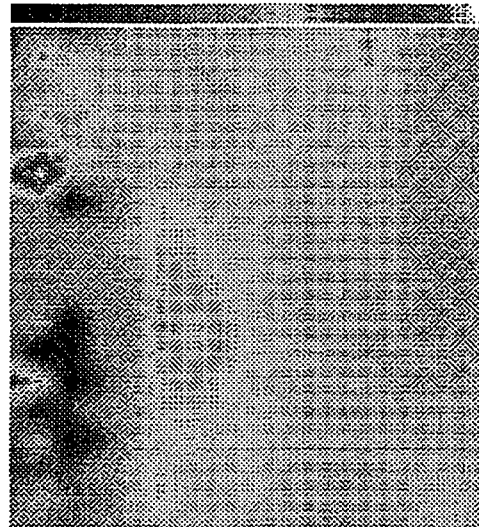
A021-022  
-0.0030 0.0045 0.0120



C075-076  
-0.0040 0.0040 0.0120

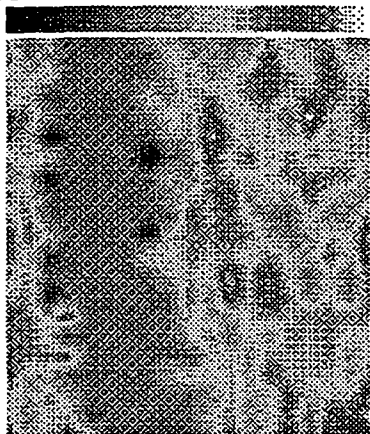


C081-082  
-0.0220 0.0020 0.0260



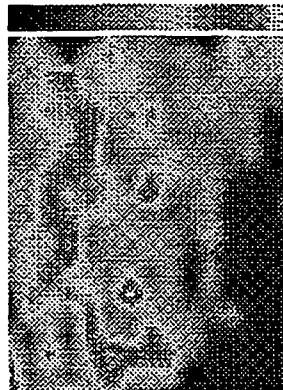
C083-084

-0.00500 0.00300 0.01100



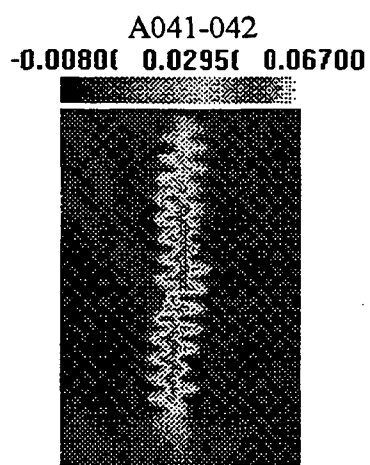
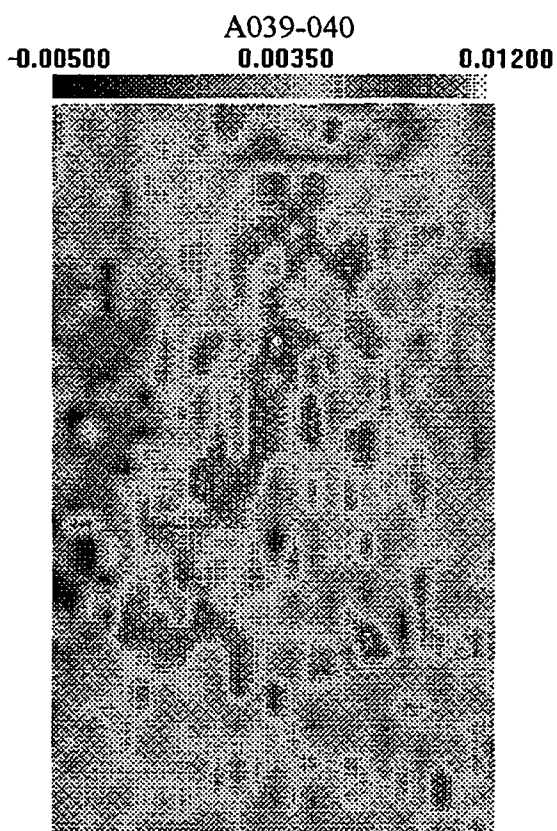
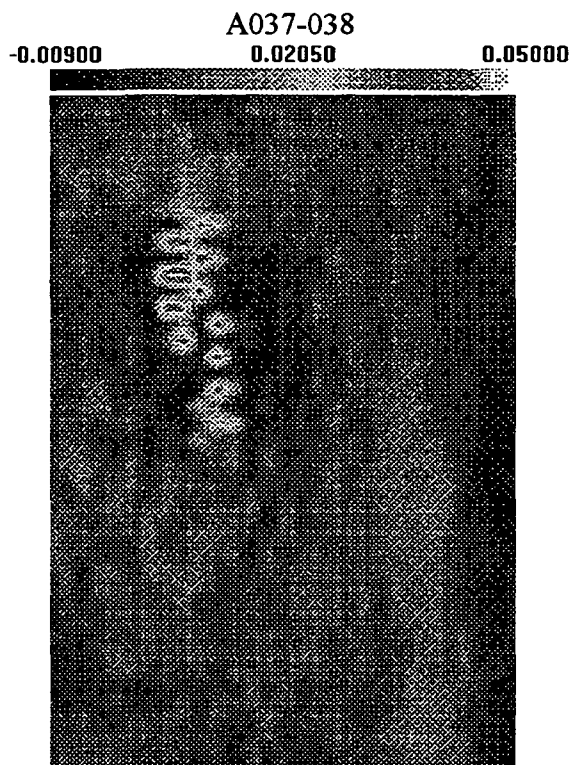
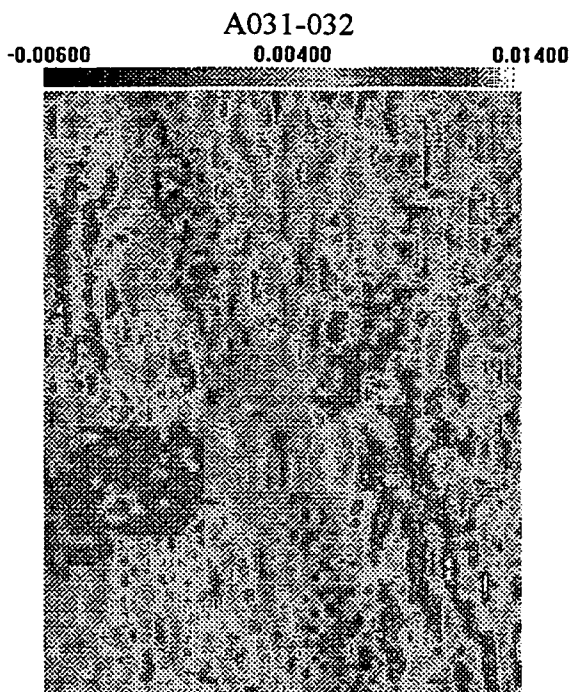
C085-086

-0.00200 0.00550 0.01300





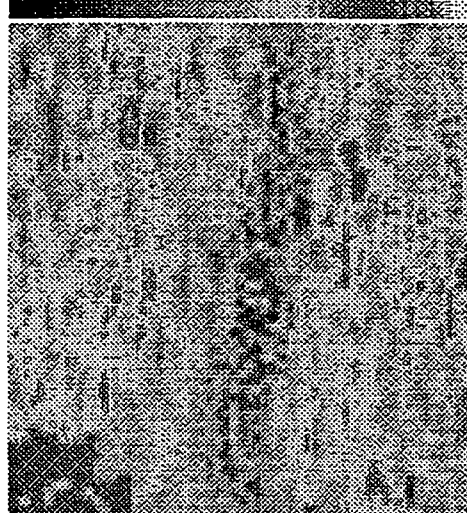
8553-6 Resin



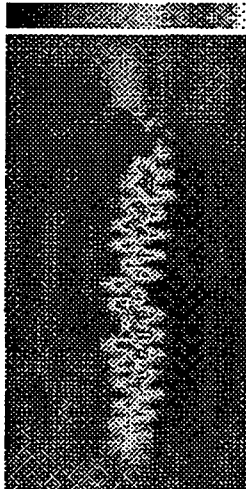
C097-098  
-0.00300 0.00550 0.01400



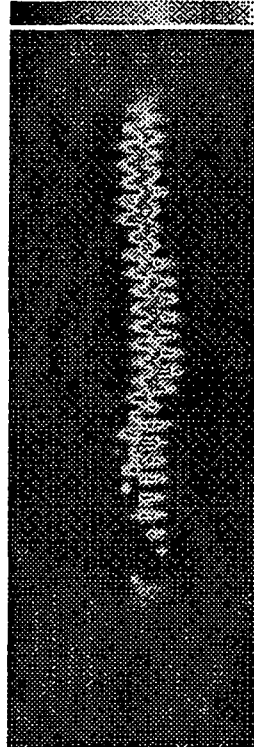
C101-102  
-0.00500 0.00450 0.01400



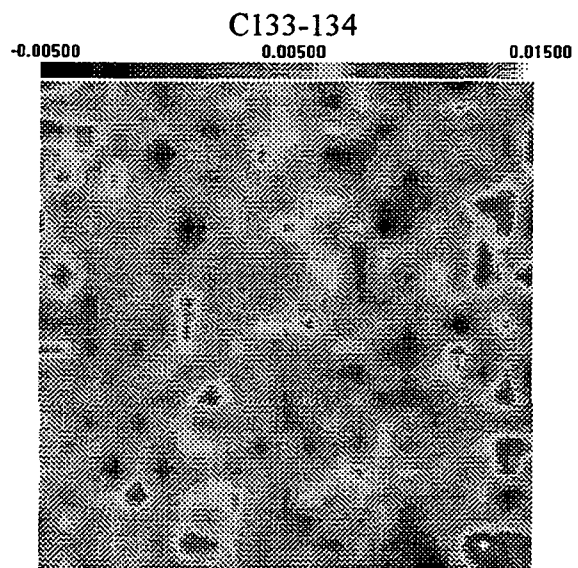
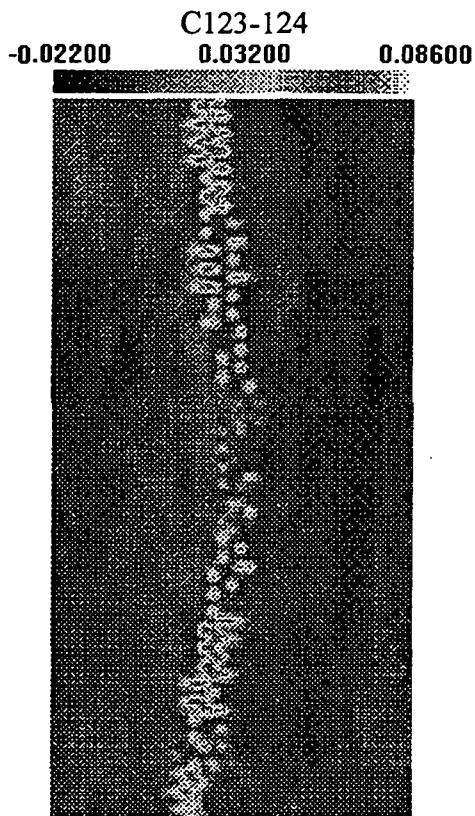
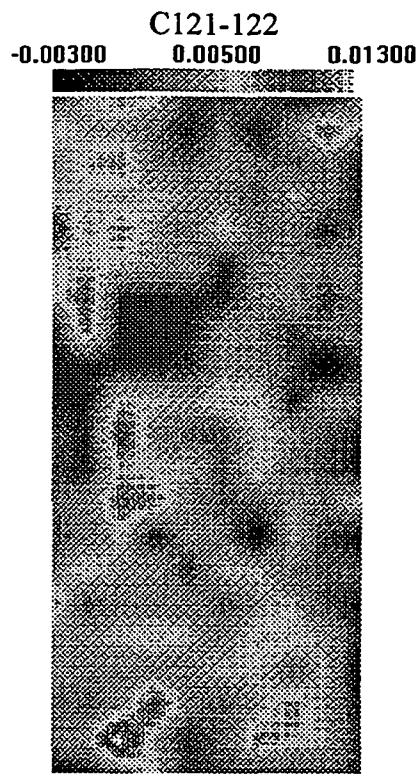
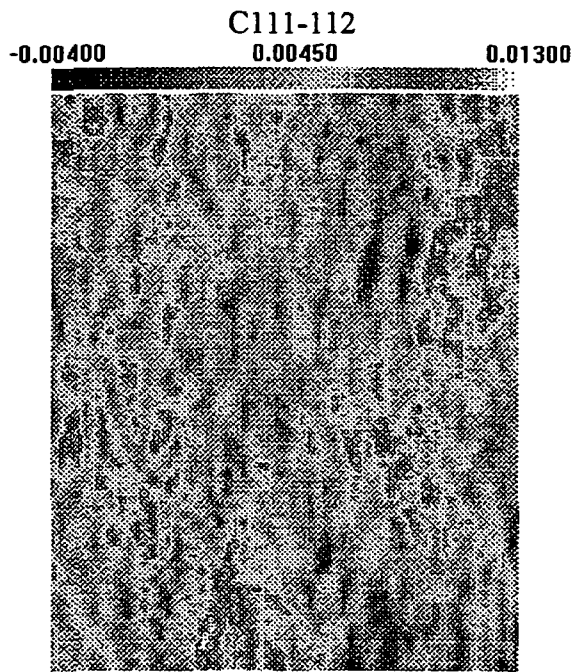
C103-104  
-0.01600 0.02500 0.06600



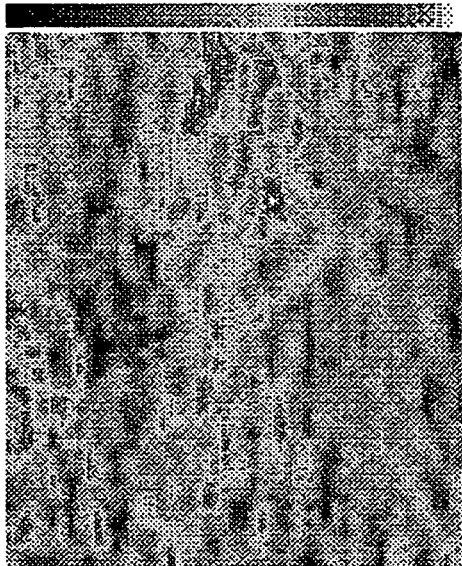
C105-106  
-0.01100 0.03050 0.07200



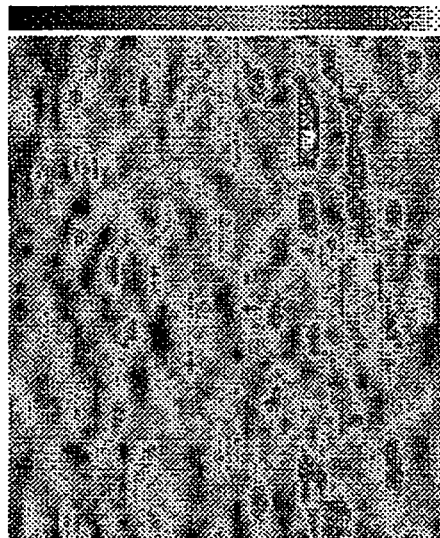
977-2 Resin



C145-146  
-0.00100 0.00450 0.01000



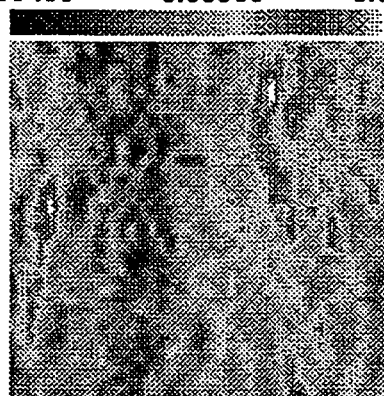
C147-148  
-0.00400 0.00450 0.01300



C149-150  
-0.00500 0.00450 0.01400

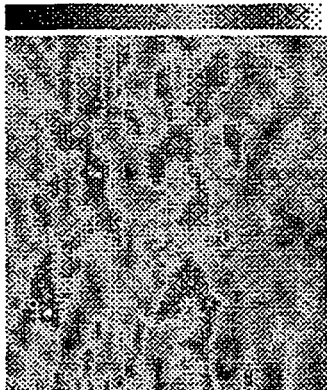


C153-154  
-0.00400 0.00600 0.01600



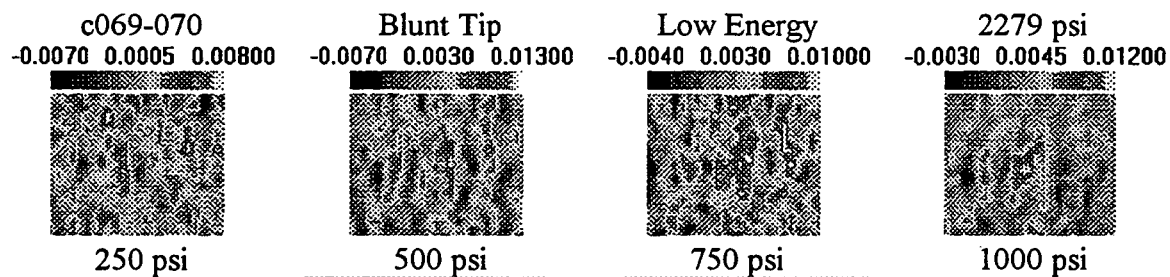
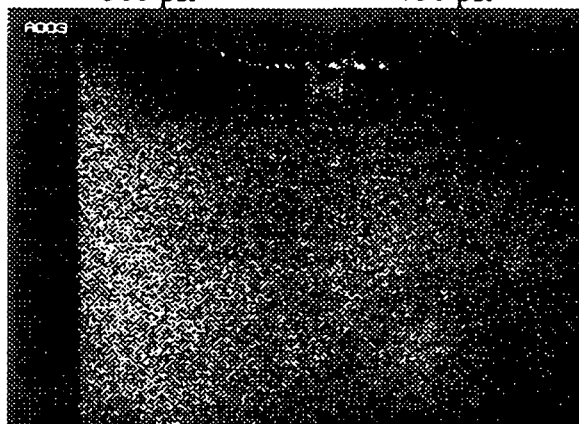
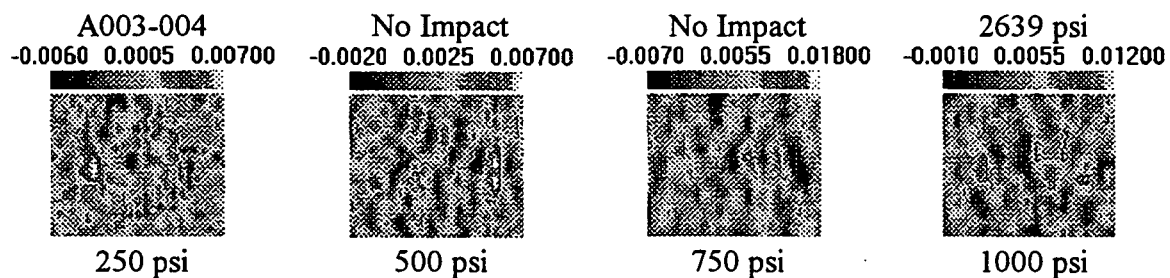
C157-158

-0.00200    0.00400    0.01000

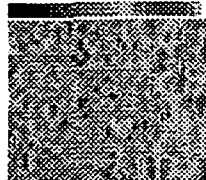


## A.2.1.2. Gr-Ep CASES FILLED WITH INERT PROPELLANT

### 3501-6 ATL Resin

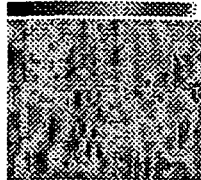


C077-078  
-0.00800 0.00100 0.01000



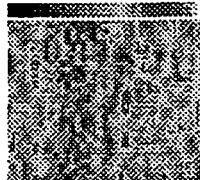
250 psi

Blunt Tip  
-0.00300 0.00200 0.00700



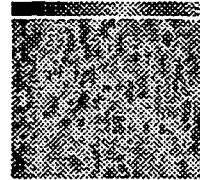
500 psi

High Energy  
-0.00500 0.00350 0.01200

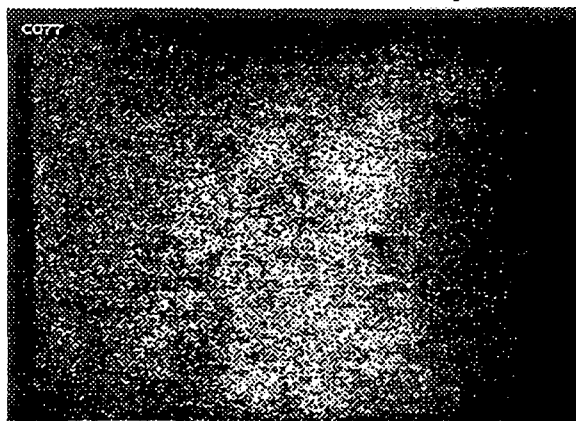


750 psi

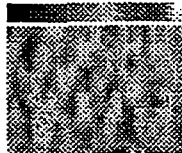
2373 psi  
-0.00400 0.00450 0.01300



1000 psi

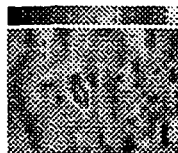


A013-014  
-0.0040 0.0005 0.00500



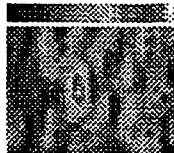
250 psi

Sharp Tip  
-0.0050 0.0035 0.01200



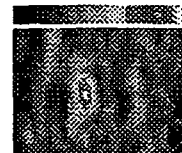
500 psi

Low Energy  
-0.0020 0.0070 0.01600



750 psi

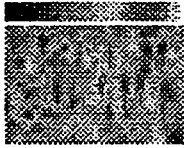
2232 psi  
-0.0020 0.0115 0.02500



1000 psi

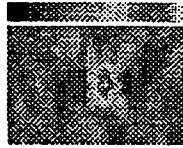


A023-024  
-0.0080f 0.0025f 0.0130f



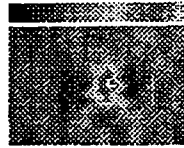
250 psi

Sharp Tip  
-0.0090f 0.0100f 0.0290f



500 psi

High Energy  
-0.0080f 0.0130f 0.0340f



750 psi

2266 psi  
-0.0120f 0.0190f 0.0500f

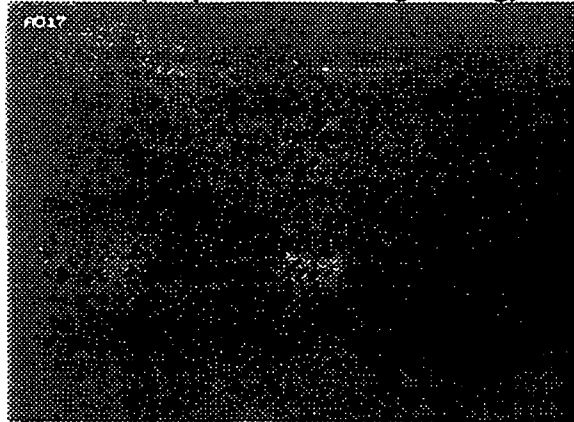


1000 psi

A017-018

Sharp Tip

High Energy





### X8553-45 Resin

A025-026  
-0.0050 0.0020 0.00900



250 psi

No Impact  
-0.0030 0.0020 0.00700



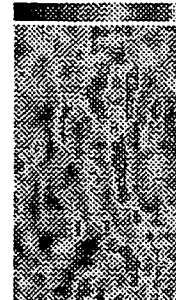
500 psi

No Impact  
-0.0040 0.0045 0.01300



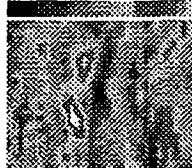
750 psi

3171 psi  
-0.0030 0.0040 0.01100



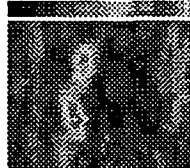
1000 psi

A029-030  
-0.00600 0.00250 0.01100



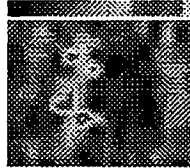
250 psi

Blunt Tip  
-0.00500 0.01150 0.02800



500 psi

Low Energy  
-0.00300 0.01000 0.02300

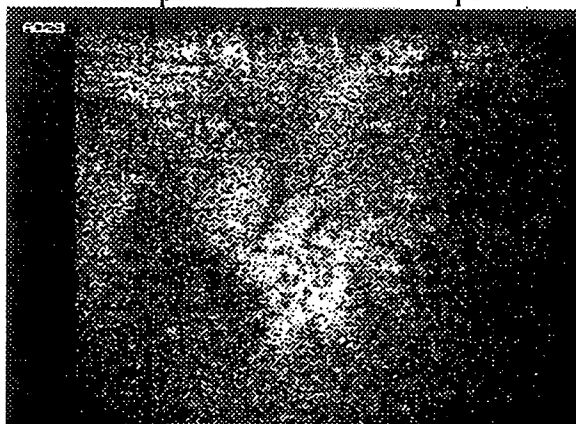


750 psi

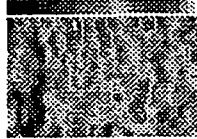
2302 psi  
-0.00700 0.01800 0.04300



1000 psi



A047-048  
-0.00300 0.00150 0.00600



250 psi

Blunt Tip  
-0.00300 0.00450 0.01200



500 psi

High Energy  
-0.00100 0.00650 0.01400

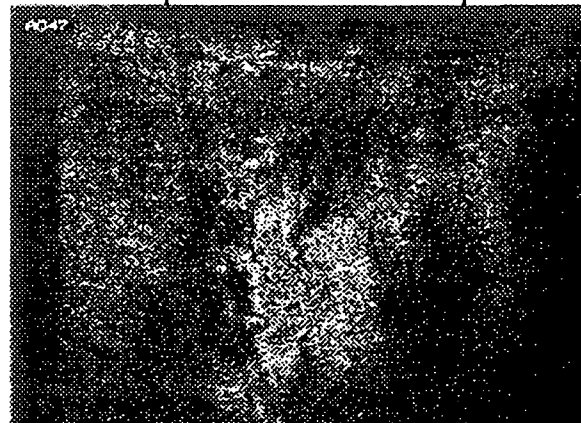


750 psi

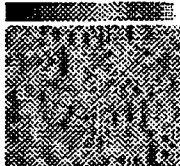
2463 psi  
-0.00200 0.00900 0.02000



1000 psi

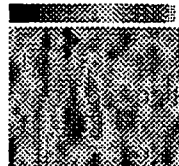


C087-088  
-0.0060 0.0010 0.00800



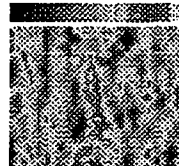
250 psi

Sharp Tip  
-0.0090 0.0035 0.01600



500 psi

Low Energy  
-0.0110 0.0035 0.01800

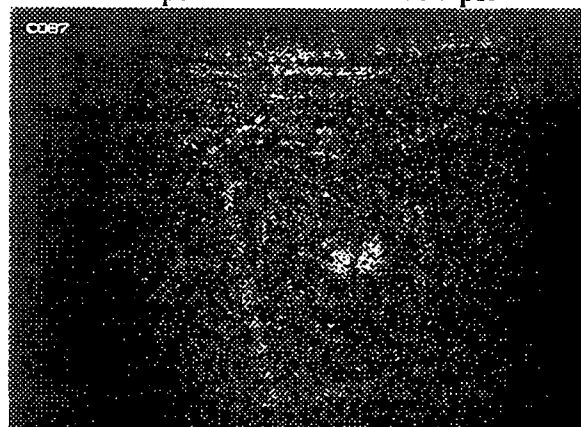


750 psi

2489 psi  
-0.0080 0.0090 0.02600



1000 psi



C-093-094  
-0.0060 0.0030 0.01200



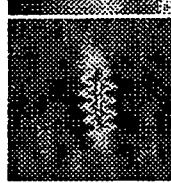
250 psi

Sharp Tip  
-0.0060 0.0135 0.03300



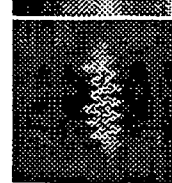
500 psi

High Energy  
-0.0070 0.0185 0.04400

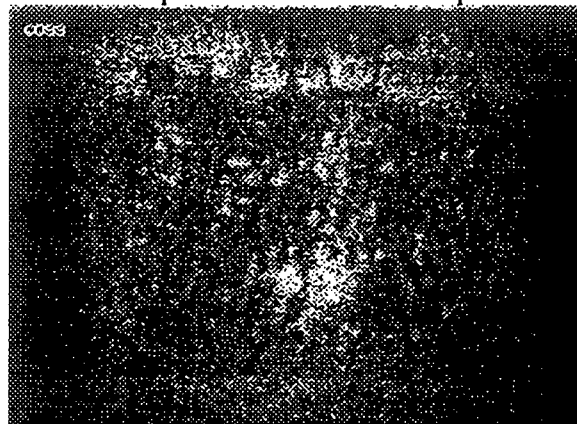


750 psi

1995 psi  
-0.0100 0.0250 0.06000

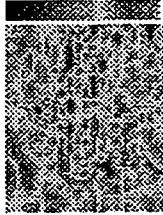


1000 psi



977-2 Resin

C-115-116  
-0.00E 0.000 0.00800



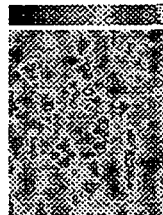
250 psi

No Impact  
-0.00E 0.001 0.01200



500 psi

No Impact  
-0.013 0.003 0.01900

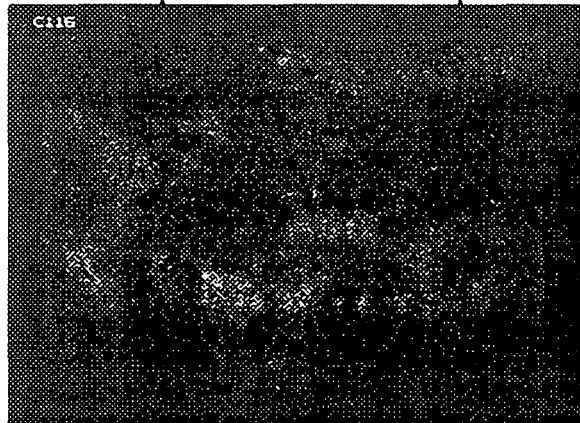


750 psi

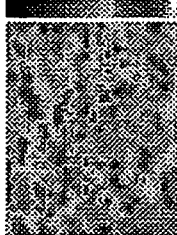
3335 psi  
-0.011 0.008 0.02700



1000 psi

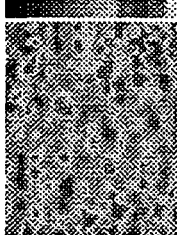


C141-142  
-0.0040 0.0010 0.00600



250 psi

Blunt Tip  
-0.0170 0.0020 0.02100



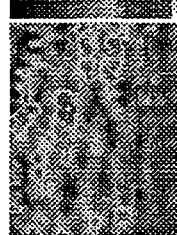
500 psi

Low Energy  
-0.0170 0.0025 0.02200

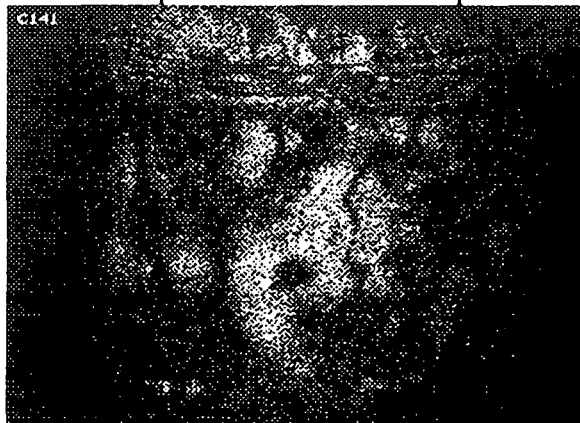


750 psi

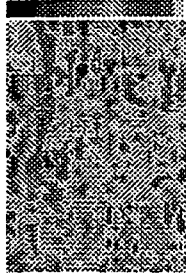
2786 psi  
-0.0160 0.0080 0.03200



1000 psi



C117-118  
-0.00700 0.00000 0.00700



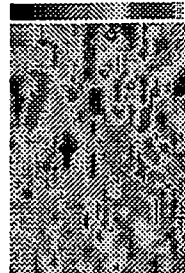
250 psi

Blunt Tip  
-0.00400 0.00250 0.00900



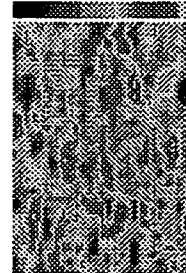
500 psi

High Energy  
-0.00400 0.00350 0.01100

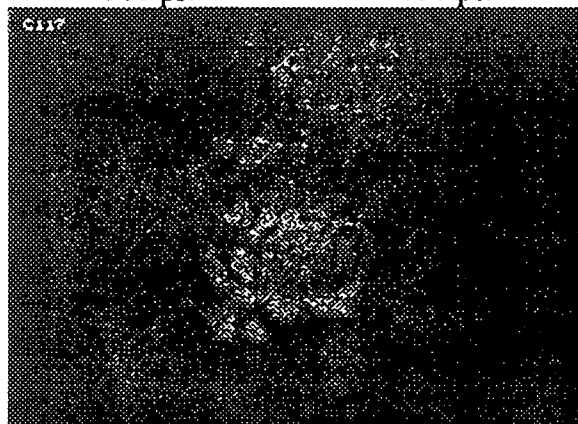


750 psi

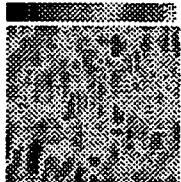
3133 psi  
-0.00300 0.00450 0.01200



1000 psi

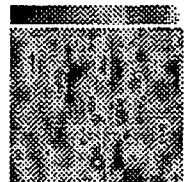


C131-132  
-0.0030 0.0010 0.00500



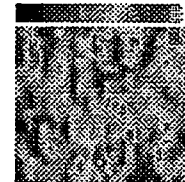
250 psi

Sharp Tip  
-0.0030 0.0030 0.00900



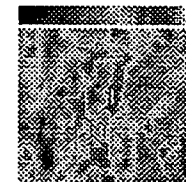
500 psi

Low Energy  
-0.0020 0.0045 0.01100

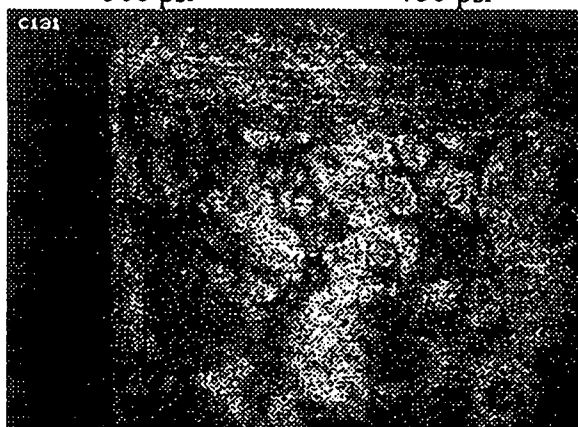


750 psi

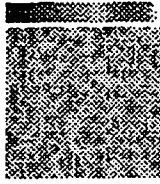
2996 psi  
-0.0040 0.0045 0.01300



1000 psi



C155-156  
-0.00E 0.000 0.00800



250 psi

Sharp Tip  
-0.00E 0.003 0.01200



500 psi

High Energy  
-0.001 0.005 0.01200

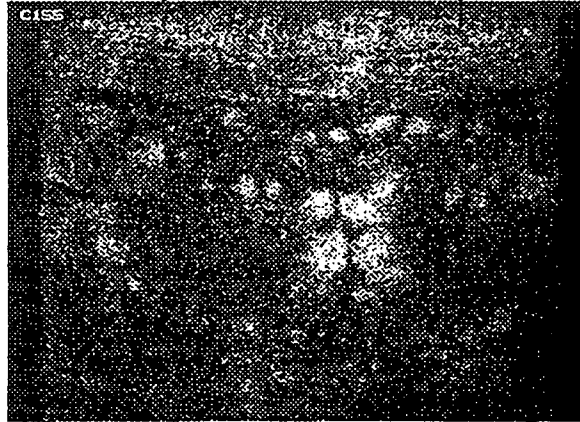


750 psi

2804 psi  
-0.00E 0.006 0.01800



1000 psi



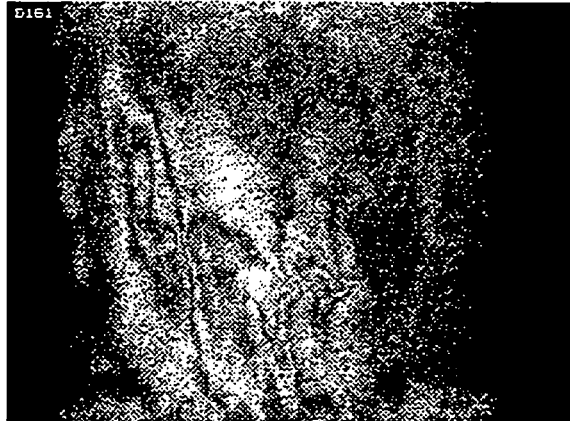
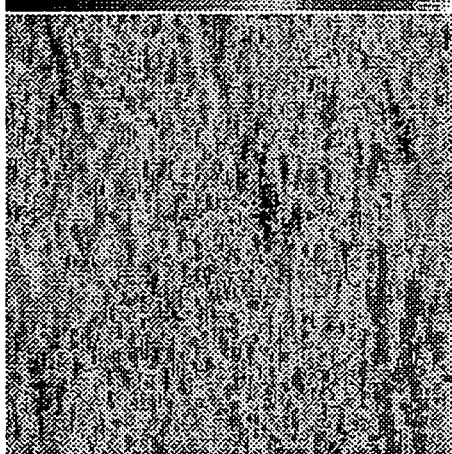
## A.2.2. KEVLAR-EPOXY

### A.2.2.1. EMPTY K-Ep CASES

D161-162      Unknown Impact

2249 psi

-0.00200      0.00550      0.01500

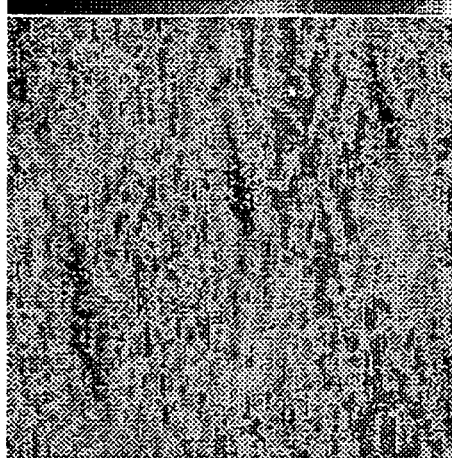


D163-164      Blunt Tip

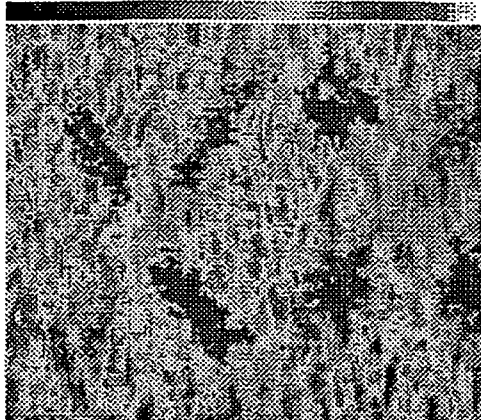
10.90 ft-lb

2194 psi

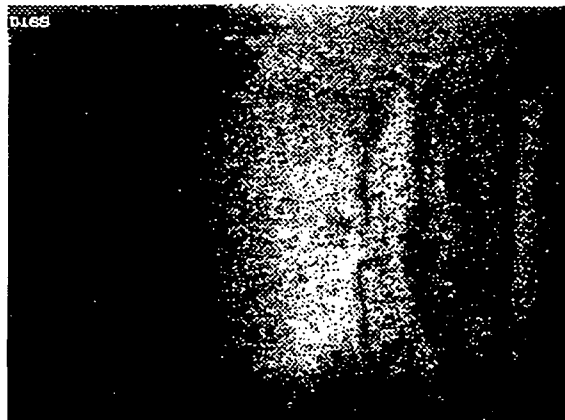
-0.00200      0.00550      0.01300



D165-166 Sharp Tip  
-0.00500 0.00600 0.01700



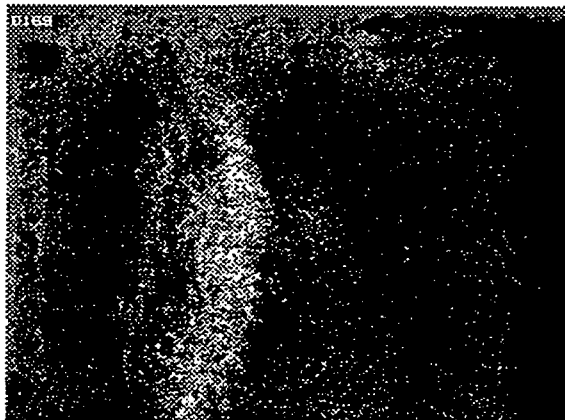
7.00 ft-lb 2353 psi



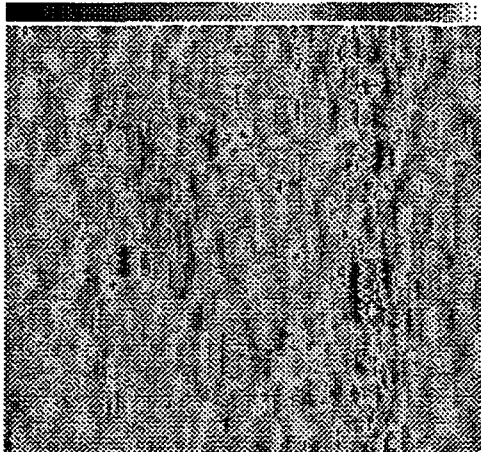
D169-170 Sharp Tip  
-0.01400 0.00450 0.02300



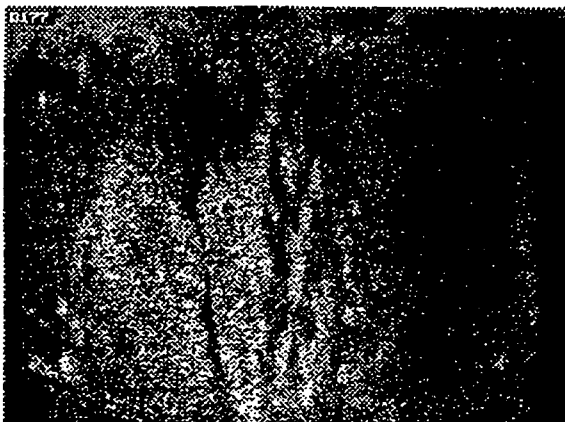
8.83 ft-lb 2608 psi



D177-178 Sharp Tip  
-0.01200 0.00750 0.02700

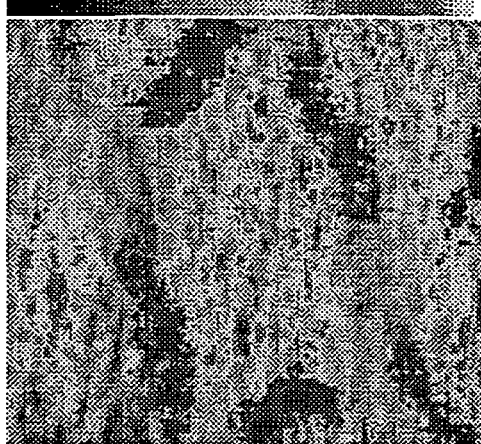


11.91 ft-lb 2237 psi

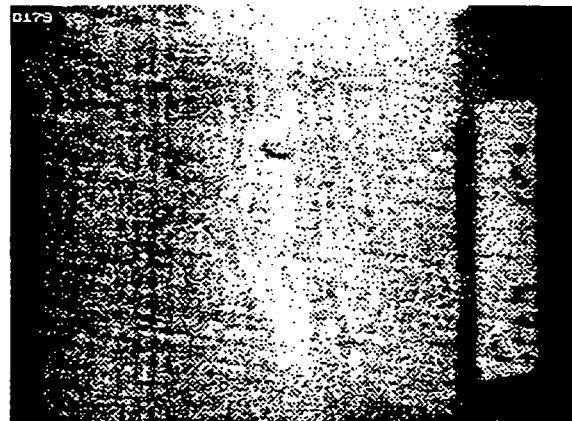




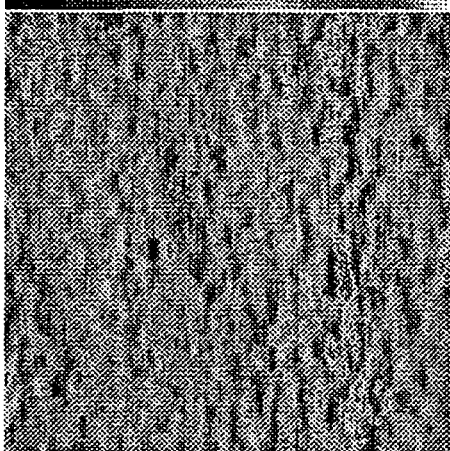
D179-180 Sharp Tip  
-0.00500 0.00650 0.01800



10.00 ft-lb 2561 psi



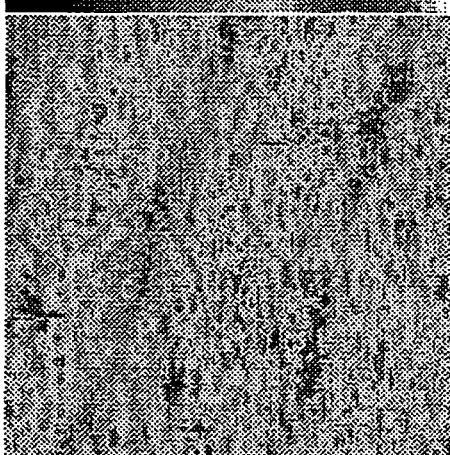
D187-188 Blunt Tip  
-0.01000 0.00950 0.02900



11.80 ft-lb 2407 psi



D201-202 Sharp Tip  
-0.00600 0.00550 0.01700



6.90 ft-lb 2597 psi



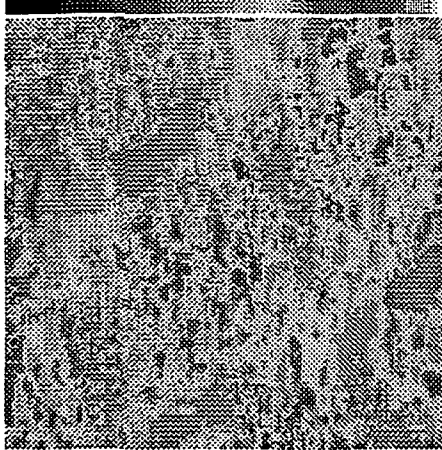
D213-214

Sharp Tip

11.00 ft-lb

2356 psi

-0.01200 0.00350 0.01900



SHEAROGRAPH NOT AVAILABLE.

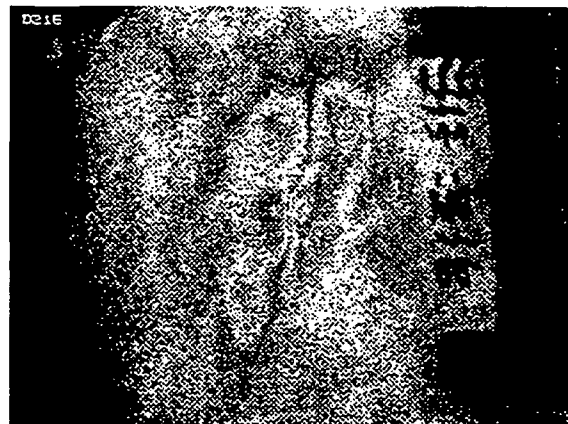
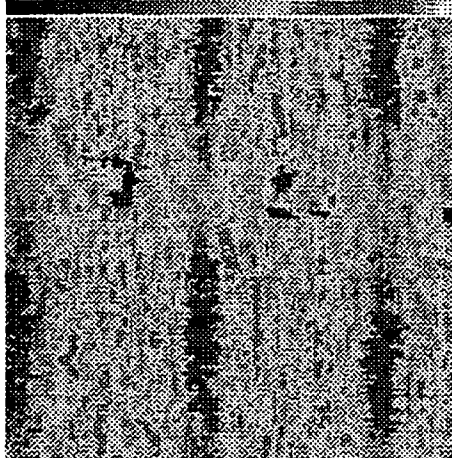
D215-216

Sharp Tip

7.10 ft-lb

2503 psi

-0.00300 0.00600 0.01500



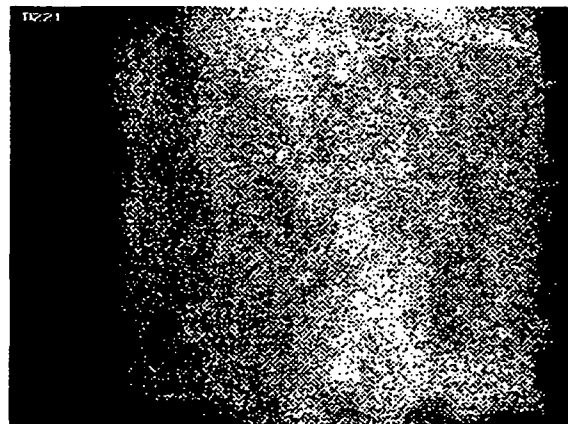
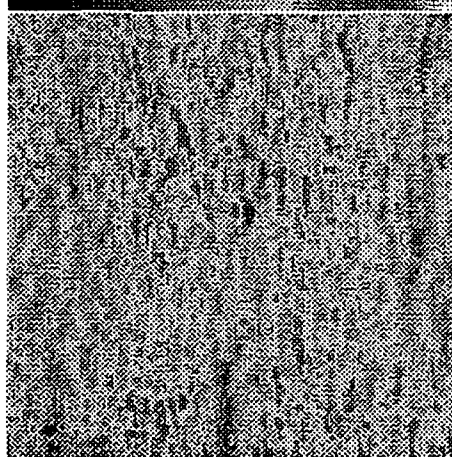
D221-222

No Impact

No Impact

2867 psi

-0.00200 0.00600 0.01400



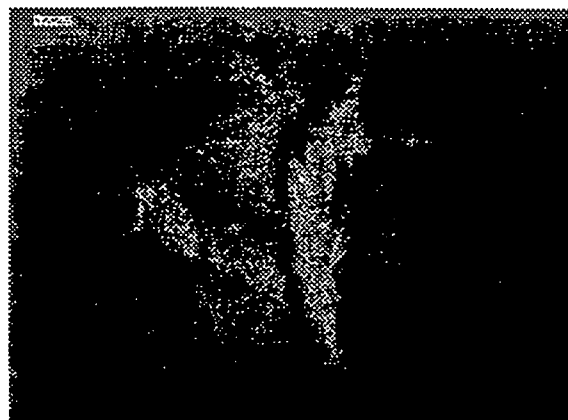
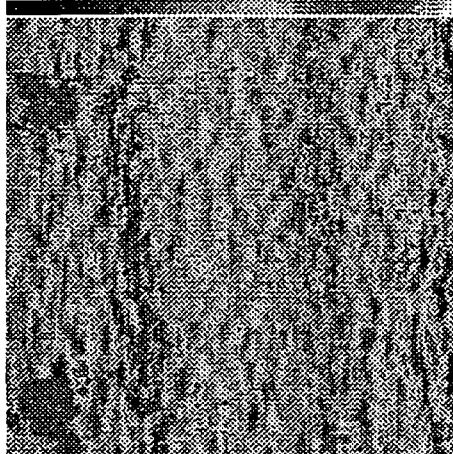
D225-226

Sharp Tip

11.80 ft-lb

2149 psi

-0.01000 0.00850 0.02700



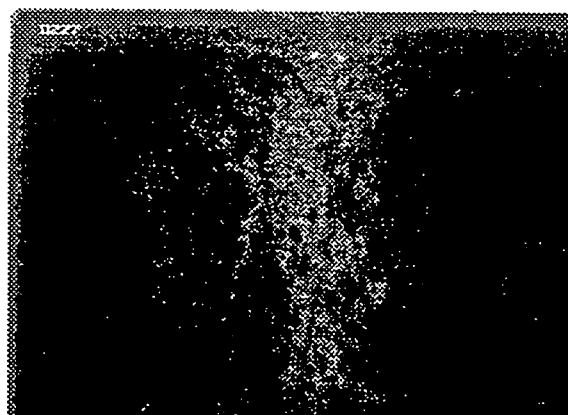
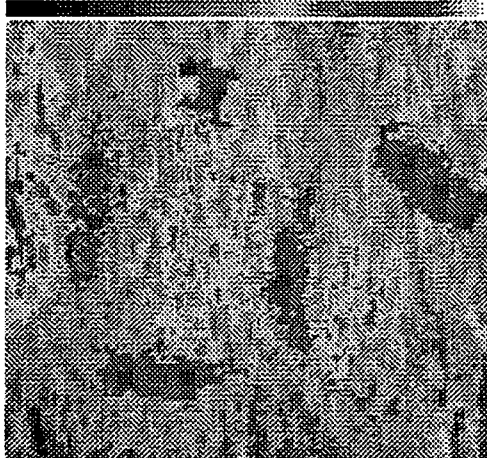
D227-228

Blunt Tip

12.00 ft-lb

2275 psi

-0.00900 0.00600 0.0210



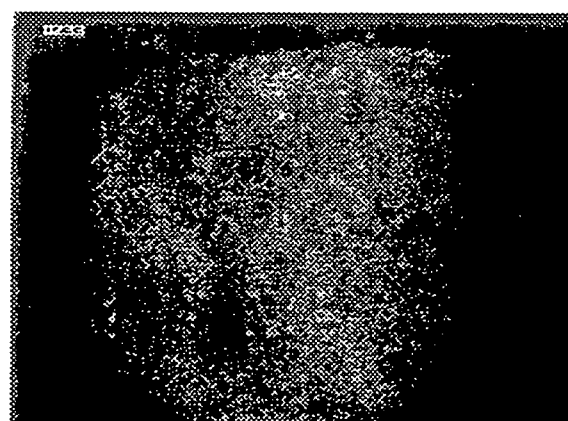
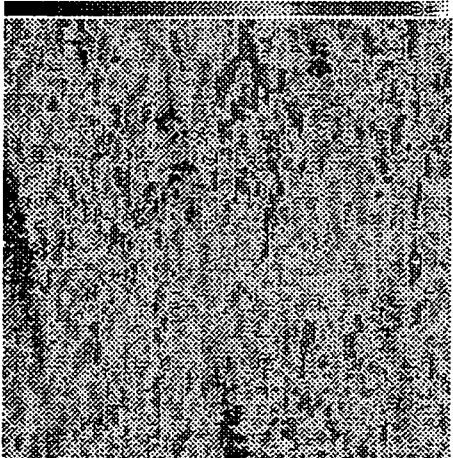
D233-234

No Impact

No Impact

3057 psi

-0.00400 0.00550 0.01500



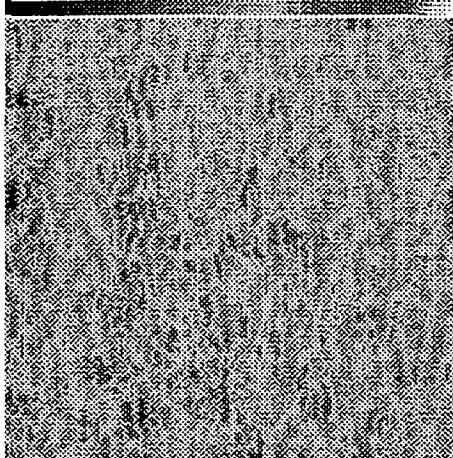
D235-236

Blunt Tip

14.41 Ft.Lbs.

1701 psi

-0.03600 0.00250 0.04100



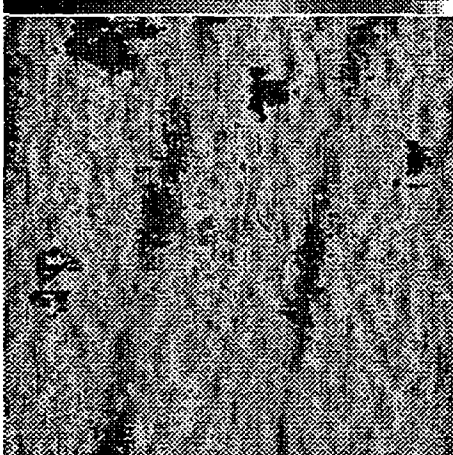
D237-238

Sharp Tip

9.80 ft-lb

2314 psi

-0.00300 0.00800 0.01900



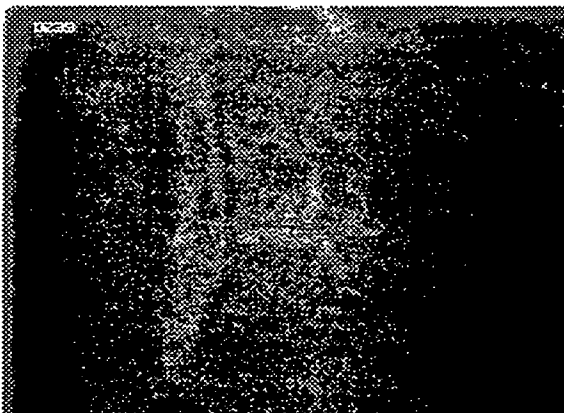
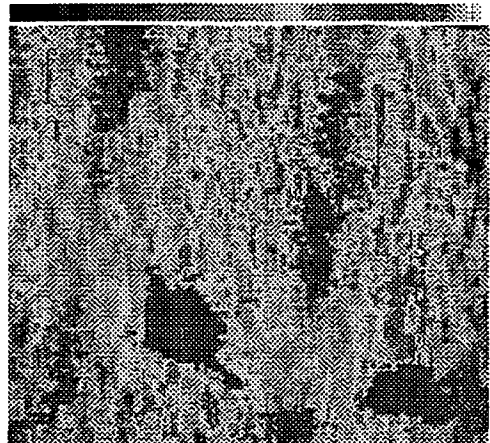
D239-240

Blunt Tip

15.50 ft-lb

1796 psi

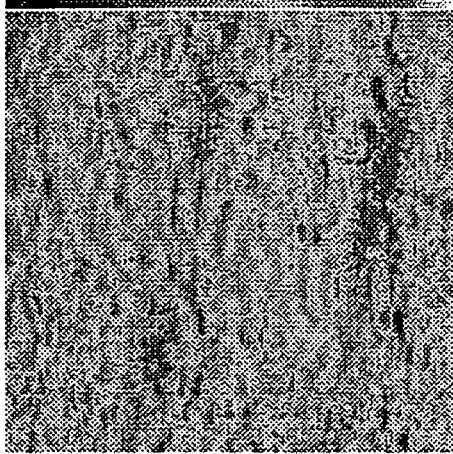
-0.00500 0.00550 0.01600



D241-242

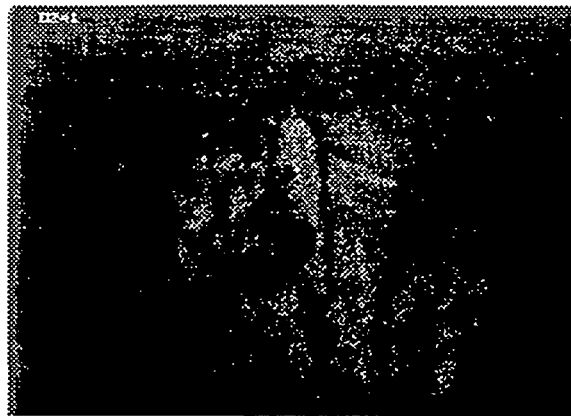
Blunt Tip

-0.00700 0.00600 0.01900



9.00 ft-lb

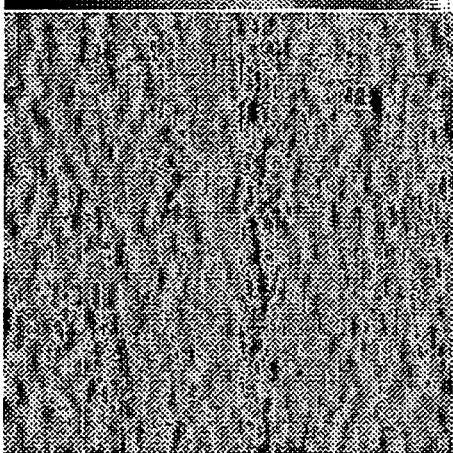
2354 psi



D253-254

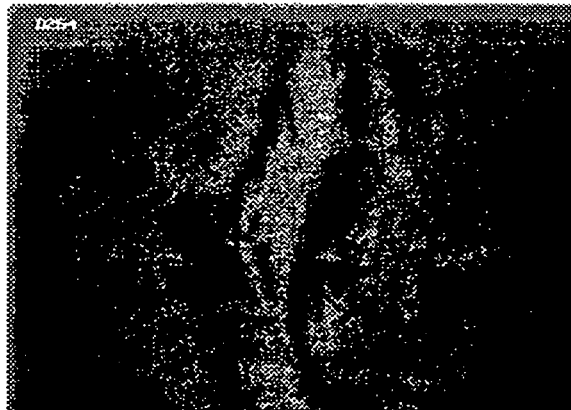
Blunt Tip

-0.01400 0.00750 0.02900



13.09 & 14.41 ft-lb

1541 psi



### A.2.2.2. K-Ep CASES FILLED WITH INERT PROPELLANT

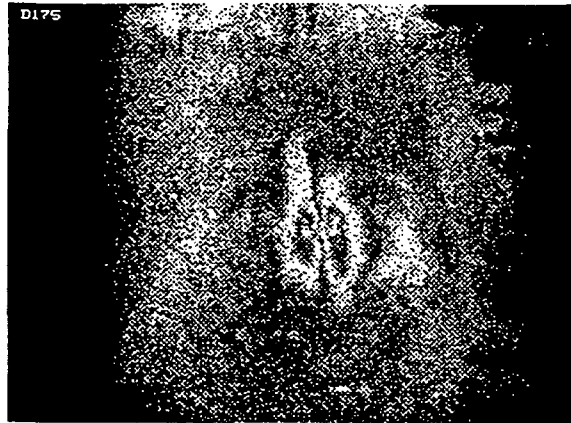
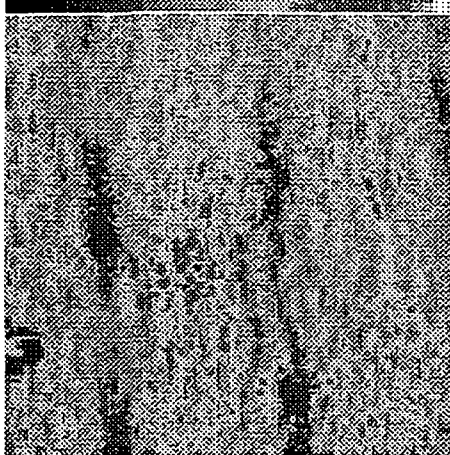
D175-176

Blunt Tip

16.5 ft-lb

1997 psi

-0.00400 0.00550 0.01700



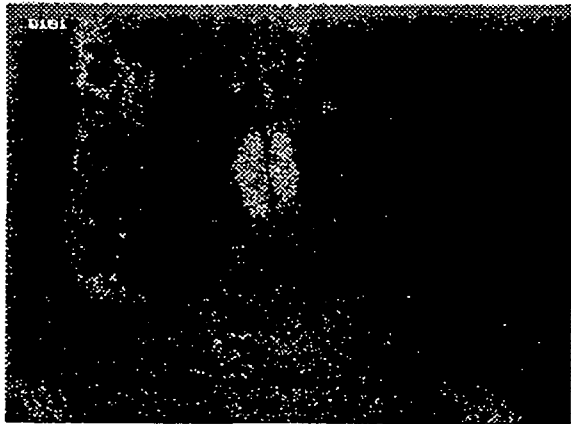
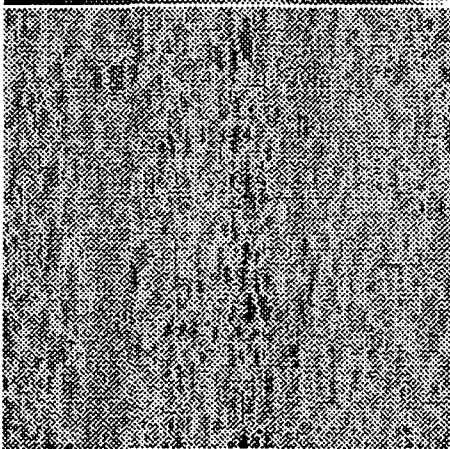
D181-182

Sharp Tip

2.89 ft-lb

2390 psi

-0.01600 0.00600 0.02800



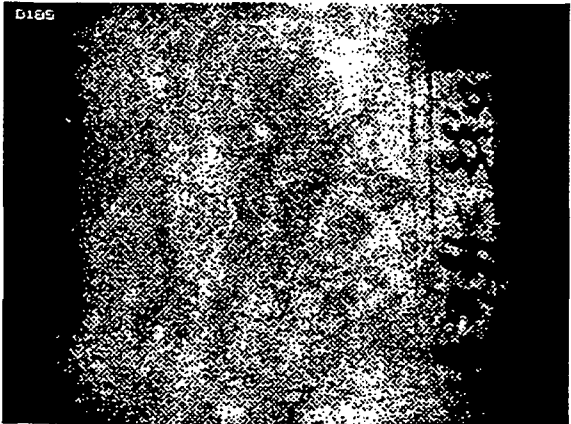
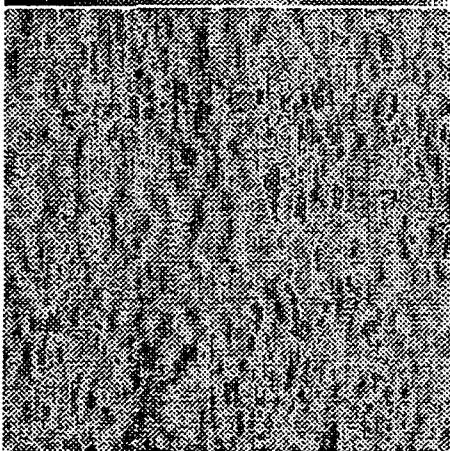
D185-186

No Impact

No Impact

3025 psi

0.00000 0.00650 0.01300



D191-192

Blunt Tip

20.28 ft-lb

2099 psi

SDVIC RESULTS NOT AVAILABLE.

Boss leak prevented image acquisition.



D197-198

Sharp Tip

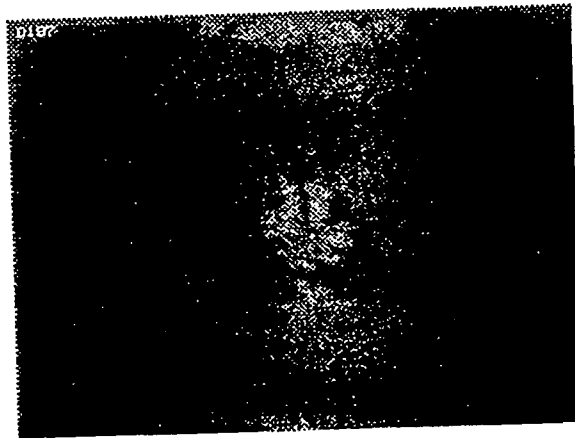
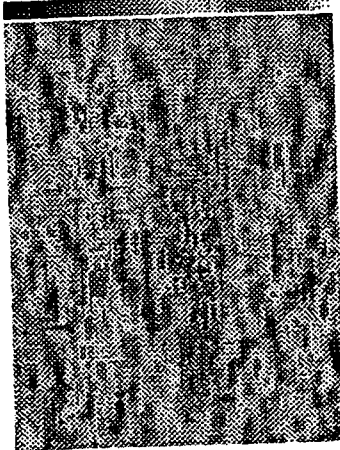
4.23 ft-lb

2319 psi

-0.00600

0.00700

0.02000



D205-206

Blunt Tip

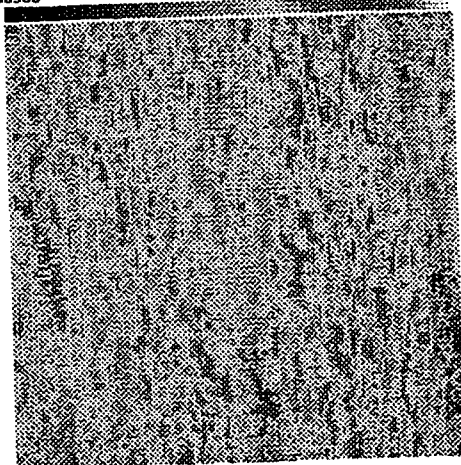
4.95 ft-lb

3071 psi

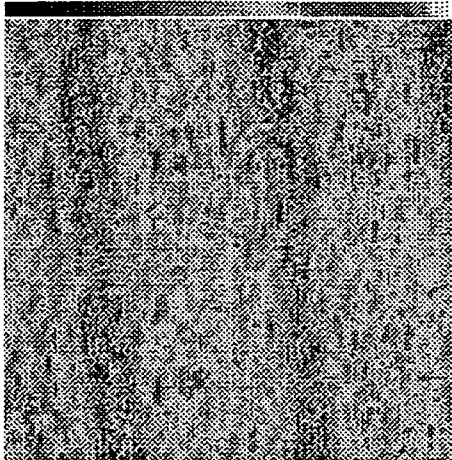
-0.00500

0.00450

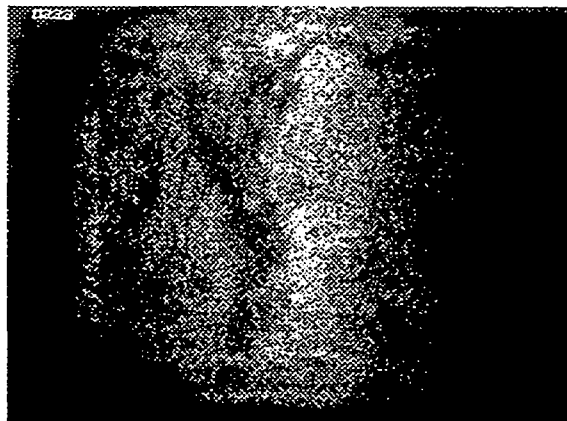
0.01400



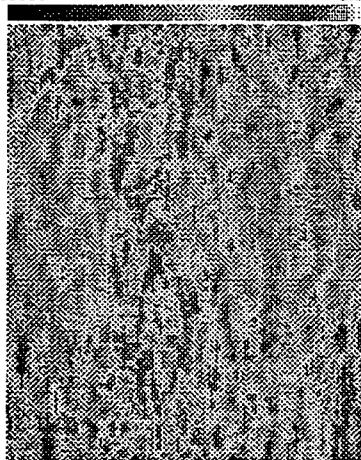
D223-224 No Impact  
-0.00700 0.00600 0.01900



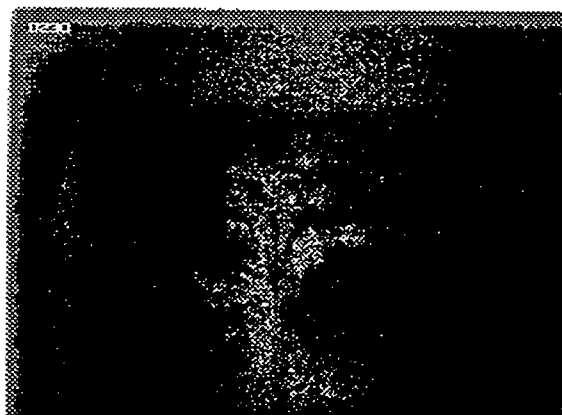
No Impact 2978 psi



D229-230 Blunt Tip  
-0.00800 0.00350 0.01500



17.00 ft-lb 2196 psi



D231-232 Sharp Tip

4.85 ft-lb 2072 psi



SDVIC RESULTS NOT AVAILABLE.

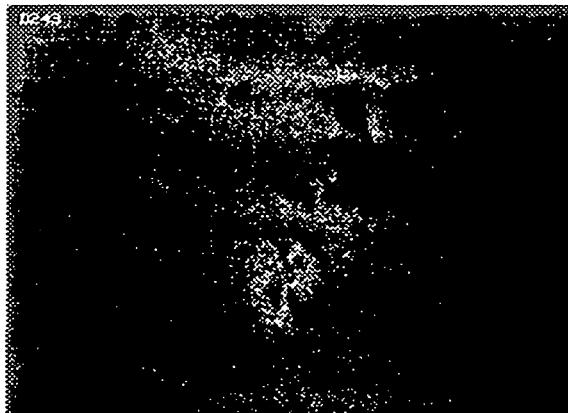
Bottle leak prevented image acquisition.



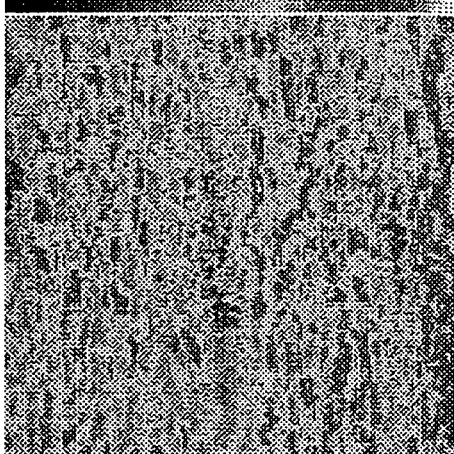
D243-244 Sharp Tip  
-0.00600 0.00600 0.0180



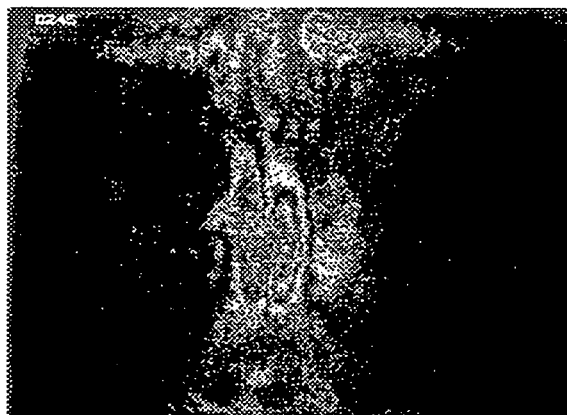
2.17 ft-lb 2588 psi



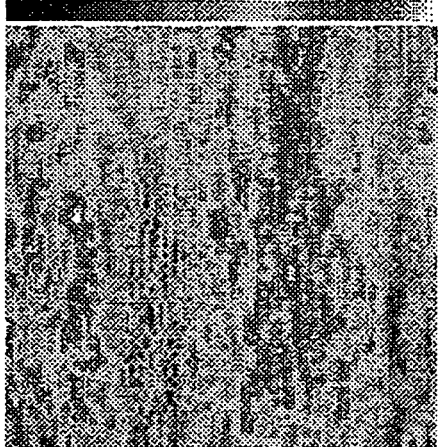
D245-246 Blunt Tip  
-0.00500 0.00450 0.01400



13.29 ft-lb 2249 psi



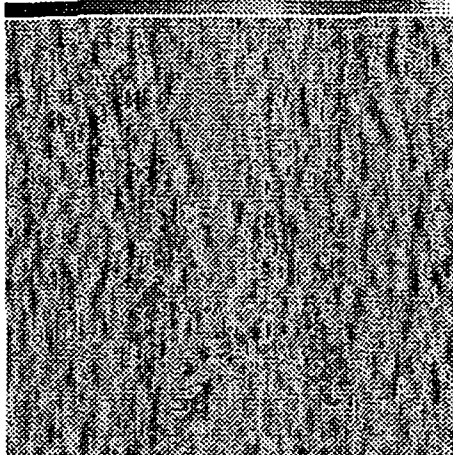
D247-248 Blunt Tip  
-0.00700 0.00400 0.01500



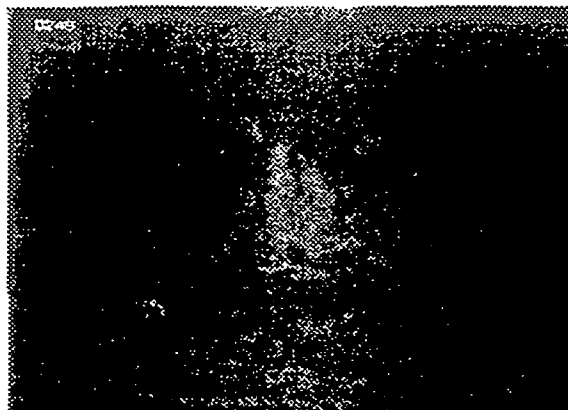
10.90 ft-lb 2541 psi



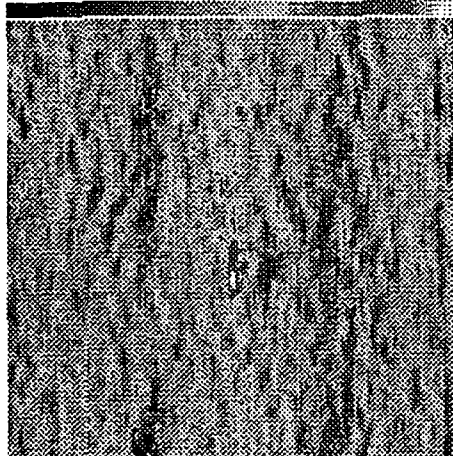
D249-250 Sharp Tip  
-0.01500 0.00850 0.03200



3.82 ft-lb 2560 psi



D255-256 Sharp Tip  
-0.00200 0.00750 0.01700

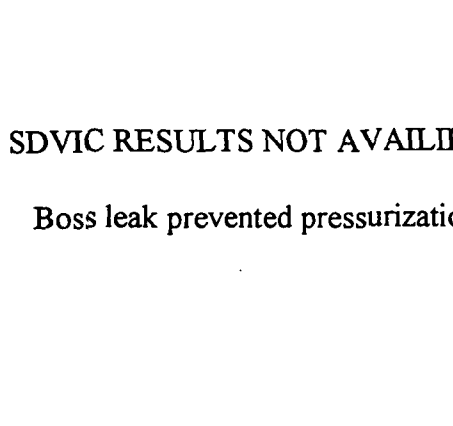


4.1 ft-lb 2682 psi



D257-258 Blunt Tip

10.90 ft-lb N/A



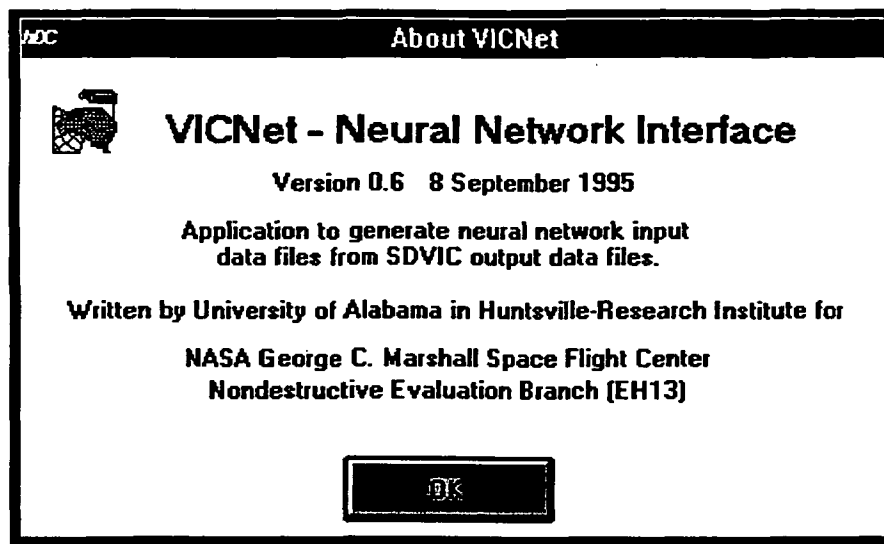
SDVIC RESULTS NOT AVAILABLE.

Boss leak prevented pressurization.



## A.3. VICNET NEURAL NETWORK INTERFACE

## A.3.1. VICNET ABOUT BOX



File: A\_VICNET.FRM

VERSION 2.00

Begin Form Frm\_AbtVICNet

BorderStyle = 3 'Fixed Double

Caption = "About VICNet"

ClientHeight = 3630

ClientLeft = 4275

ClientTop = 2595

ClientWidth = 6480

Height = 4035

Left = 4215

LinkTopic = "Form1"

MaxButton = 0 'False

MinButton = 0 'False

ScaleHeight = 3630

ScaleWidth = 6480

Top = 2250

Width = 6600

Begin CommandButton Command1

Caption = "OK"

Default = -1 'True

Height = 495

Left = 2400

TabIndex = 4

Top = 3000

Width = 1575

End

Begin PictureBox Picture1

AutoSize = -1 'True

BorderStyle = 0 'None

Height = 480

Left = 240

Picture = A\_VICNET.FRX:0000

ScaleHeight = 480

ScaleWidth = 480

TabIndex = 0

Top = 240

Width = 480

End

Begin Label Label6

Alignment = 2 'Center

Caption = "Nondestructive Evaluation  
Branch (EH13)"

Height = 255

Left = 0

TabIndex = 7

Top = 2400

Width = 6375

End

Begin Label Label5

Alignment = 2 'Center

Caption = "NASA George C.  
Marshall Space Flight Center"

Height = 255

Left = 0

TabIndex = 6

Top = 2160

Width = 6375

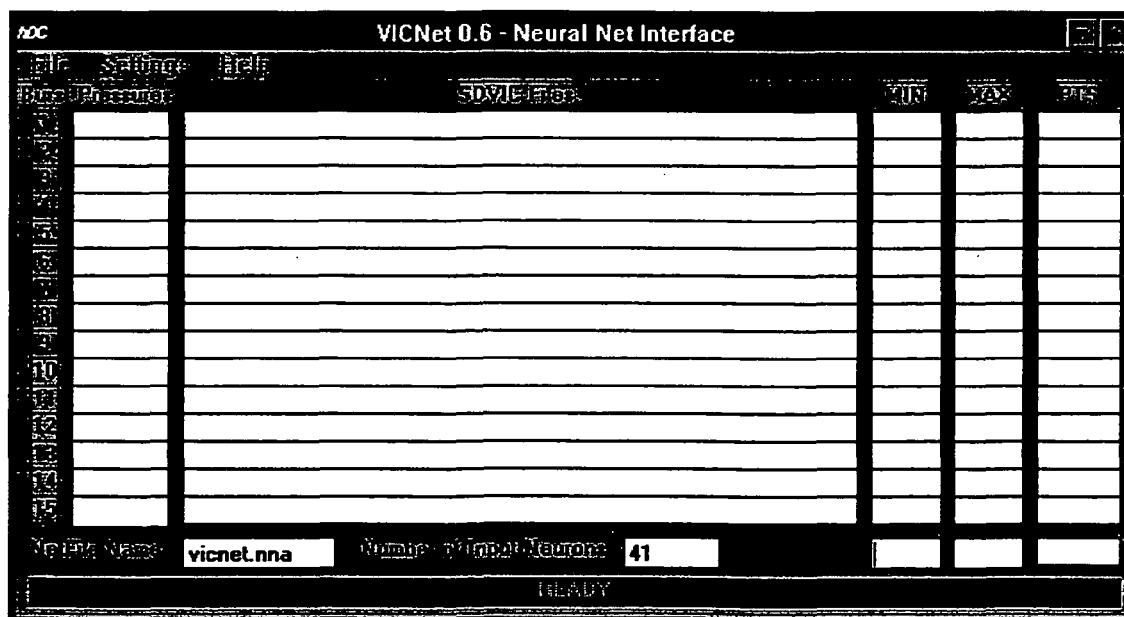
End

```

Begin Label Label4
  Alignment = 2 'Center
  Caption = "Written by University of
Alabama in Huntsville-Research Institute for"
  Height = 255
  Left = 120
  TabIndex = 5
  Top = 1800
  Width = 6255
End
Begin Label Label3
  Alignment = 2 'Center
  Caption = "Application to generate
neural network input data files from SDVIC
output data files."
  Height = 495
  Left = 1200
  TabIndex = 3
  Top = 1200
  Width = 3855
End
Begin Label Label2
  Alignment = 2 'Center
  Caption = "Version 0.6 8 September
1995"
  Height = 255
  Left = 120
  TabIndex = 2
  Top = 840
  Width = 6255
End
Begin Label Label1
  Caption = "VICNet - Neural Network
Interface"
  FontBold = -1 'True
  FontItalic = 0 'False
  FontName = "MS Sans Serif"
  FontSize = 13.5
  FontStrikethru = 0 'False
  FontUnderline = 0 'False
  Height = 375
  Left = 1080
  TabIndex = 1
  Top = 360
  Width = 5295
End
End
Sub Command1_Click ()
  Frm_AbtVICNet.Visible = False
  Frm_VICNet.Visible = True
  Frm_VICNet.SetFocus
End Sub

```

### A.3.2. VICNET MAIN WINDOW





```

Top      = 2640
Width    = 855
End
Begin TextBox Txt_Burst
Height   = 285
Index    = 9
Left     = 480
TabIndex = 29
Top      = 2400
Width    = 855
End
Begin TextBox Txt_Burst
Height   = 285
Index    = 8
Left     = 480
TabIndex = 27
Top      = 2160
Width    = 855
End
Begin TextBox Txt_Burst
Height   = 285
Index    = 7
Left     = 480
TabIndex = 25
Top      = 1920
Width    = 855
End
Begin TextBox Txt_Burst
Height   = 285
Index    = 6
Left     = 480
TabIndex = 23
Top      = 1680
Width    = 855
End
Begin TextBox Txt_Burst
Height   = 285
Index    = 5
Left     = 480
TabIndex = 21
Top      = 1440
Width    = 855
End
Begin TextBox Txt_NetFile
Height   = 285
Left     = 1440
TabIndex = 19
Text     = "vicnet.nna"
Top      = 3960
Width    = 1335
End
Begin TextBox Txt_Burst
Height   = 285
Index    = 4
Left     = 480
TabIndex = 17
Top      = 1200
Width    = 855
End
Begin TextBox Txt_Burst
Height   = 285
Index    = 3
Left     = 480
TabIndex = 16
Top      = 960
Width    = 855
End
Begin TextBox Txt_Burst
Height   = 285
Index    = 2
Left     = 480
TabIndex = 15
Top      = 720
Width    = 855
End
Begin TextBox Txt_Burst
Height   = 285
Index    = 1
Left     = 480
TabIndex = 14
Top      = 480
Width    = 855
End
Begin TextBox Txt_Burst
Height   = 285
Index    = 0
Left     = 480
TabIndex = 13
Top      = 240
Width    = 855
End
Begin TextBox Txt_Num
Alignment = 2 'Center
Height   = 285
Left     = 5280
TabIndex = 12
Text     = "41"
Top      = 3960
Width    = 855
End
Begin TextBox Txt_Max
Alignment = 2 'Center
Height   = 285
Left     = 8160
TabIndex = 11
Top      = 3960
Width    = 615
End

```

```

Begin Label Lbl_Dval
  Alignment = 2 'Center
  BorderStyle = 1 'Fixed Single
  Height = 255
  Left = 8880
  TabIndex = 102
  Top = 3960
  Width = 735

```

```
End
```

```

Begin Label Lbl_DatPts
  Alignment = 1 'Right Justify
  BorderStyle = 1 'Fixed Single
  Height = 255
  Index = 14
  Left = 8880
  TabIndex = 101
  Top = 3600
  Width = 735

```

```
End
```

```

Begin Label Lbl_DatPts
  Alignment = 1 'Right Justify
  BorderStyle = 1 'Fixed Single
  Height = 255
  Index = 13
  Left = 8880
  TabIndex = 100
  Top = 3360
  Width = 735

```

```
End
```

```

Begin Label Lbl_DatPts
  Alignment = 1 'Right Justify
  BorderStyle = 1 'Fixed Single
  Height = 255
  Index = 12
  Left = 8880
  TabIndex = 99
  Top = 3120
  Width = 735

```

```
End
```

```

Begin Label Lbl_DatPts
  Alignment = 1 'Right Justify
  BorderStyle = 1 'Fixed Single
  Height = 255
  Index = 11
  Left = 8880
  TabIndex = 98
  Top = 2880
  Width = 735

```

```
End
```

```

Begin Label Lbl_DatPts
  Alignment = 1 'Right Justify
  BorderStyle = 1 'Fixed Single
  Height = 255
  Index = 10

```

```

  Left = 8880
  TabIndex = 97
  Top = 2640
  Width = 735

```

```
End
```

```

Begin Label Lbl_DatPts
  Alignment = 1 'Right Justify
  BorderStyle = 1 'Fixed Single
  Height = 255
  Index = 9
  Left = 8880
  TabIndex = 96
  Top = 2400
  Width = 735

```

```
End
```

```

Begin Label Lbl_DatPts
  Alignment = 1 'Right Justify
  BorderStyle = 1 'Fixed Single
  Height = 255
  Index = 8
  Left = 8880
  TabIndex = 95
  Top = 2160
  Width = 735

```

```
End
```

```

Begin Label Lbl_DatPts
  Alignment = 1 'Right Justify
  BorderStyle = 1 'Fixed Single
  Height = 255
  Index = 7
  Left = 8880
  TabIndex = 94
  Top = 1920
  Width = 735

```

```
End
```

```

Begin Label Lbl_DatPts
  Alignment = 1 'Right Justify
  BorderStyle = 1 'Fixed Single
  Height = 255
  Index = 6
  Left = 8880
  TabIndex = 93
  Top = 1680
  Width = 735

```

```
End
```

```

Begin Label Lbl_DatPts
  Alignment = 1 'Right Justify
  BorderStyle = 1 'Fixed Single
  Height = 255
  Index = 5
  Left = 8880
  TabIndex = 92
  Top = 1440
  Width = 735

```

```

End
Begin Label Lbl_DatPts
  Alignment = 1 'Right Justify
  BorderStyle = 1 'Fixed Single
  Height = 255
  Index = 4
  Left = 8880
  TabIndex = 91
  Top = 1200
  Width = 735
End
Begin Label Lbl_DatPts
  Alignment = 1 'Right Justify
  BorderStyle = 1 'Fixed Single
  Height = 255
  Index = 3
  Left = 8880
  TabIndex = 90
  Top = 960
  Width = 735
End
Begin Label Lbl_DatPts
  Alignment = 1 'Right Justify
  BorderStyle = 1 'Fixed Single
  Height = 255
  Index = 2
  Left = 8880
  TabIndex = 89
  Top = 720
  Width = 735
End
Begin Label Lbl_DatPts
  Alignment = 1 'Right Justify
  BorderStyle = 1 'Fixed Single
  Height = 255
  Index = 1
  Left = 8880
  TabIndex = 88
  Top = 480
  Width = 735
End
Begin Label Label4
  Alignment = 2 'Center
  AutoSize = -1 'True
  BackColor = &H00C0C0C0&
  Caption = "PTS"
  Height = 195
  Left = 8880
  TabIndex = 87
  Top = 0
  Width = 735
End
Begin Label Lbl_DatPts
  Alignment = 1 'Right Justify
  BorderStyle = 1 'Fixed Single
  Height = 255
  Index = 0
  Left = 8880
  TabIndex = 86
  Top = 240
  Width = 735
End
Begin Label Lbl_Max
  Alignment = 1 'Right Justify
  BorderStyle = 1 'Fixed Single
  Height = 255
  Index = 14
  Left = 8160
  TabIndex = 85
  Top = 3600
  Width = 615
End
Begin Label Lbl_Min
  Alignment = 1 'Right Justify
  BorderStyle = 1 'Fixed Single
  Height = 255
  Index = 14
  Left = 7440
  TabIndex = 84
  Top = 3600
  Width = 615
End
Begin Label Lbl_Max
  Alignment = 1 'Right Justify
  BorderStyle = 1 'Fixed Single
  Height = 255
  Index = 13
  Left = 8160
  TabIndex = 83
  Top = 3360
  Width = 615
End
Begin Label Lbl_Min
  Alignment = 1 'Right Justify
  BorderStyle = 1 'Fixed Single
  Height = 255
  Index = 13
  Left = 7440
  TabIndex = 82
  Top = 3360
  Width = 615
End
Begin Label Lbl_Max
  Alignment = 1 'Right Justify
  BorderStyle = 1 'Fixed Single
  Height = 255
  Index = 12
  Left = 8160

```



```

    TabIndex    = 81
    Top         = 3120
    Width      = 615
End
Begin Label Lbl_Min
    Alignment   = 1 'Right Justify
    BorderStyle = 1 'Fixed Single
    Height     = 255
    Index      = 12
    Left       = 7440
    TabIndex   = 80
    Top        = 3120
    Width      = 615
End
Begin Label Lbl_Max
    Alignment   = 1 'Right Justify
    BorderStyle = 1 'Fixed Single
    Height     = 255
    Index      = 11
    Left       = 8160
    TabIndex   = 79
    Top        = 2880
    Width      = 615
End
Begin Label Lbl_Min
    Alignment   = 1 'Right Justify
    BorderStyle = 1 'Fixed Single
    Height     = 255
    Index      = 11
    Left       = 7440
    TabIndex   = 78
    Top        = 2880
    Width      = 615
End
Begin Label Lbl_Max
    Alignment   = 1 'Right Justify
    BorderStyle = 1 'Fixed Single
    Height     = 255
    Index      = 10
    Left       = 8160
    TabIndex   = 77
    Top        = 2640
    Width      = 615
End
Begin Label Lbl_Min
    Alignment   = 1 'Right Justify
    BorderStyle = 1 'Fixed Single
    Height     = 255
    Index      = 10
    Left       = 7440
    TabIndex   = 76
    Top        = 2640
    Width      = 615
End
Begin Label Lbl_Max
    Alignment   = 1 'Right Justify
    BorderStyle = 1 'Fixed Single
    Height     = 255
    Index      = 9
    Left       = 8160
    TabIndex   = 75
    Top        = 2400
    Width      = 615
End
Begin Label Lbl_Min
    Alignment   = 1 'Right Justify
    BorderStyle = 1 'Fixed Single
    Height     = 255
    Index      = 9
    Left       = 7440
    TabIndex   = 74
    Top        = 2400
    Width      = 615
End
Begin Label Lbl_Max
    Alignment   = 1 'Right Justify
    BorderStyle = 1 'Fixed Single
    Height     = 255
    Index      = 8
    Left       = 8160
    TabIndex   = 73
    Top        = 2160
    Width      = 615
End
Begin Label Lbl_Min
    Alignment   = 1 'Right Justify
    BorderStyle = 1 'Fixed Single
    Height     = 255
    Index      = 8
    Left       = 7440
    TabIndex   = 72
    Top        = 2160
    Width      = 615
End
Begin Label Lbl_Max
    Alignment   = 1 'Right Justify
    BorderStyle = 1 'Fixed Single
    Height     = 255
    Index      = 7
    Left       = 8160
    TabIndex   = 71
    Top        = 1920
    Width      = 615
End
Begin Label Lbl_Min
    Alignment   = 1 'Right Justify
    BorderStyle = 1 'Fixed Single
    Height     = 255

```

```

Index      = 7
Left       = 7440
TabIndex  = 70
Top        = 1920
Width     = 615
End
Begin Label Lbl_Max
Alignment  = 1 'Right Justify
BorderStyle = 1 'Fixed Single
Height    = 255
Index     = 6
Left      = 8160
TabIndex  = 69
Top       = 1680
Width    = 615
End
Begin Label Lbl_Min
Alignment  = 1 'Right Justify
BorderStyle = 1 'Fixed Single
Height    = 255
Index     = 6
Left      = 7440
TabIndex  = 68
Top       = 1680
Width    = 615
End
Begin Label Lbl_Max
Alignment  = 1 'Right Justify
BorderStyle = 1 'Fixed Single
Height    = 255
Index     = 5
Left      = 8160
TabIndex  = 67
Top       = 1440
Width    = 615
End
Begin Label Lbl_Min
Alignment  = 1 'Right Justify
BorderStyle = 1 'Fixed Single
Height    = 255
Index     = 5
Left      = 7440
TabIndex  = 66
Top       = 1440
Width    = 615
End
Begin Label Lbl_Max
Alignment  = 1 'Right Justify
BorderStyle = 1 'Fixed Single
Height    = 255
Index     = 4
Left      = 8160
TabIndex  = 65
Top       = 1200
Width    = 615
End
Begin Label Lbl_Min
Alignment  = 1 'Right Justify
BorderStyle = 1 'Fixed Single
Height    = 255
Index     = 3
Left      = 8160
TabIndex  = 63
Top       = 960
Width    = 615
End
Begin Label Lbl_Min
Alignment  = 1 'Right Justify
BorderStyle = 1 'Fixed Single
Height    = 255
Index     = 3
Left      = 7440
TabIndex  = 62
Top       = 960
Width    = 615
End
Begin Label Lbl_Max
Alignment  = 1 'Right Justify
BorderStyle = 1 'Fixed Single
Height    = 255
Index     = 2
Left      = 8160
TabIndex  = 61
Top       = 720
Width    = 615
End
Begin Label Lbl_Min
Alignment  = 1 'Right Justify
BorderStyle = 1 'Fixed Single
Height    = 255
Index     = 2
Left      = 7440
TabIndex  = 60
Top       = 720
Width    = 615
End
Begin Label Lbl_Max
Alignment  = 1 'Right Justify

```

```

BorderStyle = 1 'Fixed Single
Height      = 255
Index       = 1
Left        = 8160
TabIndex    = 59
Top         = 480
Width       = 615
End
Begin Label Lbl_Min
Alignment   = 1 'Right Justify
BorderStyle = 1 'Fixed Single
Height      = 255
Index       = 1
Left        = 7440
TabIndex    = 58
Top         = 480
Width       = 615
End
Begin Label Lbl_Max
Alignment   = 1 'Right Justify
BorderStyle = 1 'Fixed Single
Height      = 255
Index       = 0
Left        = 8160
TabIndex    = 57
Top         = 240
Width       = 615
End
Begin Label Lbl_Min
Alignment   = 1 'Right Justify
BorderStyle = 1 'Fixed Single
Height      = 255
Index       = 0
Left        = 7440
TabIndex    = 56
Top         = 240
Width       = 615
End
Begin Label Label2
Alignment   = 2 'Center
BackColor   = &H00C0C0C0&
BorderStyle = 1 'Fixed Single
Caption     = "15"
Height      = 255
Index       = 14
Left        = 120
TabIndex    = 42
Top         = 3600
Width       = 255
End
Begin Label Label2
Alignment   = 2 'Center
BackColor   = &H00C0C0C0&
BorderStyle = 1 'Fixed Single
Caption     = "14"
Height      = 255
Index       = 13
Left        = 120
TabIndex    = 43
Top         = 3360
Width       = 255
End
Begin Label Label2
Alignment   = 2 'Center
BackColor   = &H00C0C0C0&
BorderStyle = 1 'Fixed Single
Caption     = "13"
Height      = 255
Index       = 12
Left        = 120
TabIndex    = 44
Top         = 3120
Width       = 255
End
Begin Label Label2
Alignment   = 2 'Center
BackColor   = &H00C0C0C0&
BorderStyle = 1 'Fixed Single
Caption     = "12"
Height      = 255
Index       = 11
Left        = 120
TabIndex    = 45
Top         = 2880
Width       = 255
End
Begin Label Label2
Alignment   = 2 'Center
BackColor   = &H00C0C0C0&
BorderStyle = 1 'Fixed Single
Caption     = "11"
Height      = 255
Index       = 10
Left        = 120
TabIndex    = 46
Top         = 2640
Width       = 255
End
Begin Label Label2
Alignment   = 2 'Center
BackColor   = &H00C0C0C0&
BorderStyle = 1 'Fixed Single
Caption     = "10"
Height      = 255
Index       = 9
Left        = 120
TabIndex    = 47
Top         = 2400

```

```

Width      = 255
End
Begin Label Label2
Alignment  = 2 'Center
BackColor  = &H00C0C0C0&
BorderStyle = 1 'Fixed Single
Caption    = "9"
Height     = 255
Index      = 8
Left       = 120
TabIndex   = 48
Top        = 2160
Width      = 255
End
Begin Label Label2
Alignment  = 2 'Center
BackColor  = &H00C0C0C0&
BorderStyle = 1 'Fixed Single
Caption    = "8"
Height     = 255
Index      = 7
Left       = 120
TabIndex   = 55
Top        = 1920
Width      = 255
End
Begin Label Label2
Alignment  = 2 'Center
BackColor  = &H00C0C0C0&
BorderStyle = 1 'Fixed Single
Caption    = "7"
Height     = 255
Index      = 6
Left       = 120
TabIndex   = 54
Top        = 1680
Width      = 255
End
Begin Label Label2
Alignment  = 2 'Center
BackColor  = &H00C0C0C0&
BorderStyle = 1 'Fixed Single
Caption    = "6"
Height     = 255
Index      = 5
Left       = 120
TabIndex   = 53
Top        = 1440
Width      = 255
End
Begin Label Label2
Alignment  = 2 'Center
BackColor  = &H00C0C0C0&
BorderStyle = 1 'Fixed Single
Caption    = "5"
Height     = 255
Index      = 4
Left       = 120
TabIndex   = 52
Top        = 1200
Width      = 255
End
Begin Label Label2
Alignment  = 2 'Center
BackColor  = &H00C0C0C0&
BorderStyle = 1 'Fixed Single
Caption    = "4"
Height     = 255
Index      = 3
Left       = 120
TabIndex   = 51
Top        = 960
Width      = 255
End
Begin Label Label2
Alignment  = 2 'Center
BackColor  = &H00C0C0C0&
BorderStyle = 1 'Fixed Single
Caption    = "3"
Height     = 255
Index      = 2
Left       = 120
TabIndex   = 50
Top        = 720
Width      = 255
End
Begin Label Label2
Alignment  = 2 'Center
BackColor  = &H00C0C0C0&
BorderStyle = 1 'Fixed Single
Caption    = "2"
Height     = 255
Index      = 1
Left       = 120
TabIndex   = 49
Top        = 480
Width      = 255
End
Begin Label Label2
Alignment  = 2 'Center
BackColor  = &H00C0C0C0&
BorderStyle = 1 'Fixed Single
Caption    = "1"
ForeColor  = &H00000000&
Height     = 255
Index      = 0
Left       = 120
TabIndex   = 41

```

```

    Top      = 240
    Width    = 255
End
Begin Label Lbl_DatFile
    BorderStyle = 1 'Fixed Single
    Height     = 255
    Index      = 14
    Left       = 1440
    TabIndex   = 40
    Top        = 3600
    Width      = 5895
End
Begin Label Lbl_DatFile
    BorderStyle = 1 'Fixed Single
    Height     = 255
    Index      = 13
    Left       = 1440
    TabIndex   = 38
    Top        = 3360
    Width      = 5895
End
Begin Label Lbl_DatFile
    BorderStyle = 1 'Fixed Single
    Height     = 255
    Index      = 12
    Left       = 1440
    TabIndex   = 36
    Top        = 3120
    Width      = 5895
End
Begin Label Lbl_DatFile
    BorderStyle = 1 'Fixed Single
    Height     = 255
    Index      = 11
    Left       = 1440
    TabIndex   = 34
    Top        = 2880
    Width      = 5895
End
Begin Label Lbl_DatFile
    BorderStyle = 1 'Fixed Single
    Height     = 255
    Index      = 10
    Left       = 1440
    TabIndex   = 32
    Top        = 2640
    Width      = 5895
End
Begin Label Lbl_DatFile
    BorderStyle = 1 'Fixed Single
    Height     = 255
    Index      = 9
    Left       = 1440
    TabIndex   = 30
    Top        = 2400
    Width      = 5895
End
Begin Label Lbl_DatFile
    BorderStyle = 1 'Fixed Single
    Height     = 255
    Index      = 8
    Left       = 1440
    TabIndex   = 28
    Top        = 2160
    Width      = 5895
End
Begin Label Lbl_DatFile
    BorderStyle = 1 'Fixed Single
    Height     = 255
    Index      = 7
    Left       = 1440
    TabIndex   = 26
    Top        = 1920
    Width      = 5895
End
Begin Label Lbl_DatFile
    BorderStyle = 1 'Fixed Single
    Height     = 255
    Index      = 6
    Left       = 1440
    TabIndex   = 24
    Top        = 1680
    Width      = 5895
End
Begin Label Lbl_DatFile
    BorderStyle = 1 'Fixed Single
    Height     = 255
    Index      = 5
    Left       = 1440
    TabIndex   = 22
    Top        = 1440
    Width      = 5895
End
Begin Label Lbl_Status
    Alignment   = 2 'Center
    BackColor   = &H00000000&
    Caption     = "READY"
    ForeColor   = &H0000FF00&
    Height     = 255
    Left       = 120
    TabIndex   = 20
    Top        = 4320
    Width      = 9495
End
Begin Label Label8
    BackColor   = &H00C0C0C0&
    Caption     = "NetFile Name:"
    Height     = 255

```

```

Left      = 120
TabIndex = 18
Top      = 3960
Width    = 1335
End
Begin Label Label7
  BackColor = &H00C0C0C0&
  Caption   = "Number of Input
Neurons:"
  Height    = 255
  Left     = 3000
 TabIndex  = 9
  Top      = 3960
  Width    = 2295
End
Begin Label Label6
  Alignment = 2 'Center
  BackColor = &H00C0C0C0&
  Caption   = "MAX"
  Height    = 255
  Left     = 8160
 TabIndex  = 8
  Top      = 0
  Width    = 615
End
Begin Label Label5
  Alignment = 2 'Center
  BackColor = &H00C0C0C0&
  Caption   = "MIN"
  Height    = 255
  Left     = 7440
 TabIndex  = 7
  Top      = 0
  Width    = 615
End
Begin Label Label3
  Alignment = 2 'Center
  BackColor = &H00C0C0C0&
  Caption   = "Burst Pressures."
  Height    = 255
  Left     = 0
 TabIndex  = 6
  Top      = 0
  Width    = 1455
End
Begin Label Lbl_DatFile
  BorderStyle = 1 'Fixed Single
  Height     = 255
  Index      = 4
  Left      = 1440
  TabIndex  = 5
  Top       = 1200
  Width     = 5895
End
Begin Label Lbl_DatFile
  BorderStyle = 1 'Fixed Single
  Height     = 255
  Index      = 3
  Left      = 1440
  TabIndex  = 4
  Top       = 960
  Width     = 5895
End
Begin Label Lbl_DatFile
  BorderStyle = 1 'Fixed Single
  Height     = 255
  Index      = 2
  Left      = 1440
  TabIndex  = 3
  Top       = 720
  Width     = 5895
End
Begin Label Lbl_DatFile
  BorderStyle = 1 'Fixed Single
  Height     = 255
  Index      = 1
  Left      = 1440
  TabIndex  = 2
  Top       = 480
  Width     = 5895
End
Begin Label Lbl_DatFile
  BorderStyle = 1 'Fixed Single
  Height     = 255
  Index      = 0
  Left      = 1440
  TabIndex  = 1
  Top       = 240
  Width     = 5895
End
Begin Label Label1
  Alignment = 2 'Center
  BackColor = &H00C0C0C0&
  Caption   = "SDVIC Files:"
  Height    = 255
  Left     = 1440
  TabIndex = 0
  Top      = 0
  Width    = 5895
End
Begin Menu Mnu_File
  Caption = "&File"
  Begin Menu Mnu_FileAdd
    Caption = "&Add"
    Shortcut = {F1}
  End
  Begin Menu Mnu_FileDelete
    Caption = "&Delete"

```

```

    Shortcut    = {F2}
End
Begin Menu Mnu_FileRange
    Caption    = "&Range"
    Shortcut    = {F5}
End
Begin Menu Mnu_FileNet
    Caption    = "&Net"
    Shortcut    = {F6}
End
Begin Menu Mnu_FileExit
    Caption    = "E&xit"
    Shortcut    = {F7}
End
End
Begin Menu Mnu_Settings
    Caption    = "&Settings"
Begin Menu Mnu_SetClear
    Caption    = "&Clear"
End
Begin Menu Mnu_SetSave
    Caption    = "&Save"
    Shortcut    = {F3}
End
Begin Menu Mnu_SetRestore
    Caption    = "&Restore"
    Shortcut    = {F4}
End
End
Begin Menu Mnu_Help
    Caption    = "&Help"
Begin Menu Mnu_HelpAbout
    Caption    = "&About VICNet"
End
End
End

Sub Btn_Select_Click (Index As Integer)
    Flag% = Index
End Sub

Sub Form_Load ()
    Flag% = 0
End Sub

Sub Lbl_DatFile_Click (Index As Integer)
    Flag% = Index
    Frm_FName.Visible = True
    Frm_FName.SetFocus
End Sub

Sub Mnu_FileAdd_Click ()
    Frm_FName.Visible = True
    Frm_FName.SetFocus
End Sub

Sub Mnu_FileBoth_Click ()
    Mnu_FileRange = True
    Mnu_FileNet = True
End Sub

Sub Mnu_FileDelete_Click ()
    Flag% = Flag% - 1
    Lbl_DatFile(Flag%).Caption = ""
End Sub

Sub Mnu_FileExit_Click ()
    Close
End
End Sub

Sub Mnu_FileNet_Click ()
    Lbl_Status.Caption = "Generating Neural Net File..."
    Lbl_Status.Refresh
    netfile$ = Txt_Netfile.Text
    Open "c:\vic\" + netfile$ For Output As #2
    'Count Files in List
    For i% = 0 To 14
        If Len(Lbl_DatFile(i%).Caption) > 4 Then
            NumFiles% = i% + 1
        End If
    Next i%
    'Read Interface Values
    minval! = Val(Txt_Min.Text)
    numval% = Int(Val(Txt_Num.Text))
    dval! = (Val(Txt_Max.Text) - Val(Txt_Min.Text)) / numval%
    If dval! < .5 Then
        Mess$ = Str$(dval!) + " > 0.5"
        MsgBox Mess$, 0, "VICNet : Net"
    End If
    'Step Through Data Files
    For i% = 0 To NumFiles% - 1
        burst% = Int(Val(Txt_Burst(i%).Text))
        infile$ = Lbl_DatFile(i%).Caption
        numpts% = Val(Lbl_DatPts(i%).Caption)
        Open infile$ For Input As #1
        Idiot$ = "(" + Str$(i% + 1) + "/" + Str$(NumFiles%) + ")"
        Lbl_Status.Caption = "Analyzing SDVIC Data File " + Idiot$
        Label2(i%).BackColor = &HFF0000
        Label2(i%).ForeColor = &HFFFFFF
        Frm_VICNet.Refresh
        'Call Analysis Routine
    Next i%
End Sub

```

```

    Actual burst%, numval%, minval!, dval!,
numpts%
    Close #1
    DoEvents
Next i%
Close #2
Beep
MsgBox "Neural Net Data File Complete.", 0,
"Message from VICNet"
For j% = 0 To 14
    Frm_VICNet.Label2(j%).BackColor =
    &HC0C0C0
    Frm_VICNet.Label2(j%).ForeColor = &H0
Next j%
Lbl_Status.Caption = "READY"
End Sub

Sub Mnu_FileRange_Click ()
MinStrain! = 1000!
MaxStrain! = -1000!
For i% = 0 To 14
    If
Len(Frm_VICNet.Lbl_DatFile(i%).Caption) > 4
Then NumFiles% = i% + 1
Next i%
For j% = 0 To NumFiles% - 1
    infile$ =
Frm_VICNet.Lbl_DatFile(j%).Caption
    Open infile$ For Input As #1
    Idiot$ = "(" + Str$(j% + 1) + "/" +
Str$(NumFiles%) + ")"
    Frm_VICNet.Lbl_Status.Caption = "Ranging
SDVIC Data File " + Idiot$
    Frm_VICNet.Label2(j%).BackColor =
    &HFF0000
    Frm_VICNet.Label2(j%).ForeColor =
    &HFFFFFFF
    Frm_VICNet.Refresh
    numpts% = 0
    TMin! = 1000!
    TMax! = -1000!
    Do
        buffer$ = Input$(66, #1)
        numpts% = numpts% + 1
        strain! = 1000 * Val(Mid$(buffer$, 58, 7))
        If Abs(strain!) > 1000 Then
            MsgBox "ERROR: |dv/dy=" +
Str$(strain!) + "|>1000", 0, "VICNet : Sub
Range"
        End If
        If strain! < TMin! Then
            TMin! = strain!
            Frm_VICNet.Lbl_Min(j%).Caption =
Str$(TMin!)

```

```

        Frm_VICNet.Lbl_Max(j%).Caption =
Str$(TMax!)
    End If
    If strain! > TMax! Then
        TMax! = strain!
        Frm_VICNet.Lbl_Min(j%).Caption =
Str$(TMin!)
        Frm_VICNet.Lbl_Max(j%).Caption =
Str$(TMax!)
    End If
    If TMin! < MinStrain! Then
        MinStrain! = TMin!
    End If
    If strain! > MaxStrain! Then
        MaxStrain! = TMax!
    End If
    Loop Until EOF(1)
    Close #1
    Txt_Min.Text = Str$(MinStrain!)
    Txt_Max.Text = Str$(MaxStrain!)
    Lbl_DatPts(j%).Caption = Str$(numpts%)
    Frm_VICNet.Refresh
    DoEvents
Next j%
Frm_VICNet.Txt_Min.Text = Str$(MinStrain!)
Frm_VICNet.Txt_Max.Text = Str$(MaxStrain!)
Beep
MsgBox "SDVIC Data Files Ranged.", 0,
"Message from VICNet"
For j% = 0 To 14
    Frm_VICNet.Label2(j%).BackColor =
    &HC0C0C0
    Frm_VICNet.Label2(j%).ForeColor = &H0
Next j%
Frm_VICNet.Lbl_Status.Caption = "Ranging
Completed. READY."
End Sub

Sub Mnu_HelpAbout_Click ()
Frm_AbtVICNet.Visible = True
Frm_AbtVICNet.SetFocus
End Sub

Sub Mnu_SetClear_Click ()
Lbl_Status.Caption = "Clearing Settings..."
For i% = 0 To 14
    Lbl_DatFile(i%).Caption = ""
    Txt_Burst(i%).Text = ""
    Lbl_Min(i%).Caption = ""
    Lbl_Max(i%).Caption = ""
Next i%
Txt_Netfile.Text = "*.nna"
Txt_Min.Text = ""
Txt_Max.Text = ""

```



```

Txt_Num.Text = ""
Flag% = 0
Lbl_Status.Caption = "Settings Cleared.
READY."
End Sub

Sub Mnu_SetRestore_Click ()
Frm_SName.Visible = True
Frm_SName.SetFocus
End Sub

Sub Mnu_SetSave_Click ()
x$ = "x"
setfile$ = Left$(Txt_Netfile.Text,
Len(Txt_Netfile.Text) - 3) + "set"
Lbl_Status.Caption = "Saving Settings to " +
setfile$
setfile$ = "c:\vic\" + setfile$
Open setfile$ For Output As #2
For i% = 0 To 14
    If Val(Txt_Burst(i%).Text) > 0 Then
        Print #2, Txt_Burst(i%).Text, ", ";
    Lbl_DatFile(i%).Caption = ", ";
    Lbl_Min(i%).Caption = ", ";
    Lbl_Max(i%).Caption = ", ";
    Lbl_DatPts(i%).Caption
    Else
        Print #2, x$, ", "; x$, ", "; x$, ", "; x$, ", "; x$
    End If
Next i%

Print #2, Txt_Min.Text
Print #2, Txt_Max.Text
Print #2, Txt_Num.Text
Print #2, Txt_Netfile.Text
Close
Lbl_Status.Caption = "Settings Saved.
READY."
End Sub

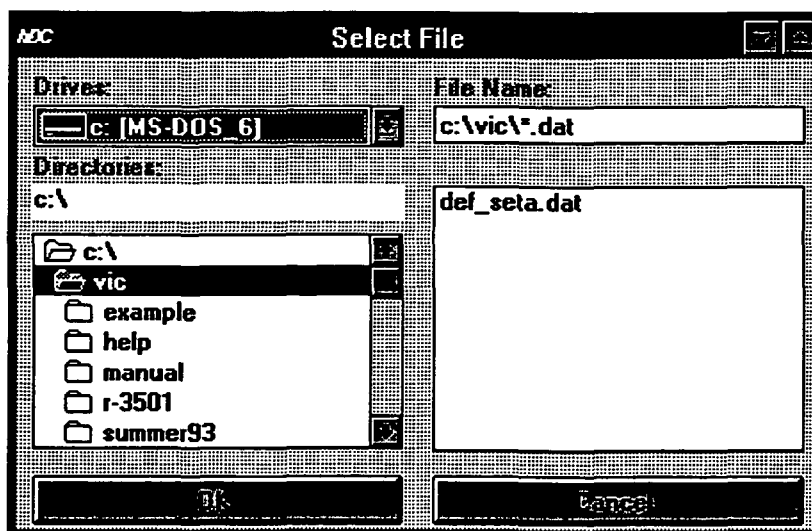
Sub Txt_Max_Change ()
Lbl_Dval.Caption =
Left$(Str$(Val(Txt_Max.Text) -
Val(Txt_Min.Text)) / Val(Txt_Num.Text)), 5)
Lbl_Dval.Refresh
End Sub

Sub Txt_Min_Change ()
Lbl_Dval.Caption =
Left$(Str$(Val(Txt_Max.Text) -
Val(Txt_Min.Text)) / (Val(Txt_Num.Text))), 5)
Lbl_Dval.Refresh
End Sub

Sub Txt_Num_Change ()
Lbl_Dval.Caption =
Left$(Str$(Val(Txt_Max.Text) -
Val(Txt_Min.Text)) / Val(Txt_Num.Text)), 5)
Lbl_Dval.Refresh
End Sub

```

### A.3.3. SDVIC DATA FILE NAME REQUEST WINDOW



File: GETFNAME.FRM

0-2

VERSION 2.00

Begin Form Frm\_FName

```

BackColor = &H00E0E0E0&
Caption = "Select File"
ClientHeight = 3525
ClientLeft = 4515
ClientTop = 2820
ClientWidth = 6000
Height = 3930
Icon = GETFNAME.FRX:0000
Left = 4455
LinkTopic = "Form1"
ScaleHeight = 3525
ScaleWidth = 6000
Top = 2475
Width = 6120

```

Begin CommandButton Btn\_Cancel

```

Caption = "Cancel"
Height = 375
Left = 3120
TabIndex = 5
Top = 3120
Width = 2775

```

End

Begin CommandButton Btn\_OK

```

Caption = "OK"
Height = 375
Left = 120
TabIndex = 4
Top = 3120
Width = 2775

```

End

Begin TextBox Txt\_FName

```

Height = 285
Left = 3120
TabIndex = 3
Text = "**.*)"
Top = 360
Width = 2775

```

End

Begin FileListBox File1

```

Height = 1980
Left = 3120
Pattern = "**.dat"
TabIndex = 2
Top = 960
Width = 2775

```

End

Begin DirListBox Dir1

```

Height = 1605
Left = 120
TabIndex = 1

```

Top = 1320

Width = 2775

End

Begin DriveListBox Drive1

```

Height = 315
Left = 120
TabIndex = 0
Top = 360
Width = 2775

```

End

Begin Label Lbl\_CurrentDir

```

BackColor = &H00FFFFFF&
Caption = "c:\\"
Height = 255
Left = 120
TabIndex = 9
Top = 960
Width = 2775

```

End

Begin Label Label4

```

BackColor = &H00E0E0E0&
Caption = "Drives:"
Height = 255
Left = 120
TabIndex = 8
Top = 120
Width = 1575

```

End

Begin Label Label3

```

BackColor = &H00E0E0E0&
Caption = "Directories:"
Height = 255
Left = 120
TabIndex = 7
Top = 720
Width = 1575

```

End

Begin Label Label2

```

BackColor = &H00E0E0E0&
Caption = "File Name:"
Height = 255
Left = 3120
TabIndex = 6
Top = 120
Width = 1575

```

End

End

Sub Btn\_Cancel\_Click ()

Frm\_FName.Visible = False

Frm\_VICNet.SetFocus

End Sub

```

Sub Btn_OK_Click ()
    Frm_FName.Visible = False
    Frm_VICNet.SetFocus
    Frm_VICNet.Lbl_DatFile(Flag%).Caption =
    Txt_FName.Text
    Flag% = Flag% + 1
End Sub

Sub Dir1_Change ()
    File1.Path = Dir1.List(-1)
    Txt_FName.Text = Dir1.List(-1) + "\*.dat"
End Sub

Sub Drive1_Change ()
    Dir1.Path = Drive1.Drive
    Txt_FName.Text = Dir1.List(-1) + "\*.dat"
End Sub

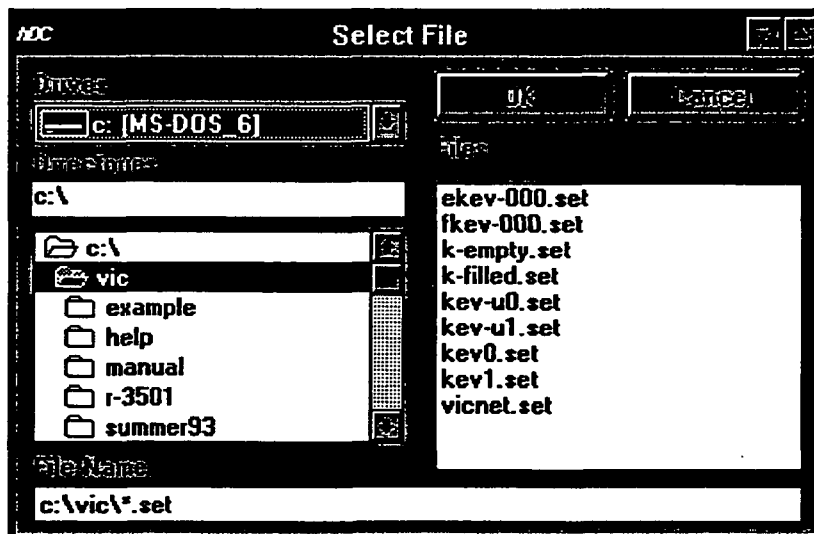
Sub File1_Click ()
    Txt_FName.Text = Dir1.List(-1) + "\" +
    File1.FileName
End Sub

Sub File1_DblClick ()
    Txt_FName.Text = Dir1.List(-1) + "\" +
    File1.FileName
    Btn_OK = True
End Sub

Sub Form_Load ()
    Dir1.Path = "c:\vic"
    Txt_FName.Text = Dir1.List(-1) + "\*.dat"
End Sub

```

#### A.3.4. SETTINGS FILE NAME REQUEST WINDOW



File: SETFNAME.FRM

```

VERSION 2.00
Begin Form Frm_SName
    BackColor = &H00C0C0C0&
    Caption = "Select File"
    ClientHeight = 3615
    ClientLeft = 4500
    ClientTop = 2820
    ClientWidth = 6015
    Height = 4020
    Icon = SETFNAME.FRX:0000
    Left = 4440
    LinkTopic = "Form1"
    ScaleHeight = 3615
    ScaleWidth = 6015
    Top = 2475
    Width = 6135
    Begin CommandButton Btn_Cancel
        Caption = "Cancel"
        Height = 375
        Left = 4560

```

```

    TabIndex    = 5
    Top         = 120
    Width      = 1335
End
Begin CommandButton Btn_OK
    Caption     = "OK"
    Height     = 375
    Left       = 3120
    TabIndex   = 4
    Top        = 120
    Width     = 1335
End
Begin TextBox Txt_FName
    Height     = 285
    Left      = 120
    TabIndex  = 3
    Text      = "*.*)"
    Top       = 3240
    Width    = 5775
End
Begin FileListBox File1
    Height     = 2175
    Left      = 3120
    Pattern   = "*.set"
    TabIndex  = 2
    Top       = 960
    Width    = 2775
End
Begin DirListBox Dir1
    Height     = 1605
    Left      = 120
    TabIndex  = 1
    Top       = 1320
    Width    = 2775
End
Begin DriveListBox Drive1
    Height     = 315
    Left      = 120
    TabIndex  = 0
    Top       = 360
    Width    = 2775
End
Begin Label Label1
    BackColor = &H00C0C0C0&
    Caption   = "Files:"
    Height   = 255
    Left    = 3120
    TabIndex = 10
    Top     = 600
    Width  = 975
End
Begin Label Lbl_CurrentDir
    BackColor = &H00FFFFFF&
    Caption   = "c:\\"
    Height   = 255
    Left    = 120
    TabIndex = 9
    Top     = 960
    Width  = 2775
End
Begin Label Label4
    BackColor = &H00C0C0C0&
    Caption   = "Drives:"
    Height   = 255
    Left    = 120
    TabIndex = 8
    Top     = 120
    Width  = 1575
End
Begin Label Label3
    BackColor = &H00C0C0C0&
    Caption   = "Directories:"
    Height   = 255
    Left    = 120
    TabIndex = 7
    Top     = 720
    Width  = 1575
End
Begin Label Label2
    BackColor = &H00C0C0C0&
    Caption   = "File Name:"
    Height   = 255
    Left    = 120
    TabIndex = 6
    Top     = 3000
    Width  = 1575
End
End
Sub Btn_Cancel_Click ()
    Frm_SName.Visible = False
    Frm_VICNet.SetFocus
End Sub
Sub Btn_OK_Click ()
    Frm_SName.Visible = False
    Frm_VICNet.SetFocus
    Frm_VICNet.Lbl_Status.Caption = "Restoring
Settings from VICNET.SET"
    setfile$ = Txt_FName.Text
    x$ = ""
    Open setfile$ For Input As #1
    For i% = 0 To 14
        Input #1, buf1$, buf2$, buf3$, buf4$, buf5$
        If buf1$ <> "x" Then
            Frm_VICNet.Txt_Burst(i%).Text = buf1$
        End If
    Next i%
End Sub

```

```

    Frm_VICNet.Lbl_DatFile(i%).Caption =
buf2$
    Frm_VICNet.Lbl_Min(i%).Caption =
buf3$
    Frm_VICNet.Lbl_Max(i%).Caption =
buf4$
    Frm_VICNet.Lbl_DatPts(i%).Caption =
buf5$
    Else
        Frm_VICNet.Txt_Burst(i%).Text = x$
        Frm_VICNet.Lbl_DatFile(i%).Caption =
x$
        Frm_VICNet.Lbl_Min(i%).Caption = x$
        Frm_VICNet.Lbl_Max(i%).Caption = x$
        Frm_VICNet.Lbl_DatPts(i%).Caption = x$
    End If
Next i%
Input #1, buf1$
Frm_VICNet.Txt_Min.Text = buf1$
Input #1, buf2$
Frm_VICNet.Txt_Max.Text = buf2$
Input #1, buf3$
Frm_VICNet.Txt_Num.Text = buf3$
Input #1, buf4$
Frm_VICNet.Txt_NetFile.Text = buf4$
Close
Frm_VICNet.Lbl_Dval.Caption =
Left$(Str$((Val(Frm_VICNet.Txt_Max.Text) -
Val(Frm_VICNet.Txt_Min.Text)) /
(Val(Frm_VICNet.Txt_Num.Text))), 5)
Frm_VICNet.Lbl_Status.Caption = "Settings
Restored. READY."
End Sub

```

### A.3.5. FORM INDEPENDENT CODE

File: VICNET.BAS

```

Global Flag%
Global temp!(10), LUT!(64)
Dim count%()

Sub Actual (burst%, numval%, minval!,
dval!, numpts%)
'Calculates histogram based upon actual dv/dy
values from SDVIC.
'Initialize variable values
ReDim count%(numval% + 1)
For i% = 0 To numval%
    count%(i%) = 0
Next i%
'Read each line, 64 char + CR + LF per line,
until end of file.

```

```

Sub Dir1_Change ()
File1.Path = Dir1.List(-1)
Txt_FName.Text = Dir1.List(-1) + "\*.dat"

End Sub

Sub Drive1_Change ()
Dir1.Path = Drive1.Drive
Txt_FName.Text = Dir1.List(-1) + "\*.dat"

End Sub

Sub File1_Click ()
Txt_FName.Text = Dir1.List(-1) + "\" +
File1.FileName
End Sub

Sub File1_DblClick ()
Txt_FName.Text = Dir1.List(-1) + "\" +
File1.FileName
Btn_OK = True

End Sub

Sub Form_Load ()
Dir1.Path = "c:\vic\"
Txt_FName.Text = Dir1.List(-1) + "\*.set"
End Sub

```

```

Do
    buffer$ = Input$(66, #1)
    dvdy! = 1000! * Val(Mid$(buffer$, 58, 7))
    'Trap for misread end of lines.
    If Abs(dvdy!) > 1000! Then
        MsgBox "ERROR: |dv/dy=" + Str$(dvdy!)
+ ">1000", 0, "VICNet : Sub Actual"
    End If
    'Determine which of the numval% histogram
bars the current dv/dy is in.
    index% = Int((((dvdy! + (dval! / 2!)) -
minval!) / dval!)
    If ((index% > 0) And (index% < (numval% +
1))) Then count%(index%) = count%(index%) +
1

```

```
Loop Until EOF(1)
DoEvents
'Output Neural Net File (netfile.nna)
total% = 0
For i% = 1 To numval%
  If count%(i%) < 0 Then      'Trap for
negative count.
    Mess$ = "Count Less Than Zero (" +
Str$(count%(i%)) + ")."
    MsgBox Mess$, 0, "VICNet : Sub Actual"
    count%(i%) = 0
  End If

  total% = total% + count%(i%)
  Print #2, count%(i%), " ";
Next i%
If total% <> numpts% Then
  Mess$ = Str$(total%) + " / " +
Str$(numpts%) + " Points Counted."
  MsgBox Mess$, 0, "VICNet : Sub Actual"
End If
Print #2, burst%
End Sub
```

NASA

National Aeronautical and  
Space Agency

## Report Document Page

1. Report No. 5-33567	2. Government Accession No.	3. Recipient's Catalog No.	
4. Title and Subtitle " Methods of Video and Shearography Inspection"		5. Report Due September 1995	
		6. Performing Organization Code Research Institute, UAH	
7. Author(s) Matthew D. Lansing, Michael W. Bullock, William J. Gnacek		8. Performing Organization Report No. 5-33567	
		10. Work Unit No. Delivery Order #119	
9. Performing Organization Name and Address UAH Research Institute RI E-47 University of Alabama in Huntsville Huntsville, AL 35899		11. Contract or Grant No. NAS8-38609	
		13. Type of report and Period covered Final Report 22 September 1994 through 21 September 1995	
12. Sponsoring Agency Name and Address National Aeronautics and Space Administration Marshall Space Flight Center Huntsville, AL 35812		14. Sponsoring Agency Code	
		15. Supplementary Notes	
16. Abstract  The goal of this research effort was to study methods of video image correlation and electronic shearography for nondestructive evaluation of aerospace components. Methods of physical load application must be developed before interrogations with these methods may be used to qualify hardware. To that end, inspection procedures were developed for a variety of aerospace components and material systems. Experiments were also conducted from which the relationship between the control settings of the electronic shearography apparatus may be related to flaw detectability. A short feasibility study was conducted to determine the applicability of electronic shearography to the determination of the stress intensity factor of a Mode I crack tip by measurement of the localized zone of three dimensional plasticity			
17. Key Words (Suggested by Author(s)) experimental mechanics, flaw detection, fracture video image correlation, NDE, nondestructive testing, NDT, nondestructive evaluation, POD, probability of detection, shearography		18. Distribution Statement TBA	
19. Security Class. (of this report) Unclassified	20. Security Class. (of this page) Unclassified	21. No. of pages 101	22. Price